Glycosphingolipid Metabolism and the Glycosphingolipid-Metabolizing Enzyme Beta-Glucosidase 2: Biochemical and Cell Biological Studies

by

Saki Sultana

Submitted in partial fulfilment of the requirements
for the degree of Doctor of Philosophy

at

Dalhousie University
Halifax, Nova Scotia
December 2019

© Copyright by Saki Sultana, 2019

TABLE OF CONTENTS

LIST OF TABLES

LIST OF FIGURES

ABSTRACT

Glycosphingolipids (GSLs) are constituents of eukaryotic cell membranes and consist of a lipid (ceramide) linked to one or more sugar residues. GSLs occur in many structurally distinct forms, varying in both their lipid and oligosaccharide domains. Most cells contain multiple structurally different GSLs. Different cell types/animal tissues have distinct and consistent GSL profiles, indicating that cellular GSL homeostasis is under strict regulation. Deviations in GSL homeostasis have pathological consequences. Our understanding of the regulation of cellular GSL levels is very limited. In the first part of my project, I have attempted to assess the kinetics of GSL turnover by testing a mathematical model correlating the rates of GSL biosynthesis and degradation. Genetic and pharmacological interventions were made in cellular models to disrupt GSL biosynthetic enzymes. This approach, however, produced inconsistent results. In the second part of the project I investigated cellular and biochemical consequences of the mutations in β-glucosidase 2 (GBA2), a GSL-metabolizing enzyme reported being mutated in SPG46, a complex neurodegenerative disorder. SPG46 (SPastic Gait locus #46) patients present with a combination of spastic paraplegia and cerebellar ataxia and suffer from muscle weakness and spasticity in the upper and lower limbs along with other neurological symptoms. Currently, the cascade of events leading from mutations in the GBA2 gene to SPG46 is largely unexplored. I have characterized ten SPG46-associated GBA2 mutations, five nonsense, and five missense mutations. All ten GBA2 mutants were catalytically inactive. The lack of enzyme activity was not associated with decreased protein expression. Native conformations of all but Gly683Arg mutants were different from the WT GBA2, confirmed by native gel electrophoresis, indicative of different protein-binding behaviors of the mutant proteins. Further, nonsense GBA2 mutants caused mitochondrial depolarization and interfered with mitochondria fusion, resulting in the formation of fragmented mitochondria. I have identified a potential mitochondrial targeting site in GBA2 causing conditional import of GBA2 in the mitochondrial matrix. My research unveils the roles of GBA2 on mitochondrial forms and functions which have not been observed before.

LIST OF ABBREVIATIONS AND SYMBOLS USED

AAA	ATPases associated with diverse cellular activities
2-AA	2-anthranilic acid
ADP	Adenosine diphosphate
ANOVA	Analysis of variance
APS	Ammonium persulfate
ATCC	American Type Culture Collection
ATP	Adenosine triphosphate
α	Alpha
BN-PAGE	Blue native-poly acrylamide gel electrophoresis
Bp	Base pairs of nucleotides
BCA	Bicinchoninic acid
BSA	Bovine serum albumin
B4GALNT1	Beta-1,4 N-acetylgalactosaminyltransferase 1
β	Beta
CCCP	2-[2-(3-chlorophenyl) hydrazinylyidene] propanedinitrile
cDNA	Complementary DNA
CMV	Cytomegalovirus
c-Myc	v-myc avian myelocytomatosis viral oncogene homolog
CoA	Co-enzyme A
CNS	Central nervous system
CS	Ceramide synthase
DMEM	Dulbecco's modified eagle medium
DMSO	Dimethyl sulfoxide
DNA	Deoxyribonuclic acid
dNTP	Deoxyribonucleotide triphosphates
DLP1	Dynamin-like protein 1
DRP1	Dynamin related protein 1
EDTA	Eythylene-diamine tetra-acetic acid (disodium salt used)
FACS	Fluorescence activated cell sorting

FBS	Fetal bovine serum
FCCP	Carbonyl cyanide-4-phenylhydrazone
FITC	Fluorescein isothiocyanate
GBA1	Gluocerebodisase 1
GBA2	Glucosylceramidase beta 2
GFP	Green fluorescent protein
GlcCer	Gluocylceramide
GSL	Glycosphingolipid
HBS	Hepes buffered saline
HEK-293T	Human embryonic kidney 293 SV40
HeLa	Henrietta Lacks
HEPES	4-(2-hydroxyethyl)-1-piperazineethanesulfonic acid
HPLC	High performance liquid chromatography
HPTLC	High performance thin layer chromatography
HSP	Hereditary spastic paraplegia
IMS	Inter membrane space of mitochondria
Kbp	Kilobase pairs
KDa	Kilo Dalton
KO	Knockout
M	Molar
mAb	Monoclonal antibody
$MgCl_2$	Magnesium chloride
MICOS	Mitochondrial contact site
MIM	Mitochondrial inner membrane
mOsM	Miliosmole
mRNA	Messenger RNA
*N*B-DGJ	*N*-(n-Butyl) deoxygalactonojirimycin
*N*B-DNJ	*N*-Butyldeoxynojirimycin
OPA1	Optic atrophy protein 1
PBS	Phosphate buffered saline
PC	Phosphatidylcholine

PCR	Polymerase chain reaction
PFA	Paraformaldehyde
PM	Plasma membrane
PVDF	Polyvinylidene difluoride
RNA	Ribonucleic acid
ROS	Reactive oxygen species
Rpm	Revolutions per minute
RT	Room temperature
SDS	Sodium dodecyl sulphate
SDS-PAGE	Sodium dodecyl sulphate-poly acrylamide gel electrophoresis
SL	Sphingolipid
SPG46	Spastic gait locus #46
TEMED	Tetramethylethylenediamine
TIM	Translocases of outer mitochondrial membrane
TOM	Translocases of inner mitochondrial membrane
TMRM	Tetramethylrhodamine methyl ester
UGCG	UDP-glucose ceramide glucosyl transferase
WT	Wild type

ACKNOWLEDGMENTS

I would like to gratefully thank my supervisor, Dr. Aarnoud C. van der Spoel, for his constant encouragement, support, and guidance throughout this journey. I sincerely thank him for his constructive feedback on my research, presentation skills, and writings. I am ever grateful to him for giving me all the flexibility I needed to balance my professional and personal life.

I would also like to thank my committee members: Dr. Barbara Karten, Dr. Roger McLeod and Dr. Stefan Krueger for the valuable suggestions and discussions that helped me improve the quality of my research. I always eagerly waited for my committee meetings as I knew that I would turn up with better ideas and inspirations after each meeting.

I would also like to express my gratitude to Dr. Stephen Bearne, the Head of the Department of Biochemistry and Molecular Biology, for being there for me during my tough times. I truly appreciate his support and prompt actions to help me finish this journey smoothly.

I would like to express my thankfulness to the graduate coordinator Dr. Jan Rainey for always being accessible whenever needed. Very special thanks to two motherly figures, Roisin McDevitt and Debbie Hayes. Thank you so very much for all the assistance and love that you have given me.

To all the members of ARC, I truly appreciate for sharing your knowledge and lab techniques with me. Special thanks to Rob Douglas for maintaining cell cultures as well as technical supports.

It would not have been possible for me to continue my study and research without the financial supports from Nova Scotia Health Research Foundations (NSERC), IWK Hospital, Natural Sciences and Engineering Research Council (NSERC), Dalhousie Medical Research Foundations (DMRF), Government of Nova Scotia for the Nova Scotia Graduate Scholarship (NSGS) and Department of Biochemistry and Molecular Biology, Dalhousie University.

I would like to thank my family for being there for me whenever I needed them the most. My father Sultan Mahmud and my mother Nasima Akther have made many sacrifices to have me achieve my goals. They have always had their full faith on my potentials and have given me the freedom to follow my dream and passion. My younger brothers, Saad and Shoaib, thank you so much for being the most caring, loving and supportive siblings. I miss being with you! Kamrul, thank you so very much for being so patient and keeping up with all my mood swings. I can't thank you enough for loving and supporting me all these years. Finally, Arham, I don't know what to tell about you! You are the best thing that have ever happened in my life. You have made me realize how strong I am! Mamma is so sorry for taking away so much time from you. Mamma loves you more than anything in the world.

Finally, I would like to show my gratitude towards the Almighty for His countless blessings. Thank you, Allah, for blessing me with the gift of family, health, learning, peace and contentment.

Chapter 1: Introduction

1.1 Glycosphingolipids

1.1.1 Sphingolipids and Glycosphingolipids

Sphingolipids are ubiquitous components of mammalian cell membranes. They are the second major category of polar lipids, represent 5-20% of total lipid mass in mammalian brain (1,2), and are particularly abundant in myelin sheaths of neurons (3,4). The basic structure of sphingolipids is a sphingoid base known as sphingosine, which is a long-chain, unsaturated amino alcohol. When the amino group of the sphingosine is attached to a fatty acid through an amide linkage, the structure is known as ceramide - the precursor of all complex sphingolipids. Attachment of different prosthetic groups to the first carbon of ceramide produces different sphingolipids (Figure 1.1.1). In sphingomyelin, the prosthetic group is phosphorylcholine, and in glycosphingolipids (GSLs), the prosthetic groups are carbohydrates.

GSLs are composite biomolecules consisting of a carbohydrate head group (either a mono- or oligosaccharide) and a ceramide backbone. They are amphipathic lipids where the ceramide is the hydrophobic moiety and the sugar head group is the hydrophilic part. GSLs are components of cellular membranes, but compared to phospholipids, GSLs are present at a lower level in eukaryotic cell membranes (5). In cells, the hydrophobic ceramide remains membrane-embedded, and the sugar head group faces the non-cytosolic space. Structurally, GSLs are extremely heterogenous. More than 60 different sphingoid bases and more than 300 different oligosaccharide chains have been identified, in combination forming thousands structurally distinct GSLs (6).

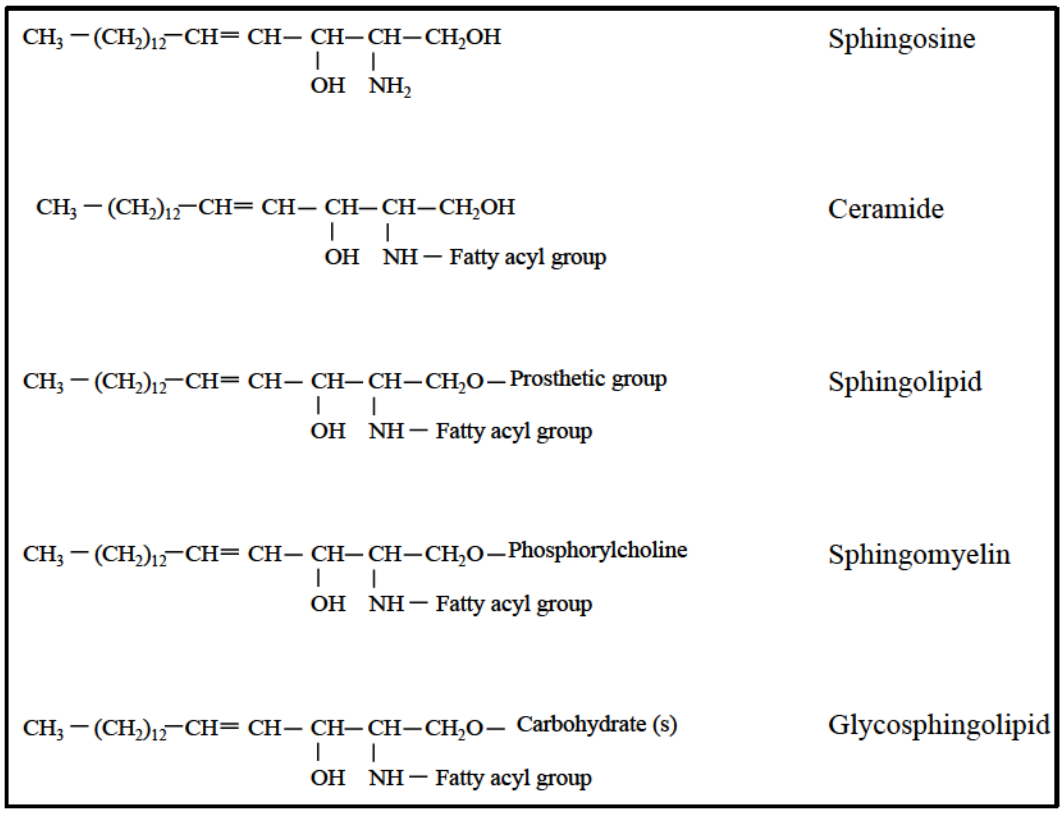

Figure 1.1.1. Structures of sphingosine (sphingoid base), ceramide and other sphingolipids.

1.1.2 Classification of Glycosphingolipids

GSLs can be classified in various ways. Based on presence or absence of an acidic group, they are classified into three categories.

(i) **Cerebrosides:** Members of this group of GSLs are also known as mono-glycosylceramides, as a single sugar moiety is attached to the first hydroxyl group of the ceramide (Figure 1.1.1). The sugar residue can be glucose or galactose, forming glucocerebrosides (glucosylceramides) and galactocerebrosides (galactosylceramides), respectively (7). Galactocerebrosides are present in neuronal cell membranes. Glucocerebrosides are not very common, they are mostly generated as intermediate products during the synthesis or degradation of gangliosides.

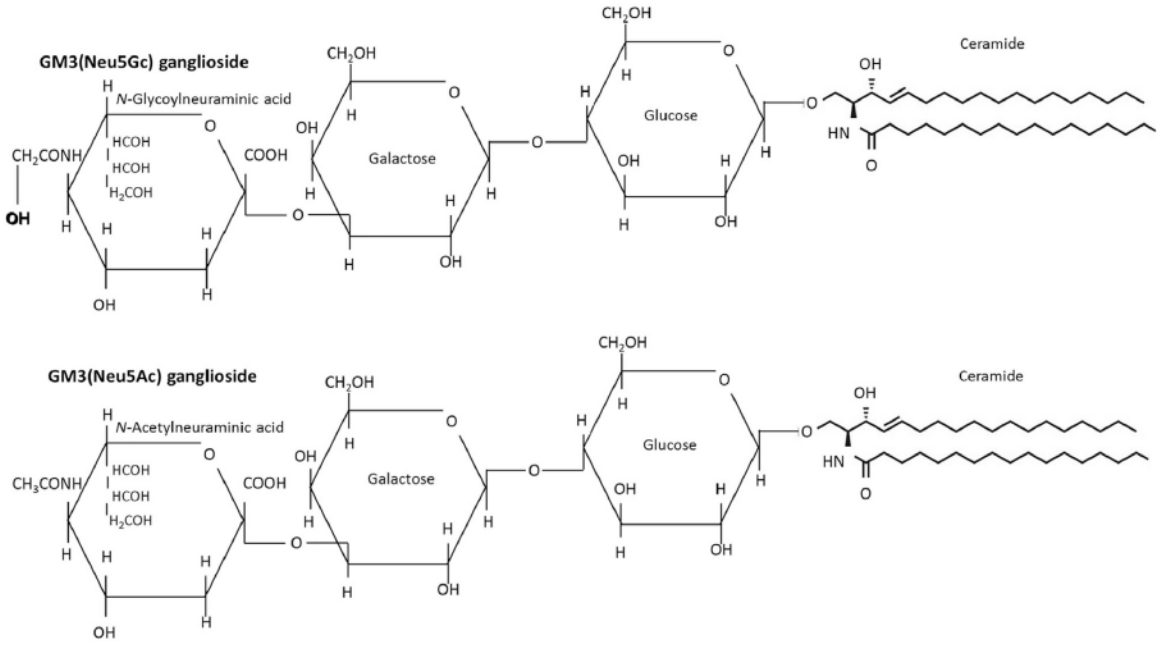

Figure 1.1.2. Structures of GM3 gangliosides. Ceramide is attached to an oligosaccharide containing glucose (Glc) and galactose (Gal), and a sialic acid residue [N-acetyl-neuraminic acid (Neu5Ac) or N-glycolyl-neuraminic acid (Neu5Gc)]. [Image source: Labrada *et al*. (8)].

(ii) **Gangliosides**: Gangliosides are glycosphingolipids containing at least one sialic acid residue (9). N-acetylneuraminic acid (Neu5Ac) and N-glycolyneuraminic acid (Neu5Gc) are the two major sialic acid variants in mammals, but human tissues do not normally contain Neu5Gc-sialoconjugates [8] (Figure 1.1.2). Gangliosides are important components of neuronal plasma membrane and intracellular membranes [10].

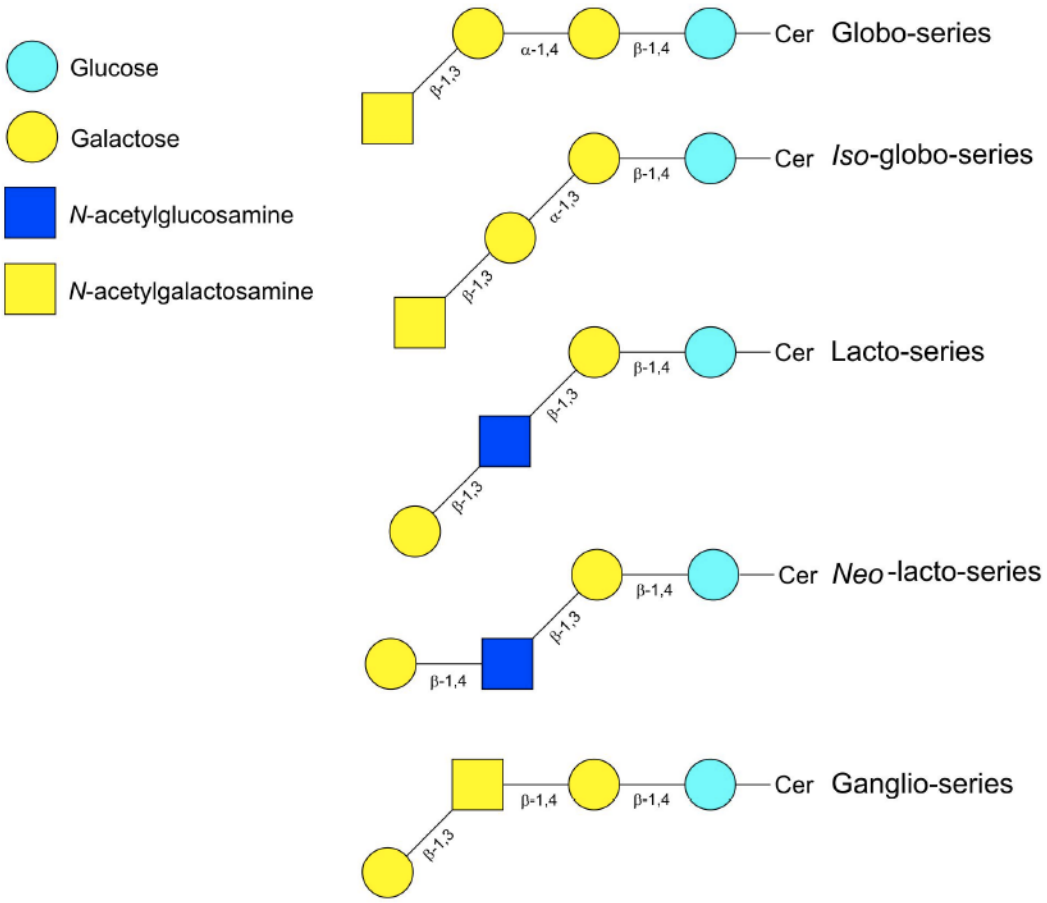

Figure 1.1.3. Schematic representation of different series of glycosphingolipids. Cer, ceramide. [Image source: Zuniga *et al.* (10)].

(iii) **Sulfatides:** Sulfatides are sulphuric acid esters of ceramide oligosaccharides. They are classified into three other subgroups - sulphated cerebroside, sulphated globosides, and sulphated gangliosides. Sulphatides are also components of neuronal cell membranes (11).

Based on the sequence of the core carbohydrate moiety and their bonds, GSLs are also classified into different series, namely the globo-, lacto- and ganglio-series [11] (Figure 1.1.3).

1.1.3 Biosynthesis and Turnover of Glycosphingolipids

GSLs undergo continuous turnover, which is reliant on intracellular transport, as GSL biosynthesis and degradation occur in different cellular compartments (12). The *de novo* synthesis of GSLs starts with the formation of ceramide at the outer membrane of endoplasmic reticulum (ER). Serine and palmitoyl CoA are precursors of ceramide. Serine is decarboxylated and CoA is released from palmitoyl CoA, forming 3-keto-dihydrosphingosine (sphinganine), catalyzed by serine palmitoyl transferase (SPT) (Figure 1.1.4) (13,14). Sphinganine is then reduced into dihydrosphingosine by 3-keto-dihydrosphingosine reductase. Dihydrosphingosine can be either phosphorylated by sphingosine kinase 1 and 2 to form dihydrosphingosine-1-phosphate, or acylated by ceramide synthases (CerS), followed by desaturation by ceramide desaturase to form ceramide. Six ceramide synthases have been reported in humans and their expression is tissue specific (15). Ceramide is also produced by hydrolysis of sphingomyelin or by the salvage pathway. After synthesis, ceramide is transported to early Golgi compartments by vesicular transport where it is glycosylated to form different GSLs. The first glycosylation step of ceramide is catalyzed by UDP-glucose ceramide transferase (UGCG), producing glucosylceramide (GlcCer) (Figure 1.1.5), which is then either transported directly to other sites within the cell or translocated to the Golgi lumen and further transformed into other GSLs by the sequential addition of monosaccharides by different glycosyltransferases (6). GlcCer is transported to other locations in the cell via FAPP2, a lipid-transfer protein located in the cytoplasm (16). From the Golgi, GSLs are carried by vesicular transport to various cellular locations, including the nucleus and the extracellular leaflet of the plasma membrane, where 70-75% of cellular GSLs reside (17).

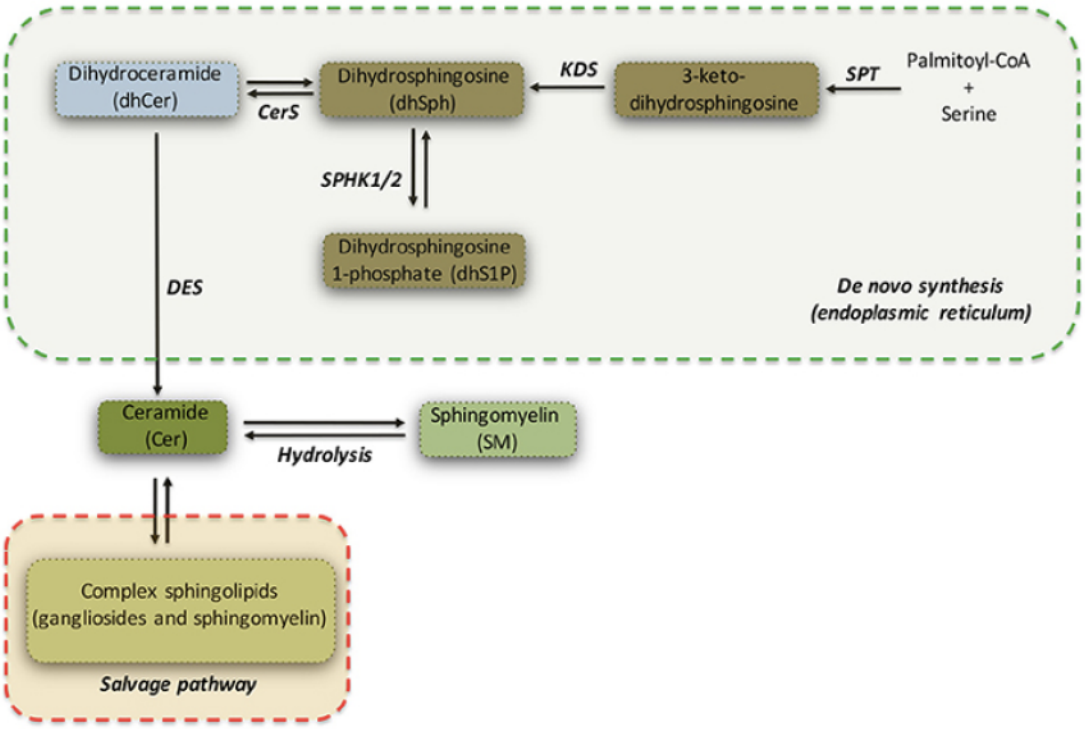

Figure 1.1.4. Simplified pathway of *de novo* biosynthesis of sphingolipids. SPT, serine palmitoyl transferase; KDS, 3-keto-dihydrosphingosine reductase; dhSPH, dihydrosphingosine; CerS, ceramide synthase; DES, ceramide desaturase; dhS1P, dihydrosphingosine-1-phosphate; SPHK1/2, sphingosine kinase 1 and 2; Cer, ceramide. [Image source: Pardo *et al.* (13)].

GSLs are endocytosed from the cell surface and are recycled back to the plasma membrane without any conversion or transformed into more complex forms after retrograde transport to the Golgi apparatus. Alternatively, GSLs are hydrolyzed by specific acid hydrolases in endolysosomes. The resulting monosaccharides, sphingoid bases, fatty acids and sialic acids leave the lysosome, are used within salvage processes or are further degraded (18-20). Failure of degradation of GSLs in the lysosome results in accumulation of different GSL species in the lysosomes, causing lipid storage diseases (21).

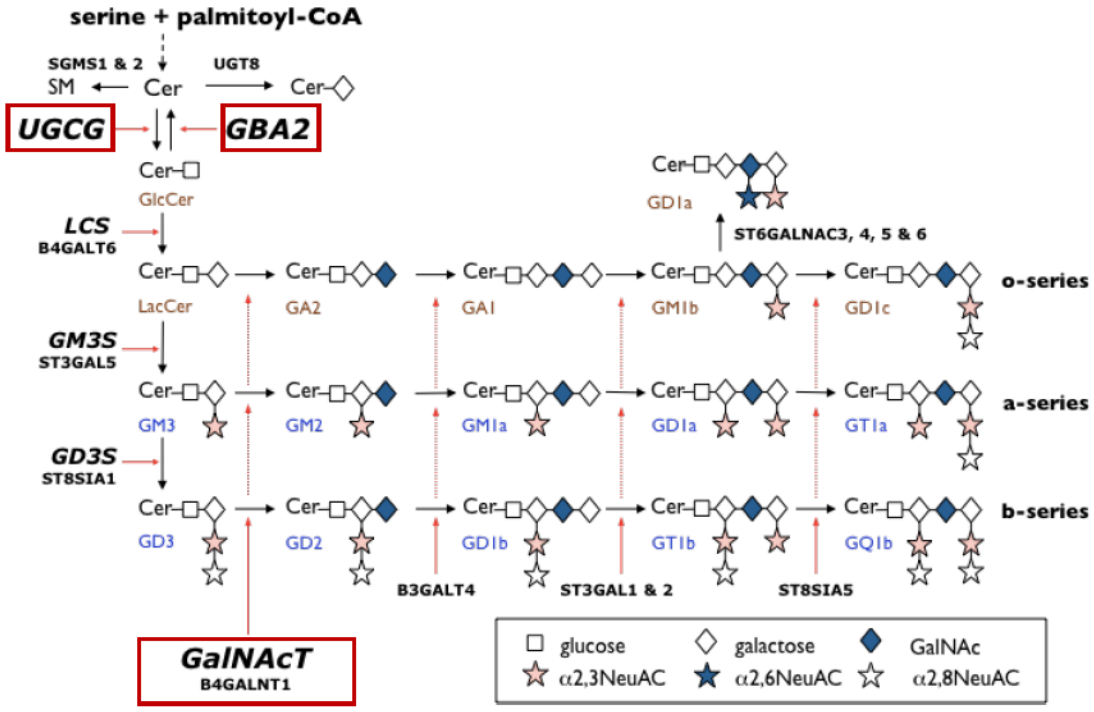

Figure 1.1.5. Glycosphingolipid biosynthetic pathways (ganglio-series). Ceramide, produced in a number of steps from serine and palmitoyl-CoA, is converted into glucosylceramide (GlcCer) by UGCG. B4GALNT1 catalyzes the formation of complex GSLs by the addition of N-acetylgalactosamine to the simpler GSLs (LacCer, GM3 and GD3). Enzymes enclosed in the red boxes are enzymes of interest of this thesis.

1.1.4 Glycosphingolipid Distribution

GSLs are expressed in a cell type-specific fashion. Animal tissues and cultured cells have distinct GSL profiles (qualitative and quantitative), which are strictly regulated. Most cells contain multiple structurally different GSLs. Further, the quantities of various GSLs in a given cell are dissimilar and may span a wide range. The GSL profile of any type of cell or tissue is often characteristic for that cell/tissue type (Figure 1.1.6). In addition, certain GSL species can be characteristically abundant in particular tissues. For example, in rats, GD1a is present in high concentration in spleen, liver, and testis (22), GM3 in intestine, GM2 in bone marrow, GM1 in erythrocytes, and GM4 in

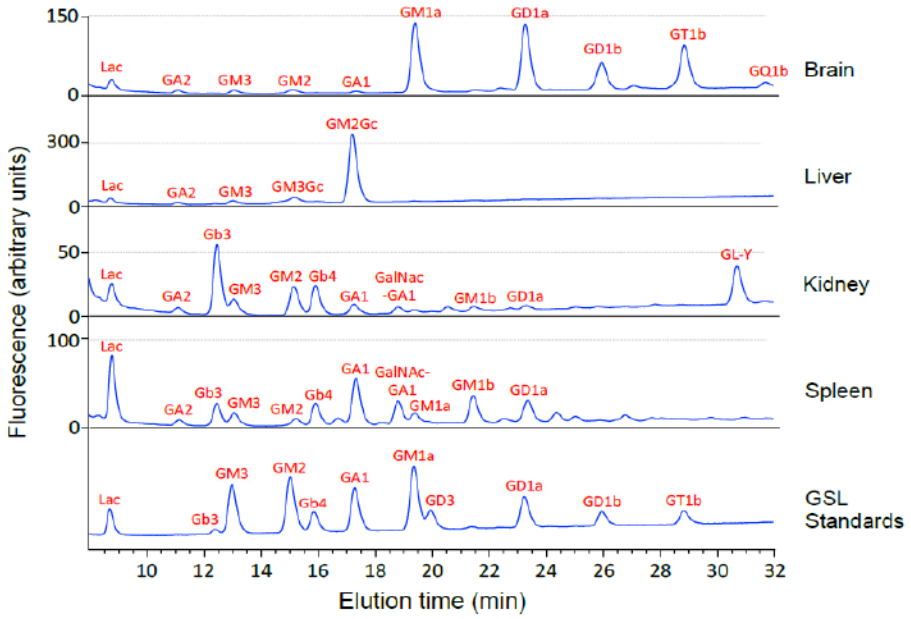

Figure 1.1.6. Glycosphingolipid profiles in mouse tissues. Mouse brain, liver, kidney and spleen contain qualitatively and quantitatively different glycosphingolipid species. (Unpublished results, David Priestman, Department of Pharmacology, University of Oxford, UK.)

kidney (23). Sphingomyelin, sulfatides and GalCer are structural components of myelin sheaths, and are major lipids in oligodendrocytes and Schwann cells in humans (24). Major gangliosides of adult human brain are GM1a, GD1a, GD1b and GT1b, comprising almost 90% of total brain gangliosides, with small amount of other gangliosides like GM2, GT1a and GQ1b, GM2, and GM3 (22,25). In skeletal muscle, membrane vesicles mostly contain neutral GSLs and gangliosides (26,27).

Under pathological conditions, cellular GSL profiles change quantitatively and qualitatively. For example, during apoptosis, GD3 is rapidly synthesized in cis-Golgi and recruited into mitochondria, altering mitochondrial permeability and membrane potential, which leads to the release of apoptotic factors into the cytoplasm (28). Similarly, in malignant hepatomas, mitochondrial GD1b and GD3 reach very high levels (29).

1.1.5 Physiological Roles of Glycosphingolipids

Glycosphingolipids play important roles in cellular interaction and differentiation (30) and are essential for embryonal development (31), postnatal brain development and functioning (32,33). In knockout mice lacking the gene for ceramide glucosyltransferase (UGCG), embryonic development is arrested just past the gastrula stage due to extensive apoptosis, which causes *in utero* death (31). Knockout mice for GM3 synthase (ST3GAL5) exhibit enhanced insulin sensitivity due to an increased phosphorylation of the insulin receptor (34). Complex gangliosides are required for spermatogenesis (35,36). KO mice for the GM2/GD2 synthase (B4GALNT1) show defects in the development, maintenance and repair of nervous tissues and also in the differentiation of spermatocytes (37). Ceramide is the major epidermal lipid in skin and plays an important role in maintaining skin's water permeability. Impaired ceramide levels due to defects in GSL biosynthesis are associated with a number of skin disorders like contact dermatitis, psoriasis, and atopic dermatitis (38-40). Double-KO mice lacking GM2/GD2 and GD3 synthases develop refractory skin injury, indicating the role of GSLs in maintaining skin integrity (41).

Excessive lysosomal GSL accumulation due to the defects in GSL-degrading enzymes results in GSL lysosomal storage diseases (glycosphingolipidoses). The majority of these disorders affect the brain and are neurodegenerative in nature (42-45). Secondary storage of GSLs is associated with a number of storage disorders where GSL catabolism is not the primary defect but the accumulation of the GSLs contributes to the disease progression (46,47). Examples of diseases in which glycosphingolipid levels are dysregulated are Fabry disease (27,48) , Niemann-Pick type C disease (27,49),

autoimmune neuropathies (50-53), polycystic kidney disease (54), hereditary spastic paraplegia (55-60), Alzheimer's disease (61), Parkinson's disease (62,63), GM3 synthase deficiency (64), Tay-Sachs disease (65), Gaucher disease (66-68), Krabbe's disease (69,70).

GSLs are also involved in the immune system. Endogenous GlcCer stimulates invariant natural killer T-cells (iNKT cells) in a CD1d-dependent manner (71,72). Gangliosides, specially GM3(Neu5Ac) poses a strong immune-suppressive effect by reducing CD4 expression in mouse and human T-lymphocytes (8). Further, GSLs are involved in the alteration of signal transduction by influencing receptor proteins on the cell surface. Gangliosides regulate the activity of the epidermal growth factor receptor, platelet-derived growth factor receptor, fibroblast growth factor receptor and neutrotrophin receptor (8,18,73,74). Glycosphingolipids also play important roles in autophagy, ER stress, necroptosis and lysosomal membrane permeabilization (75-78). Clearly, glycosphingolipids are biologically important. Therefore, it is of interest to investigate how glycosphingolipid levels are regulated and how deviation from their natural metabolism affects physiological functions.

1.2 GBA2

1.2.1 Structure and Functions of GBA2

GBA2 is also known as bile acid β-glucosidase or the non-lysosomal glucosylceramidase, which breaks down the membrane lipid glucosylceramide (GlcCer) into glucose and ceramide, and transfers glucose to other lipid substrates (Figure 1.1.5) (79). GBA2 is tightly associated with cellular membranes, mainly resides at the plasma membrane and/or endoplasmic reticulum (79). The activity of GBA2 is dependent on its

membrane association (80). Another glucosylceramidase, glucocerebrosidase (GBA, acid β-glucosidase) degrades glucosylceramide in lysosomes (81). GBA belongs to glycohydrolase family GH30. The tissue-specific expressions and subcellular localizations of the isozymes GBA and GBA2 are distinct and unrelated to each other, and they do not compensate for each other in any pathological conditions (82). A third, cytosolic, β-glucosidase (GBA3, klotho-related protein) can also degrade glucosylceramide, the physiological role of which is not clear (83,84).

Human GBA2 contains 927 amino acids,104.6 kDa. The GBA2 cDNA isolated from liver contains 3696 base pairs (85). TxGH116, a β-glucosidase from the bacterium *Thermoanaerobacterium xylanolyticum*, shares 37% sequence identity with human GBA2. Its three-dimensional structure reveals that all the sugar-binding residues are conserved between human GBA2 and TxGH116, providing valuable information regarding the active site residues of human GBA2 (Glu527 and Asp677) (86).

1.2.2 Cellular Expression of GBA2

In humans, GBA2 is expressed at the highest level in brain, heart, skeletal muscle, and kidney (80,85). In mice, GBA2 is mainly expressed in testis and brain, and in the Purkinje cells (87). Thalamus, subthalamic nucleus, substantia nigra, and caudate nucleus are GBA2-rich regions of human brain (88).

1.2.3 GBA2 in Health and Diseases

GBA2 is important for post-meiotic development of male germ cells in mouse (89). *GBA2* knockout mice accumulate GlcCer in the testes, resulting in impaired male fertility. The spermatozoa of these knockout mice have defective shapes, including abnormal acrosomes and large round heads, and are poorly motile. Bile acid and

cholesterol metabolism is normal in these mice. GBA2 knockout mice also show accumulated glucosylceramide in the brain and liver, but do not exhibit organomegaly, or a reduced lifespan (82). Pharmacological inhibition of GBA2 also causes infertility in male mice, which is reversible (90,91). However, the reproductive effects of inhibiting GBA2 are contingent on a particular genetic background (90).

Recently, mutations in *GBA2* have been reported to be associated with abnormal neurological features and impaired locomotion in humans (92). In contrast, the mouse homolog Gba2 has not been reported to be obvious for neurological or neuronal development. A recent study has reported mild gait disturbances in some, but not all *Gba2* knock-out mice (80). Otherwise, *Gba2* gene-disrupted mice have never been described with neurological or neurodegenerative symptoms.

1.2.4 GBA2 Pharmacology

β-glucosidases are inhibited by conduritol B epoxide (CBE) and alkylated imino sugars, but their sensitivity to inhibition by these compounds are different. GBA2 is less sensitive to inhibition by CBE because of the poor binding affinity of CBE to GBA2 (93). The alkylated imino sugar *N*-butyldeoxygalactonojirimycin (*N*B-DGJ) exclusively inhibits GBA2 which makes it a suitable candidate for distinguishing GBA2 from GBA (93). GBA, GBA2 and UGCG are inhibited by *N*-butyldeoxynojirimycin (*N*B-DNJ, miglustat), but GBA2 is much more sensitive to this compound, so that low-dose miglustat administration elevates GlcCer levels in mouse brain and testis (Figure 1.1.6). Miglustat is approved in over 40 countries for clinical use in type 1 Gaucher disease and Niemann–Pick type C disease (94,95). Gaucher disease is associated with mutations in *GBA*, leading to accumulation of glycolipids in macrophages. Gaucher patients treated

with miglustat show improvements in organomegaly and hematological manifestations (96), without developing neurological symptoms (97). Similarly, disruption of the *GBA2* gene in a Gaucher mouse model reduces disease severity (98). Niemann-Pick type C disease is a lysosomal glycosphingolipid storage disorder with a neurodegenerative course. Miglustat reduces the disease burden in mouse models of NPC by suppressing the central nervous system inflammation and decelerating the loss of motor control and muscle strength (87). At much higher doses miglustat inhibits glucosylceramide synthase (UGCG) along with GBA2 (89,99), but it is not clear to what extent this happens in miglustat-treated patients (93).

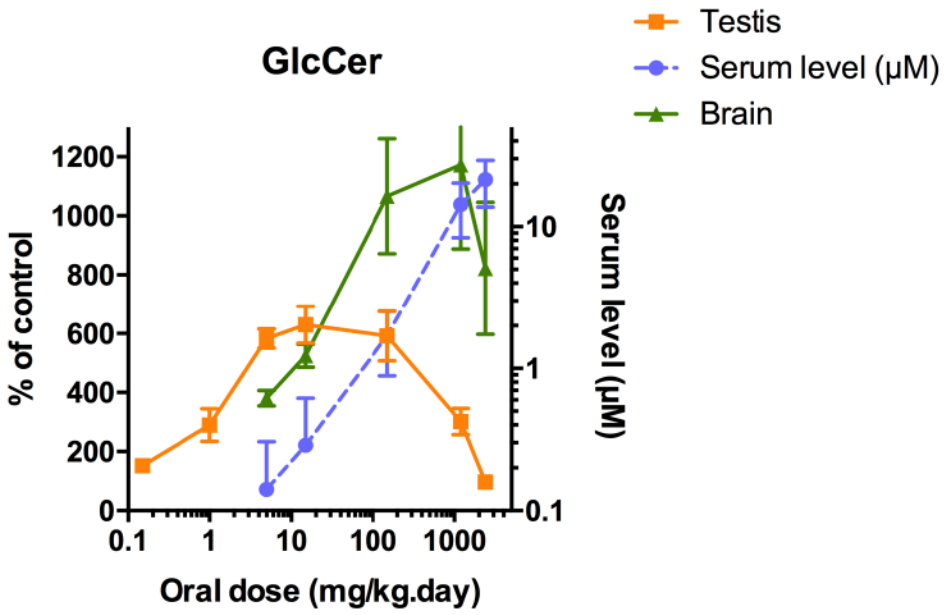

Figure 1.1.6. Pharmacological inhibition of GBA2 by miglustat (*N*-butyl-deoxynojirimycin) in mouse testis and brain. This figure indicates the concentrations of miglustat in the serum of mouse orally treated with different doses of miglustat. Brain and testis GlcCer level increases with increasing serum level of miglustat; the maximum serum levels of miglustat required to achieve the highest levels of GlcCer are different in brain and testis. [Image source Walden *et al.* (89)].

1.2.5 GBA2 Binding Partners

High-throughput interactome studies have identified a number of proteins as binding partners of GBA2 (Table 1). One of the GBA2-interactors is GBA2 itself, indicating that GBA2 is a self-interacting protein. Other than GBA2, four plasma membrane proteins have been reported to form protein complexes with GBA2. This is expected as GBA2 is present at the plasma membrane or in the ER. Interestingly, GBA2 also interacts with a number of mitochondrial proteins (100,101). Six out of 14 candidate interactors of GBA2 are located in the mitochondria, five at the inner mitochondrial membrane or matrix, and one at the outer mitochondrial membrane (Table 1).

Table 1. GBA2-Interacting Proteins Identified in High-Throughput Studies.

Protein ID	***Protein name***	***Cellular location***	***References***
GBA2	β-glucosidase 2	Plasma membrane	(100)
AFG3L2*	Paraplegin-like protein	Inner mitochondrial membrane	(100)
BAG5*	BAG family molecular chaperone regulator 5	Cytoplasm, mitochondria	(100)
ILVBL	Acetolactate synthase-like protein	Plasma membrane	(100,101)
LAMTOR5	Ragulator complex protein LAMTOR5	Cytoplasm, lysosome	(100)
MRPL44*	Mitochondrial large ribosomal subunit protein mL44	Mitochondrial matrix	(100)
MRPS22 *	Mitochondrial large ribosomal subunit protein mS22	Mitochondrial matrix	(100)
MTNR1A	Melatonin receptor type 1A	Plasma membrane	(102)
PPFIA1	Liprin-alpha-1	Plasma membrane	(100)
RDH13 *	Retinol dehydrogenase 13	Cytoplasm, inner mitochondrial Membrane	(101)
SKAP2	Src kinase-associated phosphoprotein 2	Cytoplasm	(101)
SRP68	Signal recognition particle subunit SRP68	Cytoplasm	(100)
TMEM216	Transmembrane protein 216	Plasma membrane	(101)
TUBB8	Tubulin beta-8 chain	Microtubules	(101)
VPS13C *	Vacuolar protein sorting-associated protein 13C	Cytoplasm, mitochondria	(101)
Six out of 14 proteins have a mitochondrial association (marked by *).			

1.3 Human Voluntary Movements

1.3.1 Neurons

Neurons are the structural and functional units of the nervous system. They conduct impulses that enable the body to interact with its internal and external environments. There are various types of neurons, including sensory, motor, and interneurons. Sensory neurons carry impulses form inside and outside of the body to the brain and spinal cord (central nervous system).

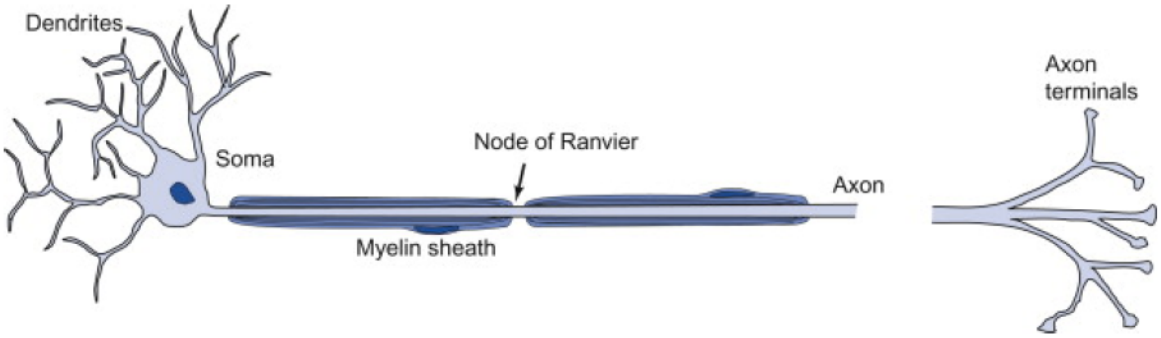

Figure 1.3.1. Schematic of a motor neuron. [Image source: (103)].

Motor neurons (Figure 1.3.1.) are located in the spinal cord and carry signals away from the CNS. Interneurons are present within the CNS, in between brain and spinal cord. They transmit nerve impulses from the sensory neurons to the motor neurons (104). In movement disorders like spinal muscular atrophy (SMA), amyotrophic lateral sclerosis (ALS), primary lateral sclerosis (PLS), and hereditary spastic paraplegia (HSP), motor neurons become damaged or degenerated, resulting in lack of proper signal transmission from brain to the muscle (103-106).

1.3.2 The Tracts of Spinal Cord

Human voluntary movement requires proper communication between the brain and the voluntary muscles. Signals for voluntary movements are transmitted through the spinal cord and the peripheral nerves in a two-way direction in between the brain and muscles, involving two different tracts – the spinocerebellar tract, and the corticospinal tract (107).

The corticospinal tract is the descending pathway that transmits signals from the brain to muscles. It is a motor tract that transmits signals from the cerebral motor cortex to the neuromuscular junctions on striated muscles. These connections enable muscle contraction. Corticospinal tract is composed of the upper and lower motor neurons. On the other hand, the spinocerebellar tract is the ascending tract carrying signals from muscles to the brain. This is a sensory tract that carries proprioceptive signals from skeletal muscles and tendons to the cerebellum. These signals are essential for the control of posture and coordination of movement (108). Both pathways are multi-synaptic pathways and contain neurons having very long axons. In fact, the distance covered by the lower motor neurons present in these tracts are sometimes as long as one meter. In spite of their lengths, these neurons have been evolved in such a way that they can relay action potentials very rapidly for proper voluntary movements (107,109). At the same time, because of their length, axons are very susceptible to degeneration or injury or dysfunction. Both of these tracts are affected in a number of genetic conditions which ultimately leads to movement disorders.

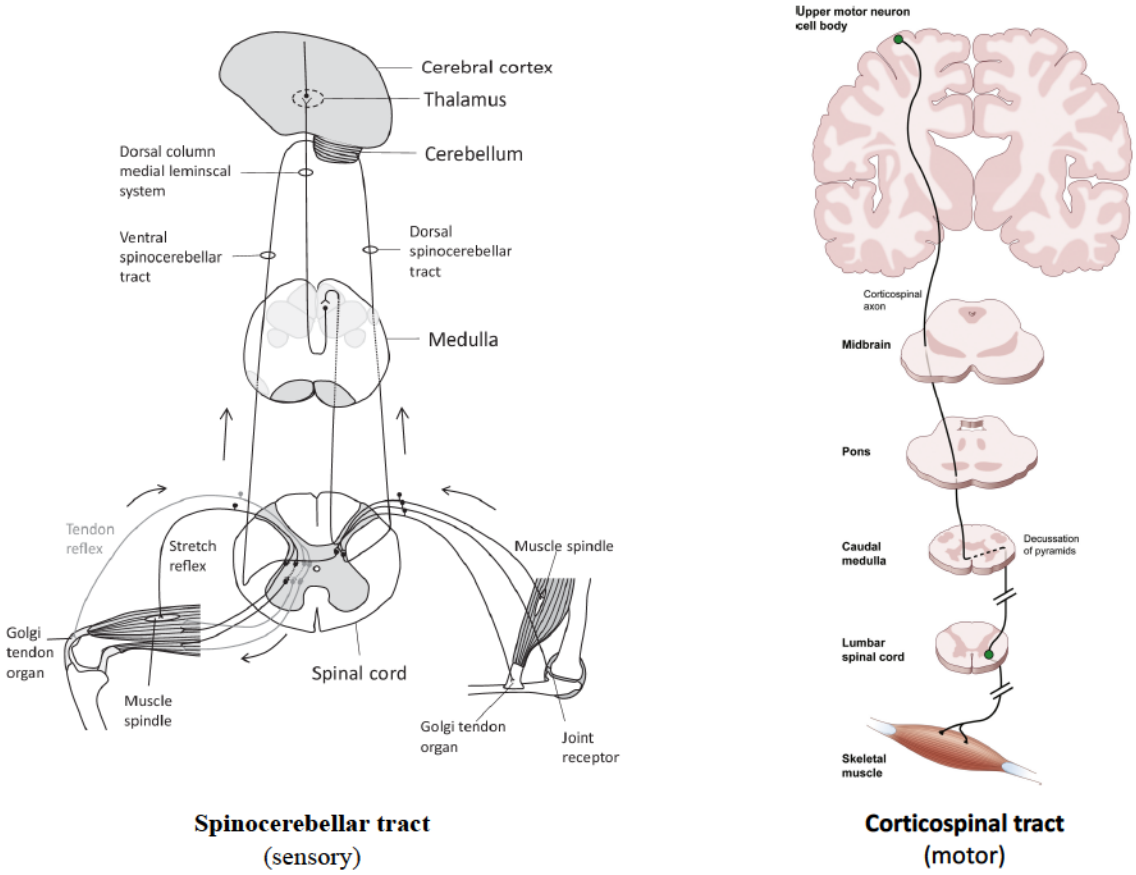

Figure 1.3.2. Spinocerebellar tract and corticospinal tract. [Image source: Blackstone C. (110)].

1.4 Hereditary Spastic Paraplegias

1.4.1 Clinical Features

Hereditary spastic paraplegias (HSP) are a group of clinically and genetically diverse, rare genetic disorders characterized by severe lower extremity weakness and spasticity. In HSP, the corticospinal tract (the motor tract) (Figure 1.3.2) is affected. Patients suffer from muscle cramps and difficulty with balance. The condition is progressive in nature; affected individuals may become severely handicapped with time and may require assistive devices [106]. HSP is associated with degeneration of upper

motor neurons, so that nerve impulses cannot be properly transmitted to lower motor neurons and corresponding muscles, leading to impaired muscle tone, muscle weakness and stiffness or spasticity of muscles. The condition is also known as familial spastic paraplegia or paraparesis (FSP) (111,112).

1.4.2 Classification

There are two different classes of HSP - pure and complex. In pure HSP, neurological impairment is limited to the lower body. In complex HSP, other systems of the body are involved and there may be other neurological symptoms, like as seizures, dementia, amyotrophy, ataxia, mental retardation, vision loss, problem with hearing, extrapyramidal disturbance, or peripheral neuropathy (113). Genetic inheritance of HSP can be autosomal dominant, autosomal recessive, and X-linked (112). More than 80 genetic types of HSP have been identified so far (114). Despite vast clinical and genetic heterogeneity of HSP, the genes affected in this condition can be grouped to number of classes based on the cellular processes regulated by the affected genes. The major cellular or physiological functions related to the affected genes in spastic paraplegia are myelination, integrity of endoplasmic reticulum, endosomal dynamics, microtubule-based transport, mitochondrial function, and lipid synthesis and metabolism (110,115). This thesis addresses some aspects related to lipid metabolism and associated cellular pathways in a group of spastic paraplegias and cerebellar ataxias known as SPG46.

1.4.3 Treatment/Management Options

To date, no effective treatment is available to prevent, retard or reverse the disease progression in HSP. Current treatment options are mostly focused on symptomatic relief and to support physical and emotional well-being of patients (112). Drugs, physical

therapies, exercises and assistive devices are used to manage the symptoms and ease the disease burden of affected individuals. Drugs are mostly administered to HSP patients for three purposes –

(i) Reduction of spasticity (muscle relaxants, like baclofen, tizanidine, clonazepam, diazepam, etc.) (112) .

(ii) Help with bladder problems, reducing bladder contraction or bladder spasm (tolterodine tartrate or hyoscyamine (112) .

(iii) To combat the depression or mental retardation (serotonin reuptake inhibitors, tricyclic anti-depressants, etc. (112).

1.5 SPG46

1.5.1 Clinical Presentations

Spastic Gait locus #46 (SPG46, OMIM #614409) falls within the spectrum of spastic paraplegia and cerebellar ataxia. In cerebellar ataxias, the spinocerebellar tract (the sensory tract) (Figure 1.3.2) is affected, resulting in ataxic conditions. Clinical presentations of SPG46 include cerebellar ataxia, spastic quadri/paraplegia, cerebellar & cerebral atrophy, thin corpus callosum, smaller brain size, cognitive impairment (very severe-mild), axonal sensorimotor (poly)neuropathy. The usual age of onset of SPG46 is 1-20 years and the median age is 7 (116).

1.5.2 GBA2 Mutations in SPG46

SPG46 is associated with mutations in *GBA2* (Table 2).

Table 2. *GBA2* Mutations in SPG46 (Cerebellar Ataxia/Spastic Paraplegia and Marinesco-Sjögren-Like Syndrome).

#	*nt #*	*WT nt*	*Mutant nt*	*aa #*	*WT aa*	*Mutant aa*	*Ref.*	*Presentation*
1	363	C	A	121	Tyr	STOP	(55)	Cerebellar ataxia
2	451+2	T	C	Donor splice site second exon-intron junction			(117)	
3	452-1	G	C	Splice acceptor site exon 3			(118)	SPG46
4	518	G	A	173	Trp	STOP	(56)	SPG46
5	700	C	T	234	Arg	STOP	(56)	SPG46
6	1018	C	T	340	Arg	STOP	(55)	Cerebellar ataxia
7	1255	T	G	419	Phe	Val	(83)	
8	1471-1474	GGCA	GGCAGGCA	492	Thr	Argfs*9	(56)	SPG46
9	1528-1529	AT	Deleted	510	Met	Valfs*17	(119)	Marinesco-Sjogren-like syndrome
10	1780	G	C	594	Asp	His	(59)	Spastic ataxia
11	1789	G	Deleted	597	Asp		(120)	
12	1888	C	T	630	Arg	Trp	(56)	SPG46
13	2048	G	C	683	Gly	Arg	(116)	SPG46
14	2054 + 62	G	A	(intron 13)			(59)	
15	2201	G	A	734	Arg	His	(59)	
16	2608	C	T	870	Arg	STOP	(83)	
17	2617	C	T	873	Arg	Cys	(121)	
18	2618	G	A	873	Arg	His	(122)	Cerebellar ataxia

1.6 Marinesco- Sjögren-Like Syndrome

1.6.1 Clinical Presentations

Marinesco- Sjögren-like syndrome (MSS, MIM 248800) is a movement disorder, distinct from SPG46. It shares some common features with SPG46, like autosomal recessive inheritance, childhood onset, difficulty in movement coordination (cerebellar ataxia), progressive muscle weakness (myopathy), and mild to moderate intellectual disability (119,123-125). Individuals affected by Marinesco- Sjögren-like syndrome may have some additional features, like cataract, strabismus (eyes do not align with each other when looking at an object), nystagmus (involuntary eye movements), short stature, and skeletal abnormalities (119,124). Affected individuals may also suffer from hypergonadotropic hypogonadism, resulting in impaired production of the gonadotropins, follicle-stimulating hormone (FSH) and luteinizing hormone (LH), leading to delayed or absent puberty (124). Patients may become severely handicapped with age, but normally MSS does not shorten patient's lifespan (119).

1.6.2 Genetics

Previously, mutations in *SIL1* were the only genetic causes of Marinesco-Sjögren-like syndrome. The protein SIL1 is located in endoplasmic reticulum and assists in the folding of newly synthesized proteins in the ER and in the refolding of damaged proteins (126,127). Recently, a mutation in *GBA2* has been associated with Marinesco-Sjögren-like syndrome (119) (Table 2).

1.7 Mitochondria

1.7.1 Structure and Function of Mitochondria

Mitochondria are double-membraned, small organelles found in the cytoplasm of most eukaryotic organisms. They are unique organelles of the cell containing their own genome and ribosomes (128). Mitochondrial divisions are independent, not coupled to the division of the cell they belong to. Mitochondria are known as the 'power-houses' of cells as they produce ATP (adenosine triphosphate), the energy unit of cells for all metabolic activities, by oxidative phosphorylation (128). The number of mitochondria in cells is subject to the type, size and functional state of the cell, in other words, to the energy requirement of the cell. Cells with high energy requirements are usually rich in mitochondria, like muscles, and neurons (128,129). Mitochondria are also involved in other cellular processes like maintenance of calcium homeostasis, apoptosis, controlling cell cycle and cell growth (129) (Figure 1.7.1.1).

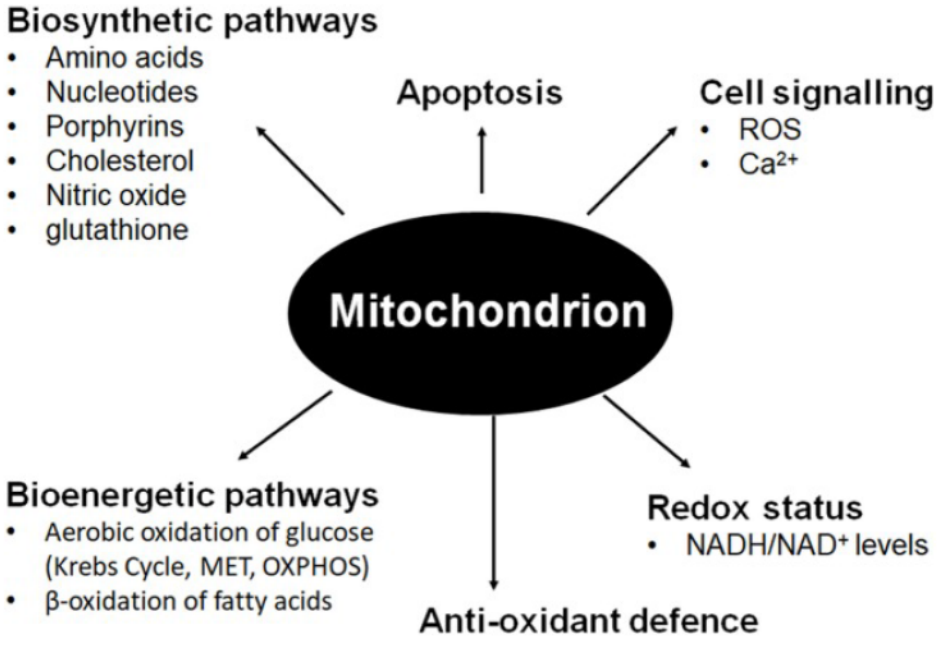

Figure 1.7.1.1. Important functions of mitochondria. [Figure source: (129)].

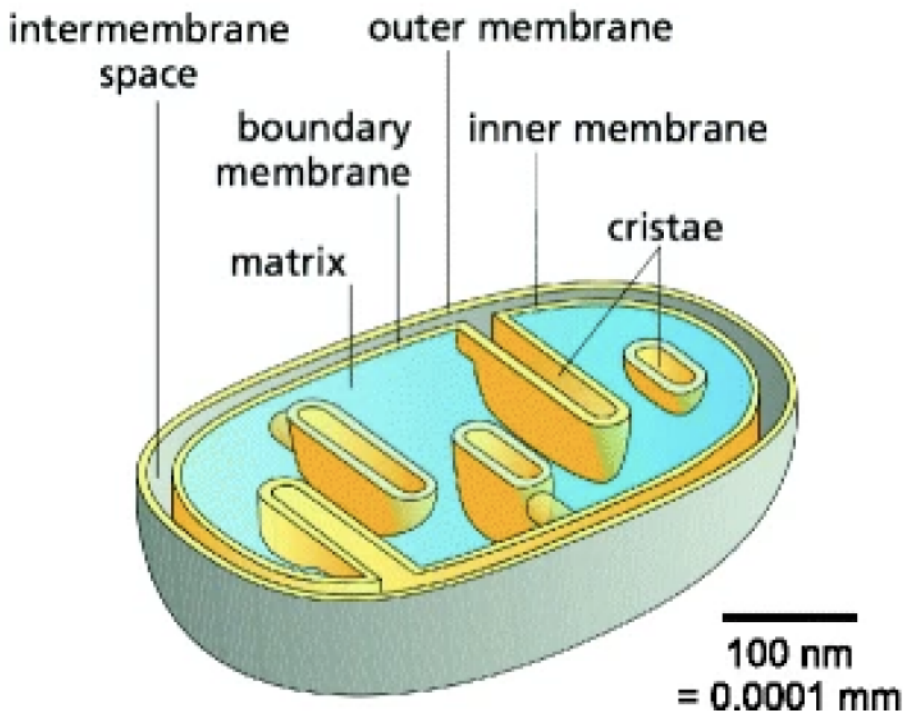

Figure 1.7.1.2. Schematic of a mitochondrion indicating the membranes and various mitochondrial sub-compartments. [Figure source: (130)].

The structure of a mitochondrion comprises of three major parts - the outer membrane, the inner membrane, and a gel-like material called the matrix (Figure 1.7.1.2). The outer and inner membranes are made of proteins and phospholipid bi-layers and are separated by the intermembrane space (130). The outer membrane encloses the entire mitochondrion and contains a large number of integral proteins known as porins. Porins facilitate diffusion of ions, nutrient molecules, energy molecules like the ADP and ATP from one side of the membrane to the other side (130) .

The intermembrane space, also known as perimitochondrial space, is the space between the inner and outer mitochondrial membrane. The inner membrane is highly folded (Figure 1.7.1.2) and enriched in phospholipids and cardiolipins. The permeability

of this membrane is restricted to oxygen, water, and carbon dioxide. It contains proteins involved in oxidative phosphorylation, ATP synthesis and electron transport (131). This membrane also contains proteins for mitochondrial fusion and fission process, and redox reactions. The inner membrane maintains an electrochemical gradient to carry out oxidative phosphorylation and electron transport (131). The folds in the inner mitochondrial membrane are known as cristae. These folds increase the surface area of the membrane, increasing the ability of mitochondria for ATP synthesis. Mitochondrial matrix is a dense, homogenous, viscous fluid enclosed by inner mitochondrial membrane. It contains mitochondrial DNA, ribosomes, transfer RNA, mitochondrial DNA, nucleotide cofactors, organic molecules, inorganic ions, etc. This is the enzyme-rich compartment of mitochondria containing enzymes of oxidation of pyruvates and fatty acids (beta oxidation), citric acid cycle, and synthesis of nucleic acids and proteins (132).

1.7.2 Protein Import into Mitochondria

More than one thousand proteins are involved in the maintenance of mitochondrial structure and functions (133). A very small fraction of mitochondrial proteins (13 in humans) is encoded by mitochondrial DNA. More than 99% of mitochondrial proteins are encoded by nuclear DNA, synthesized in the cytoplasm, and then imported into the mitochondria (134). Mitochondrial proteins can be located at the mitochondrial membranes or are transported into the intermembrane space or the matrix. The outer membrane and the inner membrane contain protein translocase complexes that recognize, sort, and transport mitochondrial proteins. Nuclear-encoded mitochondrial proteins are synthesized in the cytoplasm as preproteins containing a mitochondrial targeting sequence (MTS) (135), which is usually a positively charged N-terminal

amphipathic α-helix containing 15-70 amino acid residues (136). The translocases at the outer membrane of the mitochondria (TOM) recognize MTSs and aid preproteins to pass across the membrane to the intermembrane space. Preproteins with MTSs are further recognized by the translocases of mitochondrial inner membrane (TIM) and transported into the mitochondrial matrix (136). The MTS is then cleaved off, converting the preprotein to its functional form. Different kinds of chaperones present in the cytoplasm and in the mitochondrial matrix are associated with the transport process of proteins across mitochondrial membranes (135,137) (Figure 1.7.2).

1.7.3 Mitochondrial Dynamics

Mitochondria are dynamic organelles that undergo continuous fusion and fission to maintain their morphology, function, content, and cellular distribution (138). Fusion is important for exchange of materials among mitochondria and fission promotes replication during cell division. Mitochondrial fission and fusion are mediated by a group of guanosine-triphosphatases (GTPases) of the dynamin protein family (139). Key proteins involved in mitochondrial dynamics are dynamin-like/related protein 1 (DLP1/Drp1), mitofusin 1 (MFN1), mitofusin 2 (MFN2), and optic atrophy 1 (OPA1) (Figure 1.7.3) (139). DRP1 mediates mitochondrial fission, it is present in the cytoplasm and is recruited to mitochondria prior to fission, forming spirals around mitochondria that constrict to cut both outer and inner membranes (140). Endoplasmic reticulum (ER) is suggested to play an important role during the early stages of mitochondrial fission mediated by DRP1. Inverted formin 2 (INF2), an ER-bound protein, is recruited to mitochondria and promotes the recruitment of DRP1 to the fission-site of mitochondria (141). Studies have shown that mitochondrial constriction at the site of fission starts

immediately after recruitment of INF2, even before the activation of DRP1 (142). MFN1 and MFN2 are membrane-anchored fusion proteins located at the mitochondrial outer membrane and promote the fusion of outer mitochondrial membranes. Fusion between mitochondrial inner membranes is mediated by OPA1 in mammals. Mitochondrial fission and fusion proteins are regulated by proteolysis and posttranslational modifications (139,143).

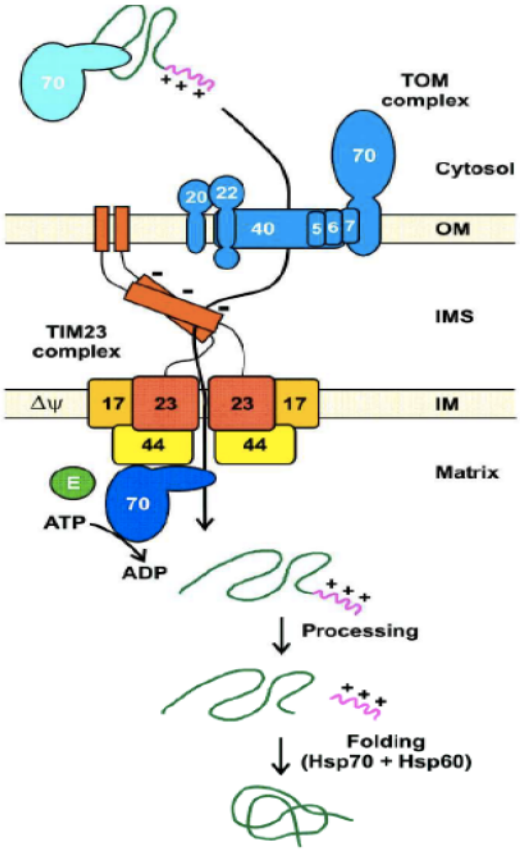

Figure 1.7.2. Mitochondrial protein import pathway for mitochondrial matrix-targeted proteins. Preproteins, synthesized in the cytosol, contain N-Terminal target sequences (purple) and bind to the cytosolic chaperone Hsp70. The signal sequence is recognized by Tom20/Tom22 located in the outer membrane; the protein-chaperone complex is transferred to the inner membrane containing the TIM23 translocase, transported into the mitochondrial matrix. In the matrix, the preprotein binds with the chaperones Hsp70 and Hsp60, the presequence is cleaved off and the protein folds into its final conformation. IM, inner membrane; IMS, intermembrane space; OM, outer membrane; HSP, heat shock protein. [Figure source: (137)].

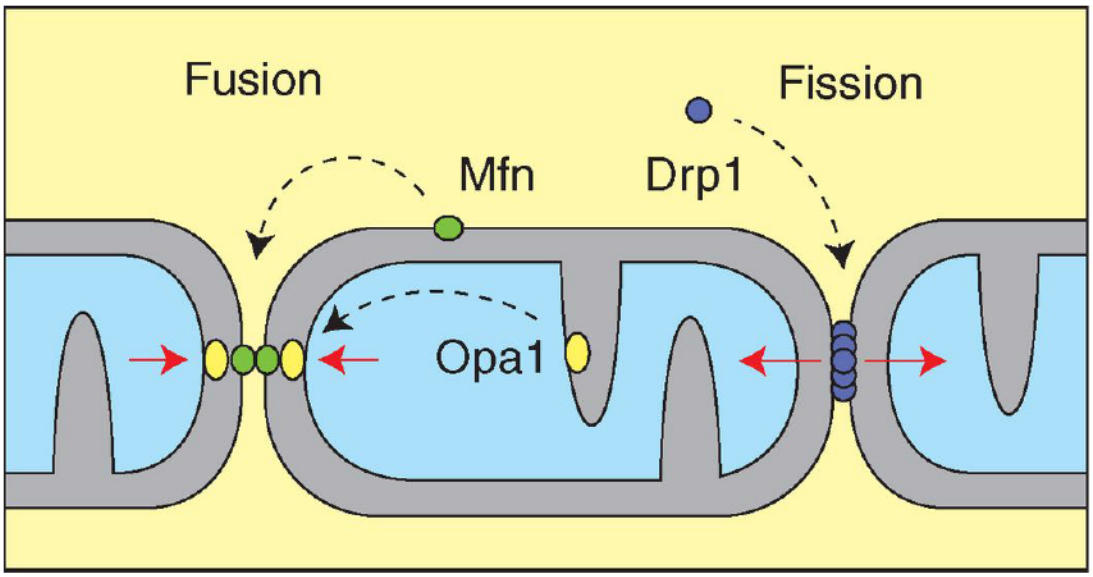

Figure 1.7.3. Proteins involved in mitochondrial fusion and fission. Mitofusions (Mfn) participate in the fusion of mitochondrial outer membranes. OPA1 regulates mitochondrial inner membrane fusion. Drp1 is distributed between the cytosol and the outer mitochondrial membrane and promotes mitochondrial fission. [Figure source: (144)].

1.8 OPA1

OPA1 (optic atrophy protein 1), is a nuclear-encoded mitochondrial protein localized in the mitochondrial inner membrane. It is a dynamin-like GTPase essential for maintenance of mitochondrial morphology and bioenergetics. In terms of maintaining mitochondrial morphology, OPA1 performs two important roles – maintenance of cristae structure and promoting inner membrane fusion (145).

Alternative splicing of *OPA1* transcripts produces eight mRNAs, producing eight different precursor forms, which are expressed in variable amounts in different tissues and undergo proteolytic cleavages, resulting in multiple variants (146). All OPA1 precursor proteins contain an N-terminal mitochondrial targeting sequence (MTS), followed by a transmembrane domain (TM). After being synthesized in the cytoplasm, its MTS assists OPA1 to be imported into the mitochondria, and its transmembrane domain

helps OPA1 to be anchored in the inner mitochondrial membrane, MTS is cleaved off and the main part of OPA1 projects into the intermembrane space (146). These are the membrane-bound long isoforms of OPA1 (L-OPA1) which are subjected to further proteolytic cleavage at either of two cleavage sites, S1 and S2, resulting in non-membrane-bound soluble forms of OPA1 (S-OPA1) (Figure 1.8) (145-147). In normal cells, long and short isoforms of OPA1 are present in almost equimolar concentrations. Long isoforms are diminished in certain conditions, like loss of membrane potential across the inner mitochondrial membrane, or in presence of apoptotic stimuli (148).

Different metallopeptidases present in the mitochondrial inner membrane are involved in the processing of OPA1 at the S1 and S2 sites. YME1L1 cleaves OPA1 at S2 and m-AAA cleaves OPA1 at the S1. AFG3L2 and paraplegin are subunits of the m-AAA protease complex (148,149). Interestingly, these subunits of m-AAA protease have been reported to be involved in neurodegenerative disorders. Mutations in *AFG3L2* are responsible for a dominant form of spinocerebellar ataxia, SCA28 (150). Mutations in *SPG7* (encodes paraplegin) causes a recessive form of hereditary spastic paraplegia (151). OPA1 undergoes accelerated cleavage by OMA1 at S1 cleavage site in case of absence or inactivity of m-AAA protease (152). Cellular stress conditions, like loss of mitochondrial membrane potential, DNA, or decreased level of ATP, reduce the activity of the m-AAA protease and induce phosphorylation/activation of OMA1. Activation of OMA1 ultimately leads to loss of membrane-anchored long isoforms of OPA1 (149,153).

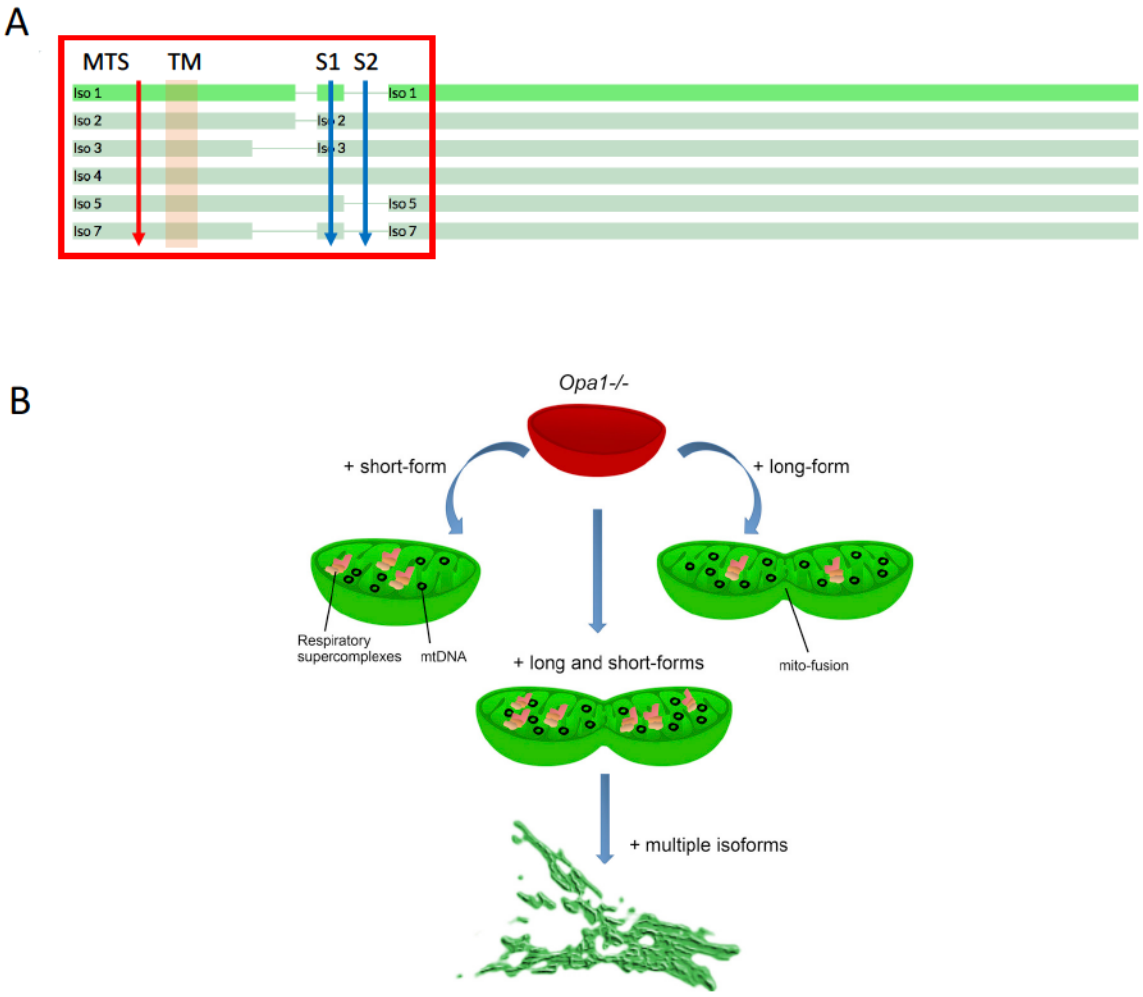

Figure 1.8. OPA1 isoforms. (A) Seven splicing isoforms of OPA1. The area within the red box contains the mitochondrial targeting sequence (MTS), the transmembrane domain (TM) and cleavage sites S1 and S2. Proteolytic cleavages at S1 and S2 generate different short, soluble isoforms of OPA1. (B) Functions of long and short forms of OPA1. [Figure A adapted from NextProt; B was obtained from Dotto, *et al*. (154)]

Chapter 2: Rationale and Objective

The cellular GSL profile is the resultant of a balance between biosynthesis, intracellular transport and endolysosomal degradation (12). The cellular "GSL profile" needs to be described in qualitative as well as quantitative terms (which GSL species are present, and at what level). GSL homeostasis is biologically relevant, because deficiencies in both GSL biosynthesis and degradation have pathological consequences, including neurological and non-neurological disorders (27,42,155). However, in spite of the importance of GSL homeostasis, we have a very limited understanding of how cells regulate GSL levels. I have addressed this gap in understanding in the first part of my PhD research, testing a simple model of the kinetics of GSL biosynthesis and degradation. I have targeted selective enzymes in the GSL biosynthetic pathways and manipulated the levels of expressions or activities of those enzymes in cellular models by using genetic or pharmacological approaches. The objective was to measure the changes in the levels of various GSL species upon genetic or pharmacological interventions in cells and determine the rates of biosynthesis and degradations of those GSL species.

Deficiencies in GSL-metabolizing enzymes associated with human genetic diseases are largely restricted to the catabolic pathway, more specifically to the endo-lysosomal pathway (42,155). For example, Gaucher disease is associated with mutations in GBA, Sandhoff disease is associated with mutations in beta-hexosaminidase, Fabry disease is associated with deficiency in alpha-galactosidase (21). Recently, however, mutations have been found in other branches of the GSL metabolic network. In patients with similar neurological conditions (lower limb spasticity and paraplegia with cerebellar dysfunction), genetic defects have been identified in a GSL-biosynthetic enzyme, β-(1,

4)-N-acetyl-galactosaminyl transferase 1 (B4GALNT1) (57,60) and in an atypical – non-lysosomal – degradative enzyme, β-glucosidase-2 (GBA2) (55,56,59,116), which cleaves glucosylceramide. The effect of cellular GSL profiles in these disorders has been largely unexplored, nor have the cellular and biochemical consequences of the mutations in *B4GALNT1* and *GBA2* been studied. In the second part of my thesis, I investigated the cellular and biochemical consequences of *GBA2* mutations and uncovered some structural and functional features of GBA2 that have not been described before, the most notable of which was involvement of GBA2 in mitochondrial dynamics and bioenergetics. So, my PhD research evolved from studying GSL homeostasis to exploring the mitochondrial involvement of GBA2.

Chapter 3: Regulation of Glycosphingolipid Homeostasis

3.1 Modelling Glycosphingolipid Homeostasis

GSL biosynthesis is thought to have zero-order kinetics, while GSL degradation may have first-order kinetics (156-158). In a zero-order kinetic reaction, the rate of synthesis of a product is constant, independent of the concentration of the substrate (s). On the other hand, a first-order reaction is linearly dependent on the concentration of one reactant (159). Previous studies thus suggest that cells synthesize GSLs at a constant rate that is not dependent on the level of GSLs present in the cell at any time but degrade GSLs at variable rates depending on the total amount of GSLs present in the cell at that time. The overall assumption can be mathematically represented in the following way:

$$\mathbf{GSL_{(t+1)} = GSL_{(t=0)} + (GSL_{(t)} + S) - ((GSL_{(t)} + S) * D)} \qquad \textbf{(i)}$$

where **S** is the amount of GSL that is newly synthesized per unit of time (molecules/cell), and **D** is the fraction of the total amount of GSL that is degraded per unit of time (with $0 < D < 1$, in $time^{-1}$). Over time, the level of a particular GSL, modeled according to equation (i), will reach a steady state level **($GSL_{(SS)}$)** expressed by equation (ii):

$$\mathbf{GSL_{(SS)} = GSL_{(t=0)} + S/D - S} \qquad \textbf{(ii)}$$

After an increase in **S** and/or a decrease of **D**, GSL levels will rise and reach a higher steady-state level, which can be described by a one-phase exponential association function:

$$\mathbf{GSL_{(t)} = GSL_{(t=0)} + (GSL_{(SS)} - GSL_{(t=0)}) * (1 - e^{-D*t})} \qquad \textbf{(iii)}$$

Conversely, a decrease in **S** and/or an increase of **D** will result in a decrease of overall GSL levels, fitting a one-phase exponential decay function (Figure 3.1).

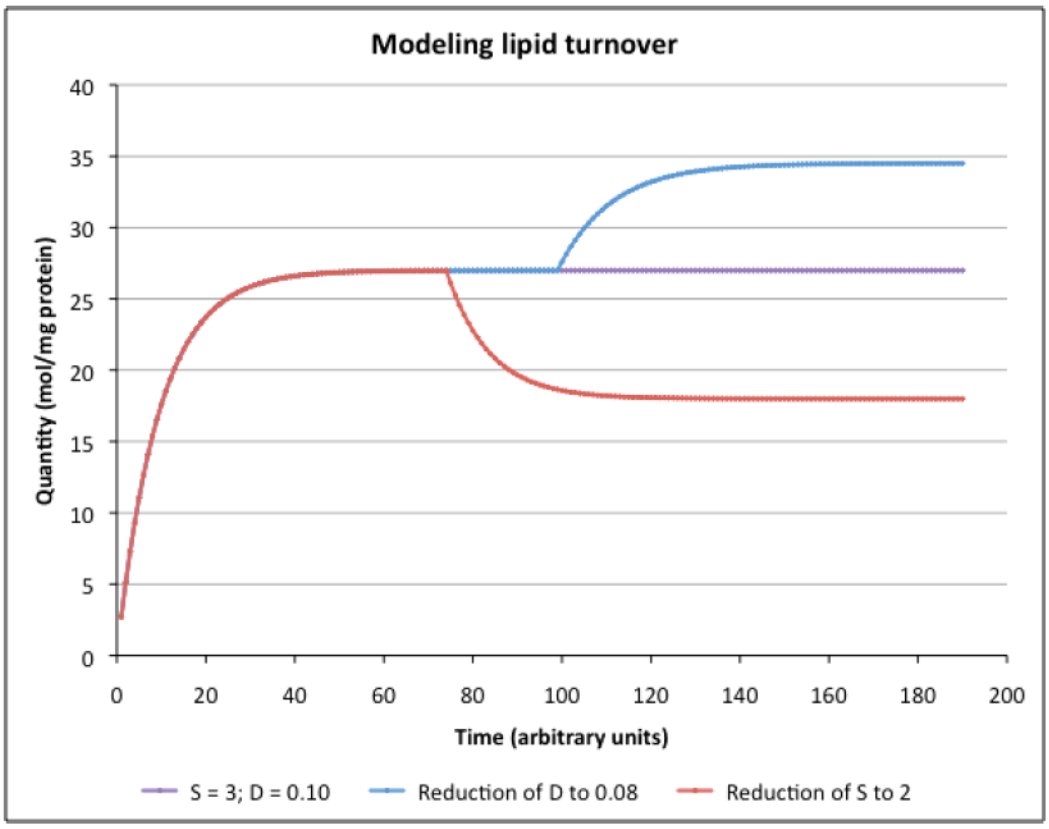

Figure 3.1. **Hypothetical model of glycosphingolipid turnover**. S, rate of biosynthesis; D, rate of degradation. The purple line shows a glycosphingolipid species arriving at its steady-state level. If the rate of synthesis (S) is decreased, the rate of degradation will be decreased (first-order kinetics) and a new lower steady-state level will be reached (red line). If the rate of degradation is decreased, the rate of synthesis will still remain constant (zero-order kinetics), and a higher steady-state level will be reached (blue line).

3.2 Hypothesis

Based on previous studies, we hypothesize that glycosphingolipid homeostasis is achieved through a balance of zero-order biosynthesis and first-order degradation.

3.3 Aims

I aimed to test whether the above-mentioned assumptions related to GSL homeostasis (biosynthesis and degradation) apply to any of the multiple

glycosphingolipid species typically present in mammalian cells. The specific aims for this project were:

Specific Aim 1: Determine the rates of biosynthesis and degradation of multiple glycosphingolipid species.

Specific Aim 2: Determine whether the experimental data fit with the theoretical model.

3.4. Experimental Approaches

I manipulated the biosynthesis and degradation of glycosphingolipids in cultured cells by different experimental approaches (Figure 3.2) and measured the levels of different glycosphingolipids species by high-performance liquid chromatography (HPLC) (Figure 3.3).

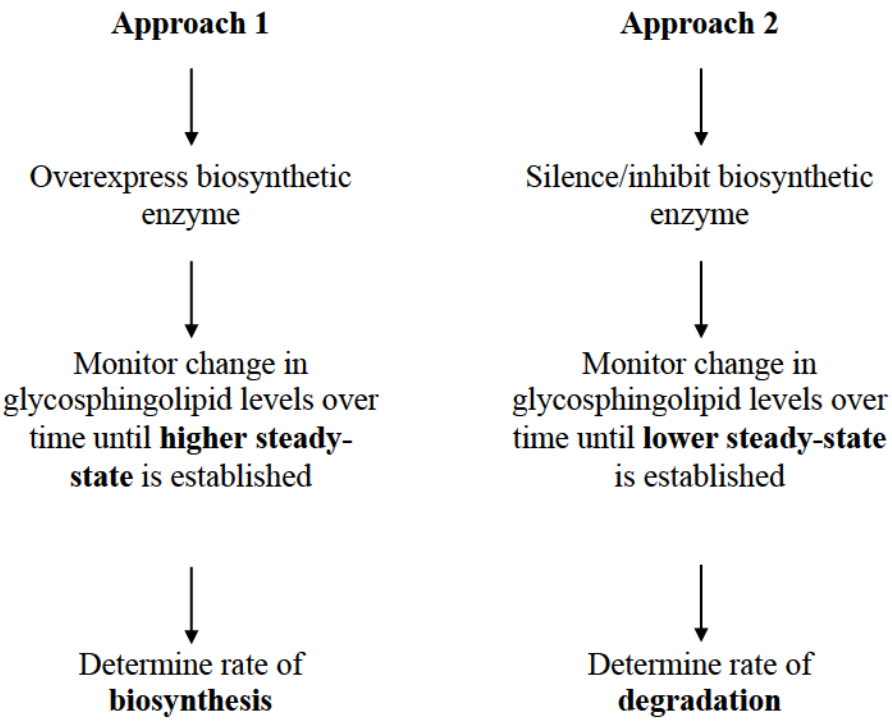

Figure 3.2. Overview of the experimental approaches and expected changes in the glycosphingolipid levels.

The experimental approaches considered to disrupt glycosphingolipid homeostasis in mammalian cells were -

(i) **Genetic Approach:** Transient overexpression of two enzymes, UDP-Glucose Ceramide Glucosyltransferase (UGCG) and beta-1,4-N-Acetyl-Galactosaminyltransferase 1 (B4GALNT1) in the glycosphingolipid biosynthetic pathway. These two enzymes work at two very important points in glycosphingolipid biosynthetic pathway (Figure 1.1.5, chapter 1). UGCG, also known as ceramide glucosyl transferase (CGT), catalyzes the first glycosylation step of ceramide and converts ceramide into glucosylceramide. B4GALNT1 catalyzes the synthesis of the ganglio-series of glycosphingolipids by transferring N-acetylgalactosamine to GM3, GD3, and globotriaosylceramide.

(ii) Pharmacological Approach: The small-molecular inhibitor *N*-butyldeoxygalactonojirimycin (*N*B-DGJ) inhibits the ceramide-specific glucosyltransferase, UDP-glucose ceramide glucosyltransferase (IC_{50} = 41.4 μM) (160) and GBA2 (IC_{50} =1-6μM), but does not affect α-glucosidases I and II or glucocerebrosidase (GBA) (79,93).

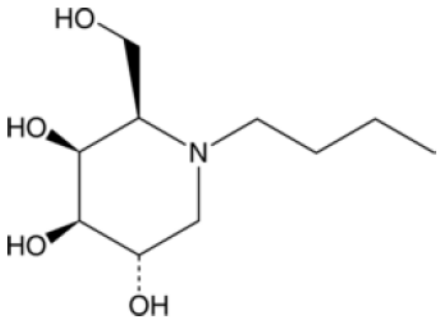

***N*-Butyldeoxygalactonojirimycin (*N*B-DGJ)**

(iii) **Biochemical Approach:** Addition of exogenous glycosphingolipids to cultured cells. Addition of exogenous glycosphingolipids was expected to either decrease the rate of biosynthesis or the increase the rate of degradation of the same glycosphingolipid added to the system to balance the level of added glycosphingolipid. This approach was not followed.

3.5 Materials and Methods

3.5.1 Pharmacological Inhibitor and Plasmids

*N*B-DGJ was obtained from Toronto Research Chemicals, Ontario or generously provided by Frances Platt (University of Oxford, UK). The human ORF clones of ceramide glucosyl transferase (UGCG), and β-1,4-N-acetyl-galactosaminyl transferase 1 (B4GALNT1) were obtained from OriGene Technologies Inc., USA. Both clones were present in pCMV6-entry vectors having a C-terminal Myc-DDK (FLAG) Tag.

3.5.2 Cell Culture

COS-7 (African green monkey kidney), SH-SY5Y (human neuroblastomas), HEK 293 (human embryonic kidney), HeLa (human cervical cancer), and MIN-6 (pancreatic beta) cells were obtained from the American Type Culture Collection (ATCC) and cultured in DMEM supplemented with 10% fetal bovine serum (Invitrogen, Carlsbad, CA). For B16-F10 (mouse melanoma) cells, low-sodium bicarbonate DMEM was used in combination with 10% fetal bovine serum. CHO-K1 cells were cultured in DMEM with a relatively lower concentration of fetal bovine serum (5%) and supplemented with 36 μg/mL proline (Life Technologies, Carlsbad, CA).

3.5.3 Transient-Transfections and Cell Harvesting

TransIT®-LT1/-2020 reagents (Mirus, Madison, WI) was used for the transient transfections of immortalized cells following manufacturers' instructions. Cells were harvested at 48 hours of post-transfection for lipid analysis by HPLC, western blot analysis, and enzyme activity assays (UGCG and GBA2). Adherent cells were harvested by washing with ice-cold PBS, scraping and washing in PBS. Cells were stored at -80°C until further use.

3.5.4 Ceramide Glycanase

Ceramide glycanase was purified from *Hirudo medicinalis* following the method described by Li and Li, 1989 (161,162). The entire isolation procedure was executed at 4°C temperature to preserve the enzymatic activity of ceramide glycanase. Briefly, lyophilized leech powder (Biopharm Leeches Ltd, Hendy, South Wales, UK) was dispersed in 50 volumes of 50 mM sodium phosphate buffer, pH 7.0, using a Tissue-Tearor (BioSpec Products Inc., Bartlesville, Oklahoma, USA). The dispersion was cleared by centrifugation at 25,000 × g for 30 minutes. The extract was then supplemented with solid ammonium sulfate to 30% saturation and stirred on ice for two hours to aid protein precipitation. After the precipitated protein was removed by centrifugation, the supernatant was brought to 55% saturation with ammonium sulfate and kept on ice for overnight. The next morning, the precipitated protein was collected by centrifugation and re-suspended in 50 mM sodium acetate buffer (pH 4.5). Insolubles were removed by centrifugation and a crude enzyme preparation was obtained. The crude enzyme was purified by a hydrophobic interaction chromatography using

Octyl-Sepharose CL-4B columns (1.0 × 23 cm; Sigma-Aldrich) equilibrated with acetate buffer (pH 4.5). After loading the crude enzyme on the column, the column was washed with 5 column volumes of acetate buffer and eluted with 3 column volumes of 2% octyl-glucoside in 50 mM potassium phosphate buffer (pH 7.0). The most pigmented fractions of the eluate were found to have the highest enzymatic activity when tested against various glycosphingolipid standards. The most pigmented fractions were pooled and concentrated 6-fold in a 10 kDa MWCO Macrosep concentration device (Pall Life Sciences; Mississauga, Ontario, Canada). The purified enzyme was stored at -20°C until further use.

3.5.5 Glycosphingolipid Analysis by HPLC

3.5.5.1 Svennerholm Glycosphingolipid Extraction

Cell pellets were resuspended in appropriate volumes of water and lysed by passing repeatedly through 23½-gauge needles. One volume cell lysate was mixed with four volumes $CHCl_3$: MeOH, 1:2 (v/v), agitated for three hours at room temperature and centrifuged at 3000 rpm for 10 minutes. The supernatant was transferred to a new tube, one volume of $CHCl_3$ and one volume of PBS were added, vortexed thoroughly and centrifuged at 3000 rpm for 10 minutes. The upper phase was transferred to a new tube and the lower phase was dried down under nitrogen gas at 42°C. The dried lower phase was resuspended in 50 µl $CHCl_3$: MeOH 1:3 (v/v) and combined with the upper phase. The resulting mixture was then purified using C18 columns (163,164).

3.5.5.2 Lipid Purification by Column Chromatography

Lipids were purified using Waters Sep-Pak 100mg C18 disposable columns, pre-equilibrated with 1 ml MeOH and water. Lipids were eluted from the columns using a

series of solvent mixtures - $CHCl_3$: MeOH (98:2), $CHCl_3$: MeOH (1:3) and MeOH. The combined eluates were then prepared for ceramide glycanase digestion (165).

3.5.5.3 Ceramide Glycanase Digestion and Fluorescent Labelling of Carbohydrates

The purified glycosphingolipids obtained by C-18 column chromatography were dried under nitrogen at 42°C, re-dissolved in 200 µl $CHCl_3$: MeOH (2:1), transferred to a screw-cap Eppendorf tube, again dried under nitrogen, re-dissolved in 25 µl $CHCl_3$: MeOH (2:1), spun in picofuge and dried under nitrogen. The dried samples were resuspended in 15 µl of 0.1% Triton X-100 and 0.25% taurocholate in 50 mM sodium acetate buffer (pH 5.0) containing 5 µl purified ceramide glycanase and were incubated at 37°C for 18 hours. After 18 hours, 10 µl water, 80 µl anthranilic acid (30 mg/ml) and sodiumcyanoborohydride (45 mg/ml) were added to the enzyme digest. Anthranilic acid and sodiumcyanoborohydride solutions were made in the labelling buffer containing 4% sodium acetate and 2% boric acid in methanol. The labelling mixture was incubated at 80°C for one hour to allow the liberated oligosaccharide to be labelled with anthranilic acid (2AA). The reaction mixture was cooled to room temperature, combined with 1 ml acetonitrile: water (97:3) and passed through prepacked and pre-equilibrated amide-2 columns (100 mg) to remove excess 2AA. The columns were washed with acetonitrile: water (95:5) and 2AA-labelled oligosaccharides were eluted with water and stored at 4° C in the dark until further use. The 2AA-labelled oligosaccharides were resolved by normal phase HPLC using a Waters Alliance 2695 separation module equipped with an in-line Waters 474 fluorescence detectors and a 4.6×250 mm TSKgel Amide-80 column (TOSOH Bioscience LLC, King of Prussia, Pennsylvania, USA), operated by Empower 3

software (165,166). The column was developed with a decreasing acetonitrile gradient in a ammonium hydroxide buffer (pH 3.85) as described by Neville *et al*. (167).

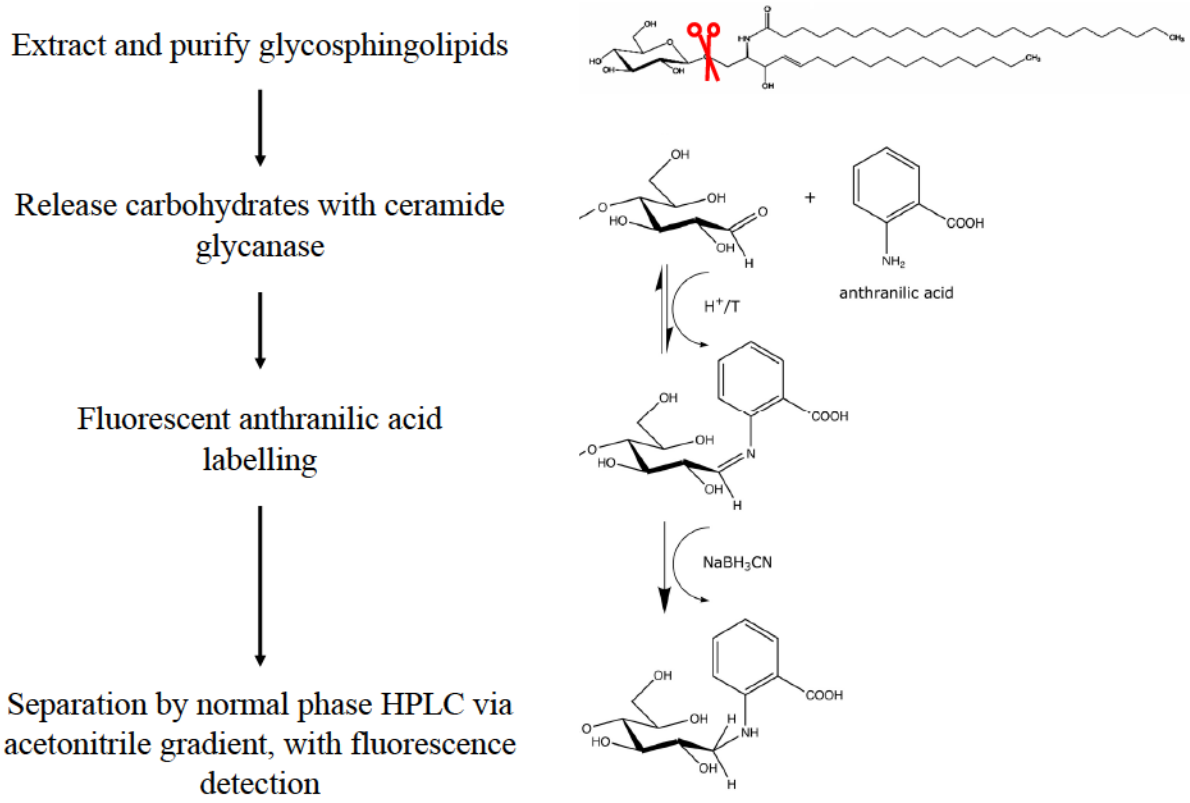

Figure 3.3. Overview of glycosphingolipid analysis by HPLC

3.5.5.4 Fluorescently-Labeled Glucose Oligomer Standards

To prepare (1-6)-linked glucose oligomers, dextran (250,000 kDa average MW; Spectrum, New Brunswick, New Jersey, USA) was mildly hydrolyzed followed by neutralization through AG 3-X4A resin (OH– form; Bio-Rad Laboratories Ltd, Mississauga, Ontario, Canada) (168). An aliquot of glucose oligomers (250 µg) was labeled with anthranilic acid as described above. The labelled oligosaccharide mixture was diluted in 1 mL acetonitrile/water (97:3, v/v) and the precipitated glucose oligomers were collected by centrifugation at 21,000×g for 5 minutes. The supernatant was passed

through prewashed Amide-2 column. Precipitated glucose oligomers were also loaded on the Amide-2 column after dissolving in distilled water. 2AA-labeled glucose oligomers were eluted with 550 µL distilled water, twice. To obtain a calibration curve, 170 ng fluorescently labeled sugars were typically injected on HPLC. One-to-four-linked glucose oligomers (n = 4–7) were obtained from Fluka/Sigma (maltotetraose to maltoheptaose).

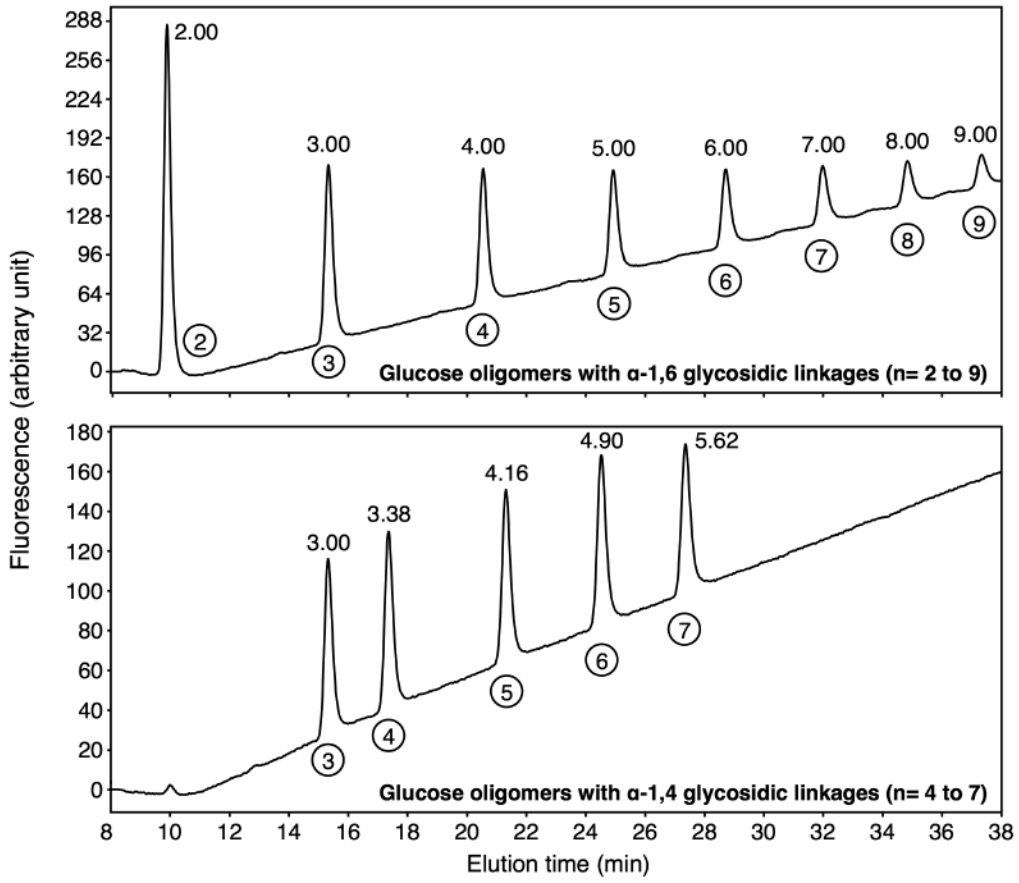

Figure 3.4. Separation of glucose oligomers with α(1-6) and α(1-4) linkages. The top panel shows peaks for α(1-6)-linked glucose oligomers obtained from partial hydrolysis of dextran (dimer to nonamer, the numbers within the circles indicate oligomers). These oligomers define the GU parameter, their GU values being identical to the number of glucose subunits. The bottom panel shows α(1-6)-linked glucose trimer and α(1-4)-linked glucose oligomers (tetramer to heptamer, oligomer numbers are within the circle) with GU values. Glucose oligomers (n= 4 to 7) having the same molecular weight but the different linkages were eluted at different times. [The figure was obtained from the paper by Vieira ***et al***. with a slight modification of the figure legend (165)].

3.5.5.5 Integration and Analysis of Chromatogram

Chromatograms were integrated using Gaussian curve fit. Elution times of chromatographic peaks obtained from cellular glycosphingolipid species were compared with the elution times of (1-6)-linked glucose oligomers and converted to glucose units (GU) using the Empower 3 GPC software add-on (Waters). Very small peaks in the chromatogram (less than 1% of total peak area) were excluded from the analysis, as the chromatograms of leech ceramide glycanase contained a range of small peaks (165). We obtained GU values obtained for neutral GSLs (Gb3, Gb4), monosialogangliosides (GM1, GM2, GM3), and di-sialogangliosides (GD3, GD1a, GD1b) (Matreya LLC, State College, Pennsylvania, USA) that were in good agreement (median difference of –0.03 GU) with previously determined values (169).

3.5.6 Ceramide Glucosyl Transferase Assay with C12-NBD-Cer

3.5.6.1 Microsome Preparation

Cell pellets harvested at 48 hours of post-transfection were resuspended in ice-cold Tris-HCl (10 mM, pH 8.0), incubated on ice for 20 minutes and lysed by passing through a 25G needle. Cellular debris was removed from the lysed cells by centrifugation at 500×g for 10 minutes at 2° C. The clear supernatant was centrifuged at 15,000×*g* for 10 minutes at 2°C using a Beckman Optima™ TLX Ultracentrifuge to pellet the crude mitochondria. The medium-speed supernatant was centrifuged at 100,000×g for 30 minutes. The resulting pellet (the microsomal preparation) was resuspended in Tris-HCl (pH 8.0) for further analysis.

3.5.6.2 Preparation of C12-NBD-Cer Bovine Serum Albumin Complex

One mg C12-NBD-Cer (Avanti Polar Lipids, Alabaster, Alabama, US) was dissolved in 1 ml $CHCl_3$/MeOH (1:2, v/v), transferred to 1.5 ml microfuge tube, dried under nitrogen followed by drying under vacuum for 30 minutes. The dried substrate was dissolved in 50 µl 100% ethanol. The resulting mixture was added dropwise to 3.42 ml 0.5 mM defatted BSA in a serum-free balanced-salt solution. The final solution became 0.5 mM C12-NBD-Cer, the substrate for the UCGC assay.

3.5.6.3 UGCG Assay

The assay buffer contained 50 mM HEPES (pH 7.4), 25 mM KCl, 5 mM $MnCl_2$ and 2.5 mM UDP-glucose (freshly prepared). For the enzyme activity assay, 25 µl microsomal preparation was mixed with 10 µl of the C12-NBD-Cer/BSA complex and 465 µl assay buffer and incubated at 37°C for 30 minutes. After the incubation period, 750 µl $CHCl_3$/MeOH (1:3, v/v), 500 µl $CHCl_3$ and 400 µl water was added to the samples and mixed by vortexing. The mixture was centrifuged at 1500×g at 8°C for 15 minutes to split the aqueous and organic phases. The top layer (aqueous phase) was carefully removed and the bottom layer was dried under nitrogen. The dried lipids were dissolved in 17.5 µl $CHCl_3$ and spotted on an HPTLC plate that was developed in a glass tank with chloroform/methanol/20% (w/v) ammonium hydroxide (70:30:5, v/v/v) (170,171) and scanned using a Typhoon Variable Mode Manager using 457 nm laser (emission was 526 SP Fluorescein, PMT 300, resolution 100 µm). Image analysis was done using ImageJ.

3.5.7 Immunostaining

Cells were seeded on glass coverslips in 35 mm dishes at a density of 100,000 – 150,000 cells/dish and transfected with the desired cDNA constructs. At 48 hours of post-

transfection, cells were washed twice with PBS, fixed with 4% PFA for 25 minutes, washed with 5 mM ammonium chloride to quench the fixative, permeabilized with 0.3% Triton X-100 in PBS for 20 minutes, washed twice with PBS to remove the TritonX-100, and blocked with 1% BSA for one hour. Cells were incubated with the primary antibody(ies) diluted in the blocking buffer at 4°C for overnight, washed twice with PBS to remove excess primary antibody, and incubated with secondary antibody for one hour. Cells were protected from light after addition of secondary antibody. Finally, the coverslips were washed with PBS, then with mQ water, dried and mounted on glass slides with Vectashield (Vector Laboratories, Burlingame, CA).

3.5.8 Western Blotting

Frozen cell pellets were resuspended in lysis buffer (20 mM Tris-HCl, 300 mM KCl, 0.5 mM EDTA, 0.5 mM EGTA, 10% glycerol, 0.25% Nonidet P-40, and protease inhibitors) and cells were lysed using a sonic dismembranator (Artek Sytems Corporation, Farmingldale, N.Y.). Cellular debris was removed by centrifuging the lysed cells at 500×g for 15 minutes at 4°C and the total protein concentration of the clear lysate was determined by BCA protein assay using BSA as standard (ThermoScientific, Waltham, MA). Cell lysates containing equal amounts of total protein were resolved by SDS-PAGE and transferred to PVDF membrane by semi-dry western blotting in 50 mM Tris-base, 40 mM glycine, 20% methanol and 0.0375% SDS. Depending on the type of the primary antibody, either 5% skimmed milk or 3% BSA in 0.1% TBST (Tris buffer saline with Tween-20) was used to block the membrane. The blots were developed using either Pierce ECL Western blot substrate (Thermo Scientific, Waltham, MA) or Amersham ECT Western blotting Detection Reagents (GE Healthcare, Chicago, IL). In

case of weak protein signals, SuperSignal West Pico PLUS Chemiluminescent Substrate (Thermo Scientific, Waltham, MA) was used.

3.6 Results

3.6.1 Genetic Approach

3.6.1.1 Cellular Glycosphingolipid Profiles

When expressed in COS-7 cells, UGCG and B4GALNT1 appeared close to their expected molecular weights (Figure 3.6.1 A). COS-7 cells overexpressing UGCG had a four-fold higher enzymatic activity compared to the mock-transfected cells at 48 hours of post-transfection (Figure 3.6.1 B). UGCG and B4GALNT1 did not change the glycosphingolipid profile of COS-7 cells at 48 hours of post-transfection (Figure 3.6.2). To verify the results obtained with COS-7 cells, I measured the GSL profiles of HeLa (cervical cancer cells), HEK293 (embryonic kidney cells), CHO-K1(monkey kidney cells), MIN-6 (pancreatic beta cells), and B-16 cells (melanoma cells) overexpressing UGCG and/or B4GALNT1. The GSL profiles of B-16 and HEK293 cells showed minor changes (Figure 3.6.2 and Figure 3.6.3), while other cell lines did not show measurable changes upon overexpression of UGCG.

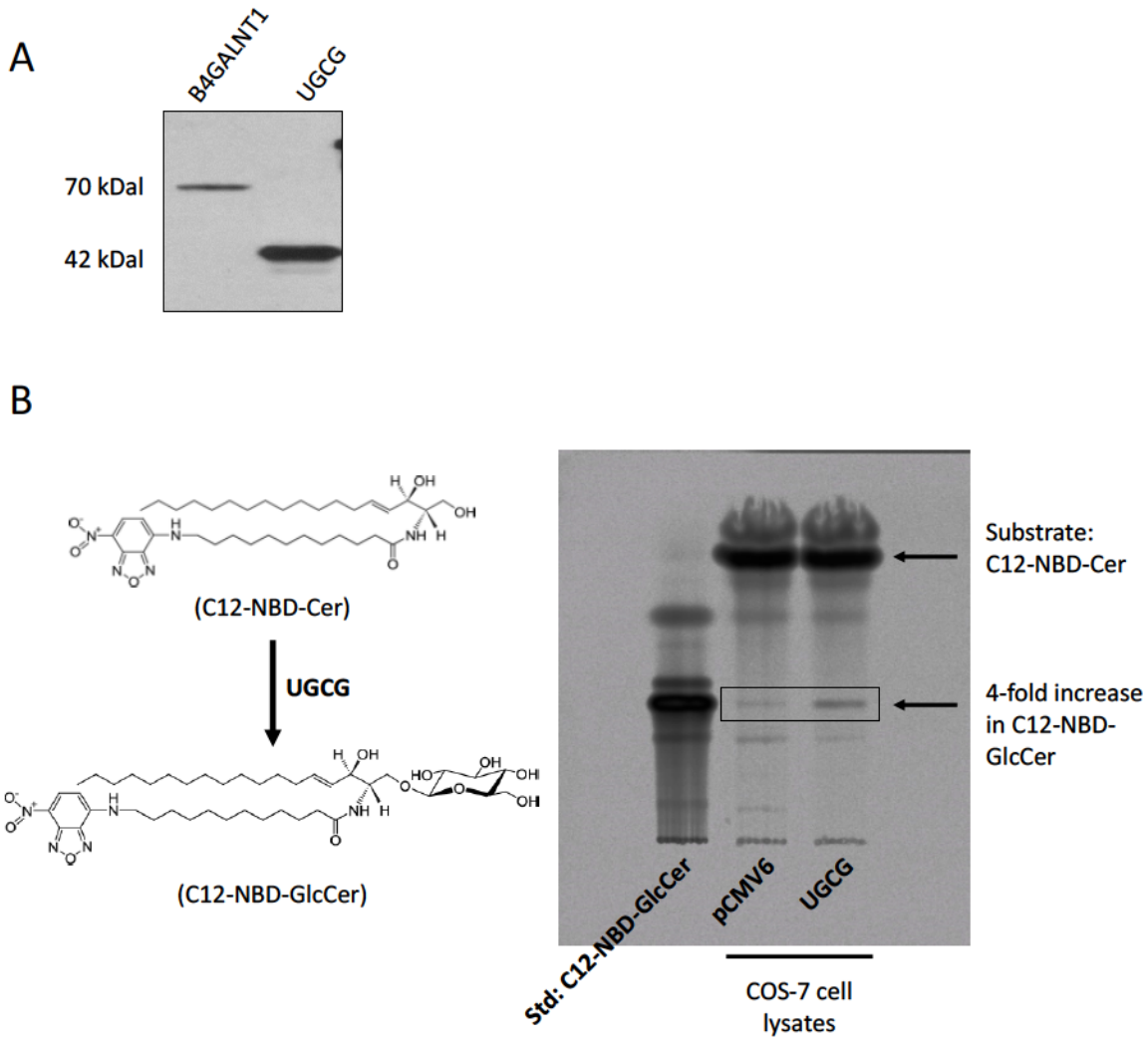

Figure 3.6.1. Expression of UGCG and B4GALNT1 and enzyme activity of UGCG.
(A) Western blot analysis (anti-FLAG) of COS-7 cells expressing UCGC and B4GALNT1. (B) HPTLC plates showing the glucosylation of C12-NBD-Ceramide by UGCG. Microsomal preparations from COS-7 cells transfected with UGCG and empty pCMV6 vector were assayed for glucosylation activities.

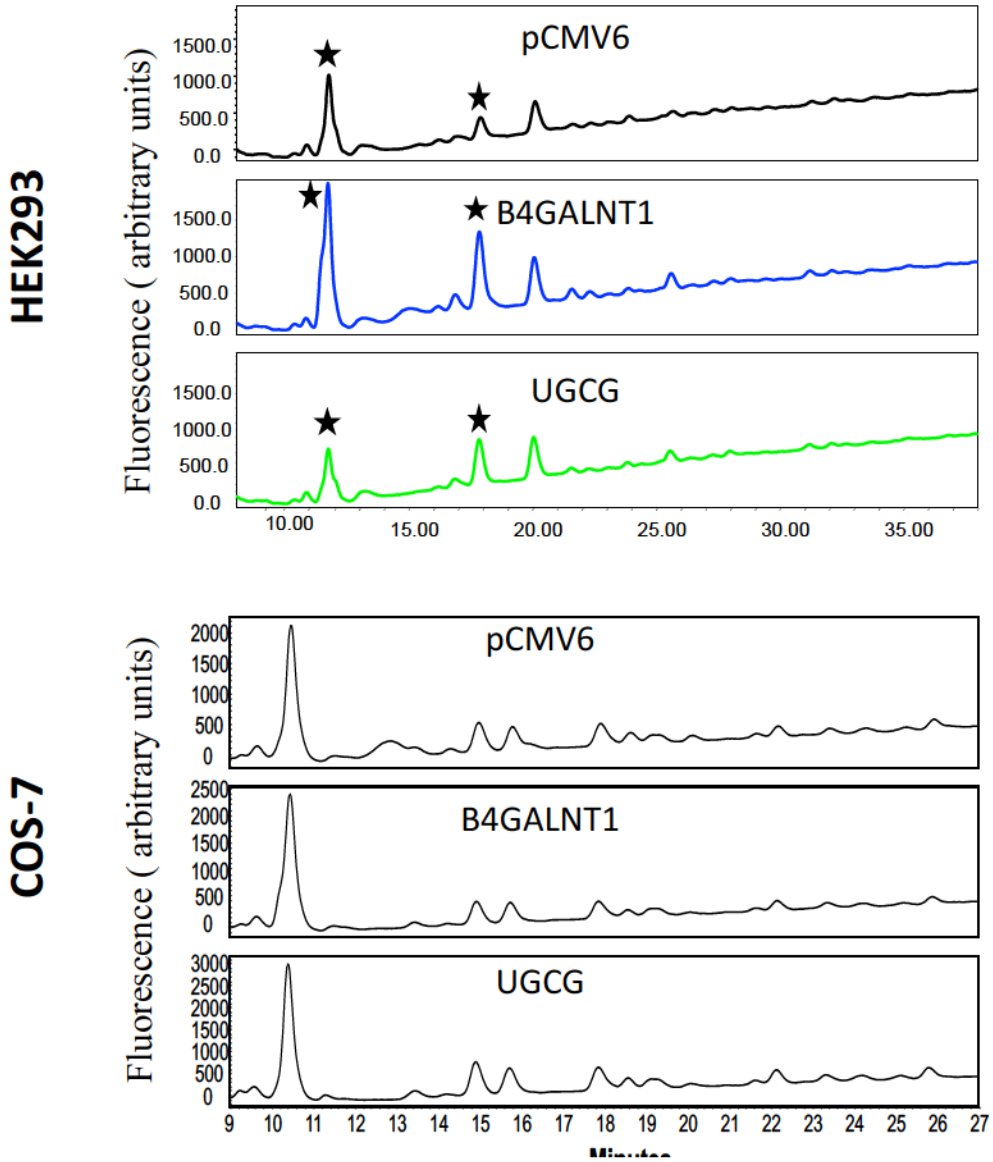

Figure 3.6.2. Glycosphingolipid profiles of HEK293 and COS-7 cells upon overexpression of UGCG and B4GALNT1. Peaks marked by the black stars indicate the GSL species that were changed in cells overexpressing UGCG and B4GALNT1.

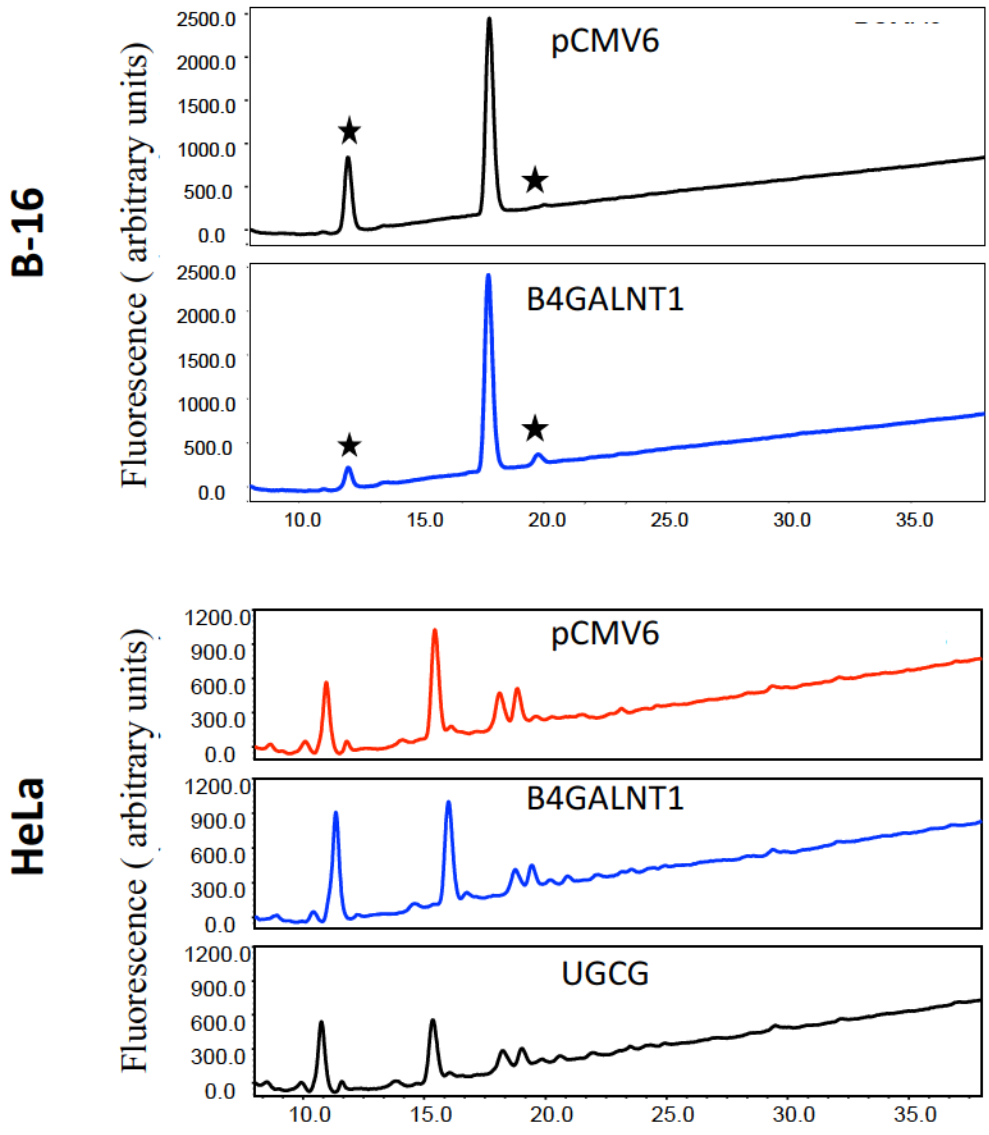

Figure 3.6.3. Glycosphingolipid profiles of B-16 and HeLa cells upon overexpression of UGCG and B4GALNT1. Peaks marked by the black stars indicate the GSL species that were changed in cells overexpressing UGCG and B4GALNT1.

3.6.1.2 Cellular Expression pattern of Overexpressed UGCG and B4GALNT1

Immunofluorescence staining showed that UGCG and B4GALNT1 were expressed throughout in COS-7 cells, indicating possible cellular localization in the plasma membrane, cytoplasm, or endoplasmic reticulum (Figure 3.6.4). Determination of subcellular localization of these enzymes in cultured cells are yet to be done.

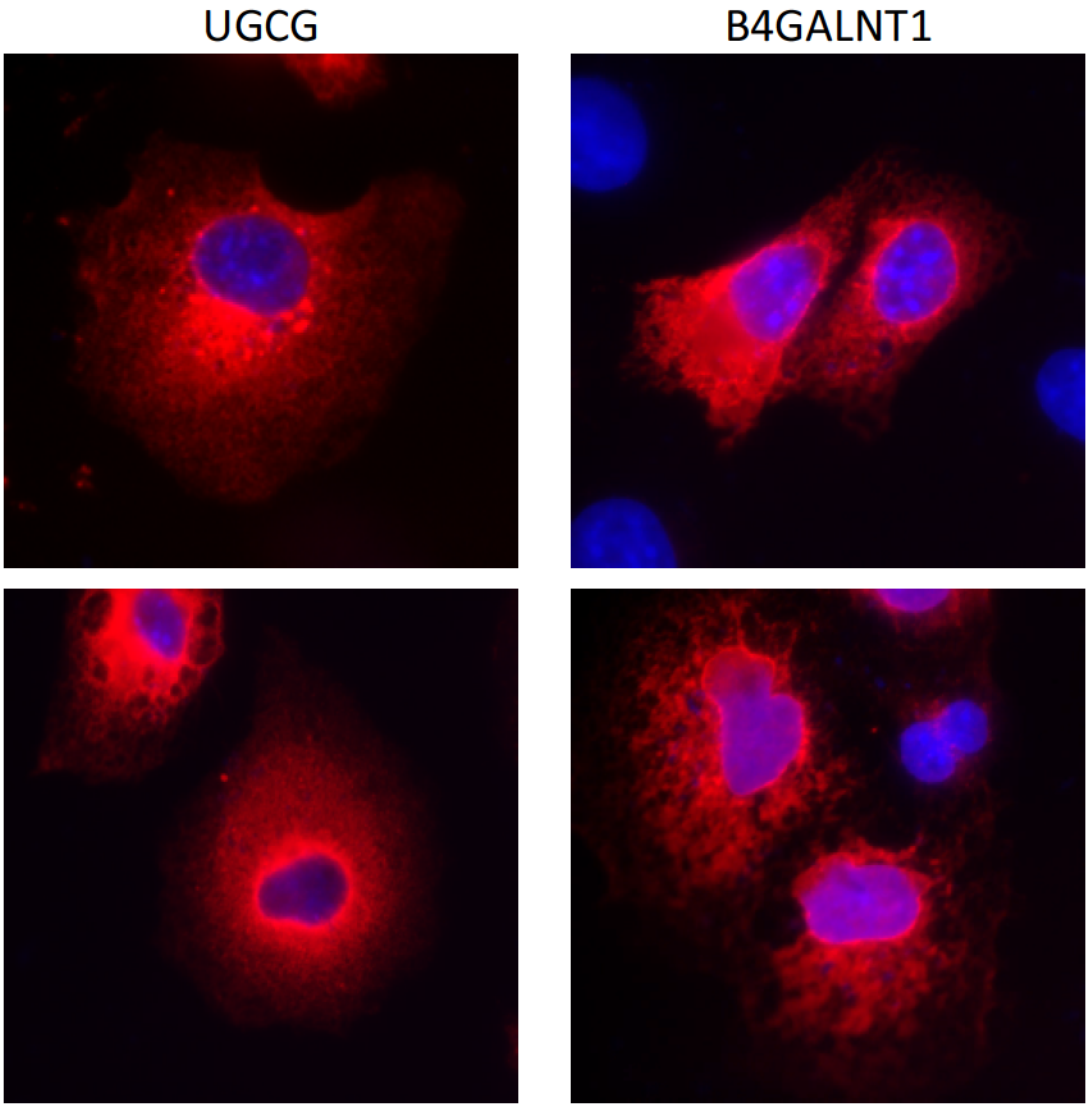

Figure 3.6.4. Immunostaining of UGCG and B4GALNT1 expressed in COS-7 cells. COS-7 cells transiently transfected with cDNAs of UGCG and B4GALNT1 and immunostained with an anti-FLAG antibody at 48 hours of post-transfection.

3.6.1.3 C-terminal FLAG-Tag Affects the Enzymatic Activity of UGCG and B4GALNT1

To assess whether the C-terminal FLAG-tag had any effect on the enzymatic activities of UGCG and B4GALNT1, I generated cDNA clones encoding UGCG and B4GALNT1 lacking the C-terminal tag and overexpressed the new constructs in B-16 cells, which have a simple glycosphingolipid profile. The transfected cells had slightly different glycosphingolipid profiles (Figure 3.6.5) compared to the cells transfected with C-terminally FLAG-tagged versions of these enzymes. The major glycosphingolipid of B-16 cell is GM3. Overexpression of B4GALNT1 in B-16 cells was expected to increase the conversion of GM3 into GM2, and overexpression of UGCG was expected to upregulate the levels of the downstream glycosphingolipids, including GM3 and GM2. Overexpression of tag-free B4GALNT1 in B-16 cells elevated GM2 by 513% and decreased GM3 by 28% (Fig. 3.6.5). On the other hand, the tag-free version of UGCG increased the levels of GM3 and GM2 in B-16 cell by 31% and 68%, respectively (Figure 3.6.5). However, these data were obtained from a single experiment. So, the experiment needs to be repeated to assess for the consistency and robustness of the data. The level of expression and cellular localization of the tag-free enzymes were not assessed by western blotting or immunofluorescence staining are yet to be determined.

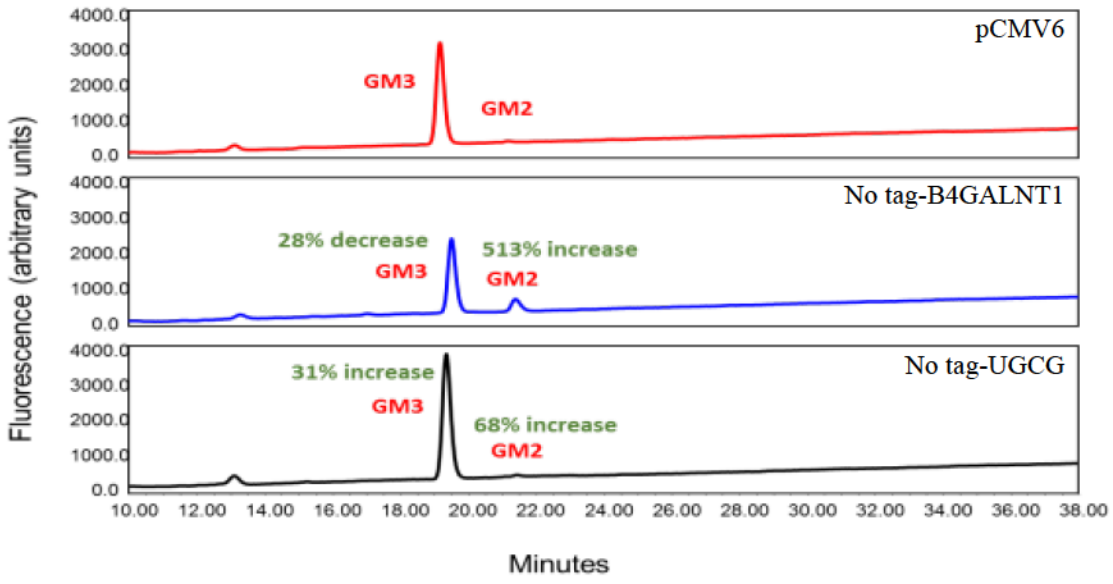

Figure 3.6.5. Glycosphingolipid profiles of B-16 cells expressing B4GALNT1 and UGCG without epitope tags. The changes in individual GSL species were quantified by using Gaussian fit curve and comparing the areas of the corresponding peaks.

3.6.2 Pharmacological Approach

To manipulate glycosphingolipid biosynthesis in cultured cells, I used *N*-butyldeoxygalactonojirimycin (*N*B-DGJ). Previously our lab found that *N*B-DGJ significantly reduced glycosphingolipid levels over 96 hours, but glycosphingolipid profiles of adherent cells changed quantitatively with increasing cell confluency (unpublished results). When adherent cells were treated with *N*B-DGJ for long periods, cells became very confluent and needed to be trypsinized while withdrawing the drug. To overcome this complication, I needed to use a cell culture system with minimal changes in glycosphingolipid profiles over time. As a starting point, I assessed the glycosphingolipid profiles of quiescent human fibroblast cells (F8) over a period of four weeks. F8 cells have a slow growth pattern and when they reach to the confluency, the growth rate reaches to an apparent halt. I observed that the GSL profile of F8 cells

remained steady over that 4-weeks period (Figure 3.6.6 A and Figure 3.6.6 B), which confirmed the suitability of F8 cells to manipulate glycosphingolipid levels by pharmacological approach. Therefore, I treated quiescent fibroblast cells with 500 μM *N*B-DGJ and measured glycosphingolipid profiles after 24, 48, 96 and 192 hours of drug treatment. The cell culture media containing the drug was replaced every 48 hours, drug was withdrawn after 192 hours and glycosphingolipid profiles were determined at 24, 48, and 96 hours post-withdrawal to assess the restoration rates of various glycosphingolipid species.

The major glycosphingolipid species of F8 cells are GM3, Gb3, Gb4, GD3 and LacCer, the overall levels of which were lower upon treatment with *N*B-DGJ, but the pattern of change was arbitrary. Upon treatment with *N*B-DGJ, GM3 and Gb3 levels were decreased for the first 48 hours, as expected, and then increased for next 144 hours until the drug was removed. After removal of the drug, GM3 and Gb3 levels drastically decreased for first 24 hours, restored over the next 24 hours and then decreased over 48 hours (3.6.6 B). LacCer showed a different trend upon treatment with *N*B-DGJ, increasing five-fold for the first 48 hours, then decreasing and leveling off. The levels of Gb4 and GD3 cells shared a similar pattern upon treatment with *N*B-DGJ, decreasing to below 2×10^7 fluorescence units and not changing much further. However, this experiment was performed once, therefore, needs to be repeated to the consistency of data and address the under underlying facts for arbitrary changes in GSL profiles upon treatment with *N*B-DGJ.

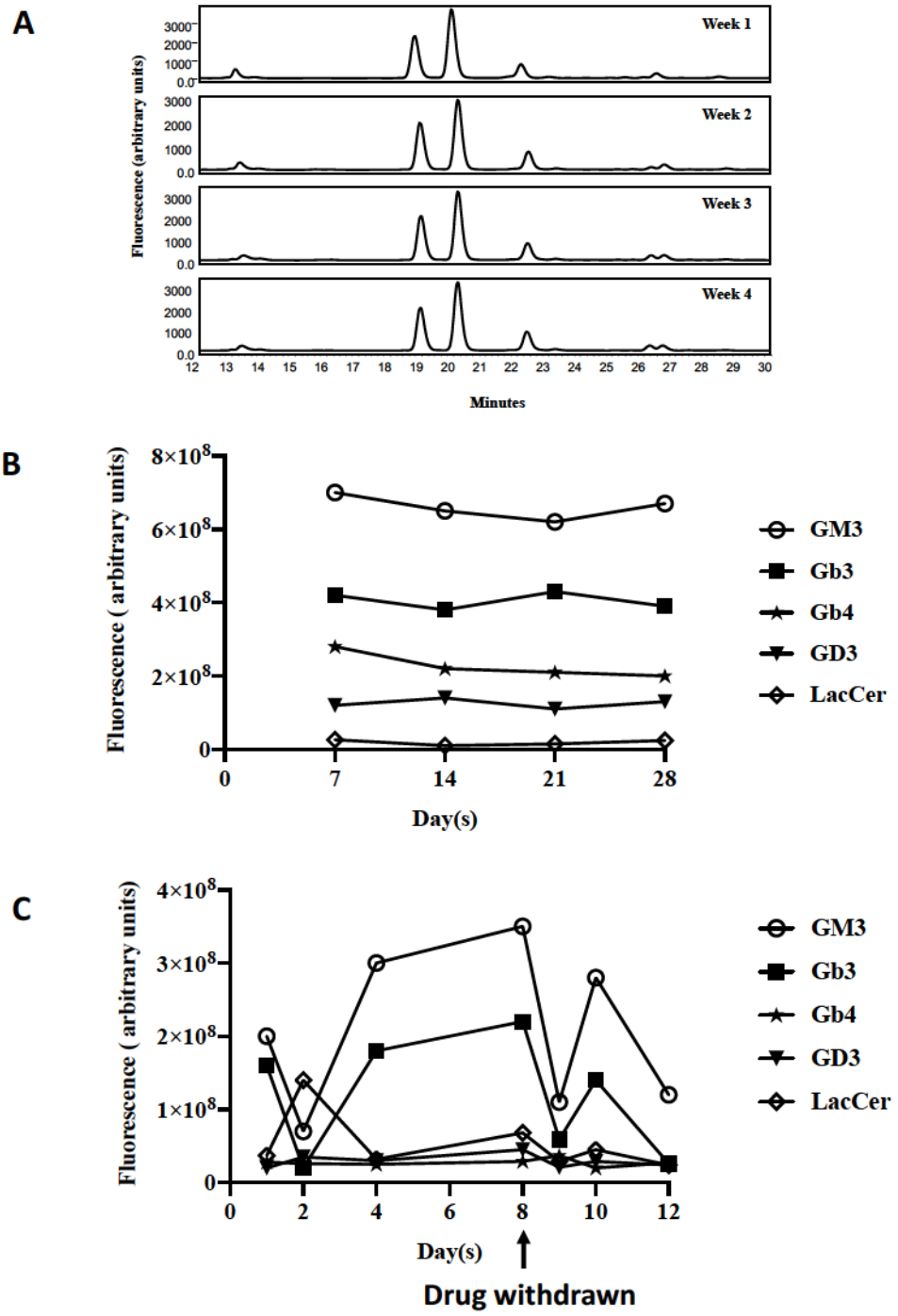

Figure 3.6.6. Glycosphingolipid profiles of F8 cells. (A) Baseline check for quiescent fibroblast cells; the major glycosphingolipids of F8 cells remained steady over four-weeks period. (B) Quantification of chromatogram data for GM3, Gb3, Gb4, GD3, and LacCer of F8 cells during the baseline check. (C) Glycosphingolipid levels upon treatment with and withdrawal of *N*B-DGJ.

3.7 Discussions

In order to manipulate cellular GSL profiles, I overexpressed two enzymes, UGCG and B4GALNT1 and treated cultured cells with *N*B-DGJ. The goal was to measure the changes in levels of GSLs over time and determine the rates of changes by kinetic analysis of that data. Unfortunately, the genetic and pharmacological interventions did not change the GSL levels in cultured cells as expected. GSL homeostasis ensues from a complex interplay among many biosynthetic and degradative enzymes. It also depends on the level of each individual GSL species present in cells at a certain time (158). Targeting one enzyme (genetic or pharmacological) in the biosynthetic or metabolic pathway may trigger or silence other enzymes involved in the same pathway due to structural or functional similarities of enzymes and substrates, and also to balance the changed profiles of metabolites or substrates in the overall system (172,173). We were not able to address what other enzymes in the GSL biosynthetic pathway were being affected due to genetic and pharmacological manipulation of certain enzymes in that pathway. Studies have shown that specific levels of GSLs in a cell are dependent on the relative ratios of the specific glycosyltransferases involved in the biosynthesis and also on the levels of enzyme substrates (174,175). Overexpression of B4GALNT1 was expected to promote the conversion of GM3 into GM2. I had the same observation when I overexpressed tag-free version of B4GALNT1in B-16 cells (Figure 3.6.5), but the levels of increase of GM2 and decrease of GM3 were disproportionate, indicating the involvement of other factors in the regulation of the levels of those two gangliosides. Furthermore, I did not assess the cellular localization of overexpressed UGCG and B4GALNT1 which is important for their enzymatic activity. The untagged versions of UGCG and B4GALNT1 changed the

GSL profiles in B-16 cells, but the assessment of their subcellular localization or level of expression are yet to be done.

The pharmacological approach changed the GSL profiles of F8 cells in an unpredictable fashion. At 500 μM, *N*B-DGJ was expected to inhibit UGCG (ceramide glucosyltransferase) and GBA2 (β-glucosidase 2). So, it was expected that the level of GlcCer and other downstream GSL species would be reduced upon treatment with *N*B-DGJ. But my observations were different. The major GSL species of F8 mostly followed an increasing trend upon addition of *N*B-DGJ over eight days (Figure 3.6.6 C), although there were some arbitrary fluctuations (increase and decrease) in their levels within first 48 hours of drug treatment. After drug withdrawal, the levels of GSL were expected to elevate, which did not happen.

In a previous study, the half-lives of gangliosides' ranged from 2 to 6.5 hours to 3 days, depending on the type of cells and other factors, including the coordination of enzymes, substrates, activators, ancillary proteins, external stimuli, etc. (175). As I did not see much difference in the GSL profiles in cells overexpressing UGCG or B4GALNT1 at 48 hours of post-transfections, there is a possibility that the GSL turnover rate was different than expected. The same expectation may apply to the pharmacological approach as well. The turnover rates need to be re-assessed choosing different time points, with more frequent sampling of cells for GSL analysis. Additionally, it is also possible that transient transfections are not good approaches for genetic manipulation of GSL biosynthetic enzymes, gene silencing or stable overexpression would be better alternatives for this study. Again, cultured cells might not be suitable models for this

study. An animal model may be a better option, as GSL profiles of animal tissues are very consistent.

In conclusion, different approaches to manipulate GSL profiles and different models' systems may be more suited for studies into the regulation of GSL homeostasis.

Chapter 4: Biochemical and Cell biological Bases of SPG46

4.1 Hypothesis

Mutations in the *GBA2* gene cause SPG46 by changing the behavior of the *GBA2* gene product.

4.2 Materials

4.2.1 Compounds

Chemical compounds used in this study were TMRM (Invitrogen, Carlsbad, CA), FCCP (Sigma, St Louis, MO), Digitonin (Invitrogen, Carlsbad, CA), Mdivi-1 (Enzo Life science, Farmingdale, NY), Lactacystin (Toronto Research Chemicals Inc., North York, ON), MG-132 (Selleckchem.com, Houston, TX). (see Appendix A for catalogue numbers).

4.2.2 Kits, Cell Culture Medium, Dishes, and Other Reagents

Dulbecco's Modified Eagle Medium (DMEM), penicillin-streptomycin, L-glutamine, puromycin, trypsin, Lipofectamine 2000, Opti-MEM, Taq DNA polymerase, 1kB-Plus DNA ladder, and T4 DNA ligase were obtained from (Gibco, Grand island, NY/Invitrogen, Carlsbad, CA). We further used HD-In Fusion cloning kit (Takara Biosciences, Mountain View, CA), T4 DNA ligase buffer (New England Biolabs, Iswich, MA), acrylamide/bis solution 37.5:1 (Bio-Rad, Hercules, CA), protease inhibitor cocktail (Roche Diagnostics, Mississauga, ON), Ammonium persulfate (Sigma, St Louis, MO), tetramethylethyl-enediamine (TEMED) (Bio-Rad, Hercules, CA), Tween-20 (Bio-Rad, Hercules, CA), Immobilon-P polyvinylidene difluoride membrane (PVDF) (Millipore Sigma, St Louis, MO), bicinchoninic acid protein assay kit (Thermo Fischer Scientific, Waltham, MA), bovine serum albumin (Sigma, St Louis, MO), enhanced

chemiluminescence reagent (GE life sciences, Pittsburgh, PA), and X-ray films (Mandel scientific, Guelph, ON). Quick change lightning mutagenesis kit, nativePAGE premade gels, DNA extraction kit, plasmid purification kit, genomic DNA extraction kit. T4 DNA ligase, DNA polymerase, and Phusion HS II enzymes were from Fisher Thermoscientific. Restriction enzymes used were from Thermoscientific, New England Biolabs, or Promega. (See Appendix A for catalogue numbers).

4.2.3 Antibodies

The following primary antibodies were used in this study: mouse anti-FLAG mAb (Sigma, St. Louis, MO), rabbit mAb anti-GAPDH (clone 14C10, Cell Signaling, Danvers, MA), rabbit monoclonal anti-α-tubulin (Cell Signaling, Danvers, MA), mouse polyclonal anti-GBA2 (Abcam, Cambridge, MA), rabbit monoclonal anti-DRP1 (Cell Signaling, Danvers, MA), rabbit monoclonal anti-DYKDDDDK (Cell Signaling, Danvers, MA), mouse monoclonal anti-HA (Roche Diagnostics, Indianapolis, IN), mouse monoclonal anti-ubiquitin (Cell Signaling, Danvers, MA), mouse monoclonal anti-OPA1 (BD Transduction Laboratories, San Jose, CA), mouse monoclonal anti-TOM20 (BD Transduction Laboratories, San Jose, CA), rabbit monoclonal anti-CLPP (Cell Signaling, Danvers, MA), rabbit monoclonal anti-COX IV (clone 3E11, Cell Signaling, Danvers, MA), rabbit monoclonal anti-HSP60 (clone DF61, Cell Signaling, Danvers, MA), rabbit monoclonal LONP1/PRSS15 (clone D8W1J, Cell Signaling, Danvers, MA), rabbit monoclonal anti-caspase-9 (Cell Signaling, Danvers, MA), rabbit monoclonal anti-caspase-3 (Cell Signaling, Danvers, MA), rabbit monoclonal anti-caspase-7 (Cell Signaling, Danvers, MA), and HRP-conjugated secondary antibodies (Jackson Immuno research Laboratories, West Grove, PA). (See Appendix A for catalogue numbers).

4.3 Methods

4.3.1 Molecular cloning

ORFs of WT and mutant GBA2 were cloned in either the pCMV6 vector having the strong cytomegalovirus (CMV) promoter or in the pMSCV vector having the 5' long-terminal repeat of the mouse stem cell virus (MSCV) as promoter.

Different cloning approaches and different plasmid purification techniques were used at different times of the project. Custom oligonucleotides were obtained from Integrated DNA Technologies (Coralville, IA) and Invitrogen (Carlsbad, CA), and plasmids from Addgene (Watertown, MA) and OriGene (Rockville, MD). QuickChange II XL Site-directed mutagenesis (Agilent, Santa, Clara, CA) and HD In-Fusion cloning (Takara Biosciences, Mountain View, CA) were used for generating some of the mutants. Qiagen plasmid miniprep kit (Qiagen, Germany), Qiagen plasmid midiprep kit (Qiagen, Germany), GeneJET plasmid miniprep kit (Thermo Fischer Scientific, Waltham, MA), GeneJET plasmid miniprep kit (Thermo Fischer Scientific, Waltham, MA) and ymopure II plasmid midiprep kit (ymo Research, Irvine, CA) were used for bacterial plasmid purification.

The template used for *in-vitro* mutagenesis was the cDNA of human GBA2 containing a C-terminal FLAG-tag (Origene, cat# RC203796). cDNAs encoding C-terminally FLAG-tagged truncation mutants Tyr121*, Trp173*, Arg234* and Arg340* of human GBA2 were generated via inverse PCR, using one forward primer and four different reverse primers. The forward primer annealed at the template from 3825 to 3845 nucleotides, and the reverse primers annealed from 1371 to 1388, 1526 to 1544, 1705 to 1726, and 2030 to 2045 nucleotides for Tyr121*, Trp173*, Arg234* and Arg340*

respectively (nucleotides are numbered as in RC203706). The reverse primers had a 15-nucleotide extension at the 3′ end, complementary to 3825 to 3839 nucleotides of GBA2 cDNA template. Phusion DNA Polymerase (Thermo Scientific, Carlsbad, CA) was used for PCR reactions. PCR was performed using a touchdown program of a Nexus Gradient Mastercycler (Eppendorf, Mississauga, ON), setting the starting temperature at 65°C and gradually reducing the temperature by 1°C after each cycle. PCR products were purified using the NucleoSpin Gel and PCR clean-up Kit (Macherey-Nagel, Bethlehem, PA), and subjected to in-fusion reaction to fuse the 15-nucleotide identical sequences at the 5′and 3′ends of the PCR products. HD In-Fusion Enzyme Premix (Clontech, Mountain View, CA) was used for the fusion reaction. QuickChange II site-directed Mutagenesis Kit (Agilent, Santa Crala, CA) was used to generate cDNAs encoding the Arg630Trp and Arg873His missense mutants where a single nucleotide was substituted at the 2916 (C>T) and 3045 (G>A) positions of the template GBA2 cDNA (cat# RC203706, OriGene). The XbaI-Bst1107I fragment (nucleotide position from 1874 to 2317) of GBA2 cDNA was replaced with a synthetic cDNA segment carrying the 2283T>G substitution to generate the cDNA encoding Phe419Val mutation. cDNAs encoding the Asp594His, Gly683Arg, andArg870* mutants were made by substituting the EcoNI-NheI segment of RC203706 (from 2536 to 3689 nucleotide, contained 1154 nucleotides) with corresponding segments of synthetic DNA carrying nucleotide substitutions at 2808 (G>C), 3075(G>C), and 3636(C>T) positions, respectively. Synthetic DNA fragments were obtained from Life Technologies/Integrated DNA Technologies (these mutagenesis techniques have been described in the paper by Sultana *et al*.(83)).

For C-terminal deletions in GBA2-339 from residue 233 towards N-terminus (Cdel 40, Cdel 80, Cdel 120, Cdel 160, Cdel 200) and N-terminal deletions in GBA2-339 from residue 1 towards C-terminus (Ndel 41, Ndel 81, Ndel 121, Ndel 161, Ndel 201 and Ndel 233) (Figure 4.4.7.2), customized synthetic DNA fragments were obtained from Twist Bioscience (San Fransico, CA). These synthetic DNA products had either BglII-XbaI or Kpn2I-XbaI or PstI-XbaI or BglII-XhoI restriction sites, which were subcloned into the template GBA2-339 cDNA via corresponding restriction digests and ligations.

Standard molecular cloning procedures were followed to expand all the resultant cDNA constructs. Sequences were verified by overlapping double-strand Sanger sequencing (Eurofins MWG Operon, Louisville, KY). Throughout, plasmid sequences were archived using SnapGene software (GSL Biotech LLC, Chicago, IL), which also allowed simulation of PCR reactions, HD In-Fusion cloning, restriction digests, agarose gel electrophoresis, ligations, and alignment of DNA sequence analysis data. Endotoxin-free transfection-grade plasmids were obtained with Endo-Free GeneJet Plasmid Maxi Prep Kit (Thermo Scientific, Rockford, IL) and Endo Free Plasmid Maxi Kit (Qiagen, Germany).

4.3.2 Cell Culture

U20S (human osteosarcoma), HeLa (human cervical cancer), COS-7 (African green monkey kidney), SH-SY5Y (human neuroblastomas), HEK 293 (human embryonic kidney), IMR-32 (neuroblastoma), Neuro-2a (neuroblastoma), CHO-K1 (Chinese hamster ovary), B-16 (mouse melanoma) and MIN-6 (pancreatic beta) cells were used in this study. All cells, except B-16 and CHO-K1 were maintained in a humidified

environment at 37°C and 5% CO_2. Culture and maintenance of B-16 and CHO-K1 cells have been described in Chapter 3.

Cultures of rat hippocampal neurons were prepared following the protocol described by Krueger *et al*, 2003 (176,177). Briefly, hippocampi were dissected from E18 Sprague-Dawley rat embryos, incubated with 0.03% trypsin for 15 minutes, and dissociated using a fire-polished Pasteur pipette. Cells were then plated on coverslips coated with 0.1% (w/v) poly-L-lysine (Peptides International, Louisville, KY) at a density of 3-6x10^3 cm^{-1} in Neurobasal Medium (Invitrogen, Carlsbad, CA) supplemented with 2% B-27 (Invitrogen, Carlsbad, CA), 0.05 mM glutamine, 25 µM glutamate, 5% fetal calf serum, 100 U/ml penicillin, and 100 µg/ml streptomycin. After 4 hours of plating, the medium was replaced with serum-free Neurobasal Medium supplemented with B-27 and 0.5 mM glutamine. One-third of the medium was replaced on a weekly basis until transfection. Primary neuronal cells were generously donated to us by Dr. Stefan Krueger, Professor, Department of Physiology and Biophysics, Dalhousie University.

4.3.3 Transient Transfections and Harvesting of Immortalized Cells

Transient transfections and harvesting of immortalized cells were performed as described in Chapter 3. For measuring the transection efficiency by luciferase assay, cells were co-transfected with the pCMV6 and the pNL1.3.CMV vectors at a ratio of 4:1 (w/w). pNL1.3.CMV encodes for NanoLuc luciferase, a smaller, brighter form of secreted luciferase (Promega, Madison, WI).

4.3.4 Neuronal Cell Transfection

Calcium phosphate-based transfection was used to transiently transfect primary rat hippocampal cells. At first, the coverslips were transferred from the original cell culture dishes to dishes containing the transfection medium (MEM supplemented with 1:100-diluted B-27, adjusted to 5mM $MgCl_2$ and 230 mOsM). The transfection mixes were made by adding DNA to the 2×HEBS mix (274 mM NaCl, 10 mM KCl, 1.4 mM Na_2HPO_4, 15 mM D-glucose, 42 mM HEPES, pH 7.05-7.15) in 1/10 increments and vortexing after each addition. The final mix was left to precipitate at room temperature for 20 minutes and then added to the transfection dishes containing the cover slips. After 3 hours, the coverslips were washed twice with wash buffer (HBS 0/5) and then transferred back to the original dishes containing the original medium.

4.3.5 CRISPR Knock-In

4.3.5.1 Transfection and Colony Selection

cDNAs encoding wild-type GBA2 or GBA2-Arg234* carrying a C-terminal 3×FLAG/twin-strep tag were inserted in the *AAVS1* safe harbor locus of U20S (osteosarcoma) cells using the CRISPR/Cas9 system. At first, the cDNAs of wild-type GBA2 or GBA2-Arg234* were cloned in the multiple cloning site (MCS) of AAVS1_Puro_PGK1_MCS_3xFLAG_Twin_Strep_ALT (Addgene #68375). A plasmid expressing an *AAVS1*-targeting gRNA in tandem with Cas9 was also obtained from Addgene (eSpCas9(1.1) No_FLAG_AAVS1_T2, #79888). Both plasmids were generously provided by Yannick Doyon (178).

For each kind of genomic knock-in, two million cells were co-transfected with eSpCas9(1.1) and AAVS1-Puro-PGK1-WT GBA2 or AAVS1-Puro-PGK1-

Arg234*GBA2. Cells were transfected in 10 cm dishes using Trans-IT-LT1 transfection reagent (Mirus BioLynx, Madison, WI) following the manufacturer's protocol. At 48 hours of post-transfection, cells from each 10 cm dish were split into 10×10 cm dishes. The cell culture medium was replaced with puromycin containing medium (3 µg/ml puromycin) at 72 hours of post-transfection and the media was changed every three days with fresh puromycin. The concentration of puromycin was decreased down to 0.5 µg/ml after one week of transfection and cell culture dishes were observed for the growth of puromycin-resistant colonies. When sufficient number of colonies were grown, the colonies were transferred into 24 well-plates using the filter disk-based clone-lift method (179,180). The colonies were gradually expanded to 12 well-plates and 75 cm^2-flasks until sufficient number of cells were obtained for genotyping and cryopreservation.

4.3.5.2 Genomic PCR

The template DNA used for genomic PCR was obtained from U20S cells using Wizard Genomic DNA purification Kit (Promega, Madison, WI) following manufacturer's protocol. QuickExtract DNA Extraction Solution (Epicentre, Madison, WI) was used for extraction of genomic DNA from stably transfected U2OS cells following manufacture's instruction. Briefly, 250 µl of QuickExtract solution was added to the cell pellet, pipetted up and down several times, extensively vortexed for 5 minutes, heated at 65° C temperature, vortexed again and finally heated at 98° C temperature to complete the extraction. Five µl of this extract was used for genomic PCR. Wizard-purified U20S DNA was used as control. Three forward primers and three reverse primers were used to assess the genomic integration at the AAVS1 locus (Figure 4.4.10).

4.3.6 Solubility Assessment of GBA2 in PBS

Frozen cell pellets were resuspended in PBS containing protease inhibitors (complete ULTRA EDTA-free protease inhibitor cocktails, Roche, Germany), pipetted up and down several times, and lysed using a sonic dismembrator (Artek Sytems Corporation, Farmingdale, NY). Cell lysates were kept on a roller for 30 minutes and then centrifuged in a table-top microcentrifuge at 21,000 × g for 30 minutes. The supernatant was transferred to a clean microcentrifuge tube and the remaining pellet was resuspended in PBS.

4.3.7 Immunofluorescence Staining

As described in Chapter 3.

4.3.8 Western Blot Analysis

As described in Chapter 3.

4.3.9 Blue-Native-PAGE

Frozen cell pellets were thawed, resuspended in 12.5 mM BisTris, 1.5 N HCl, 12.5 mM NaCl, 2.5% w/v Glycerol, 0.00025% Ponceau S, 1% digitonin and protease inhibitors, pipetted up and down several times, and kept on a roller at 4°C for 30 minutes to aid the protein solubilization. The lysates were clarified by centrifugation at 20,000 × g for 30 minutes at 4°C. The clear lysates were treated with Benzonase (1 unit/µl of sample) for 1 hour on ice to reduce the DNA content of the cell lysate. A final round of clarification of cell lysates was done by centrifuging again at 20,000 × g for 30 minutes.

Proteins were resolved under native conditions using premade NativePAGE™ 3-12% Bis-Tris Protein Gels (Thermoscientific). Electrophoresis was performed at 150V for three hours at 4°C using an XCell SureLock™ Mini-Cell Electrophoresis System

(Invitrogen, Burlington, ON) and a semi-dry transfer method to transfer proteins to PVDF membrane. The transfer buffer contained 25 mM bicine, 25 mM Bis-Tris, 1 M EDTA, and 0.05 mM chlorobutanol. Membranes were blocked using 5% skimmed milk in 0.1% TBST (Tris buffer saline with Tween-20) for two hours, quickly washed in methanol, and rewetted in TBST to remove excess blue G-250 blue dye and enhance the binding efficiency of the primary antibody. Incubation with the primary and secondary antibodies and developments of blots were done similarly as described under the SDS-PAGE method in Chapter 3.

4.3.10 GBA2 Assay Using Artificial Substrate

GBA2-specific enzymatic activity was measured as the *N*-butyldeoxygalactonojirimycin (*N*B-DGJ)-sensitive β-glucosidase activity as described by Ridley *et. al.* (93). Briefly, cell suspensions were incubated in presence or absence of *N*B-DGJ (Toronto Research Chemicals, North York, ON) at pH 5.8 for 15 minutes on ice. One volume cell suspension was combined with two volumes of 4.5 mM 4-methyllumbelliferyl-β-glucoside (Glycosynth,Warrington, UK) and incubated at 37°C temperature for 30 minutes. The enzymatic reaction was stopped by adding 20 volumes of 500 mM Na-carbonate (pH 10.7) and the fluorescence intensity of released 4-methylumbelliferone was measured with a Tecan Infinite M200 PRO plate reader (excitation 355 nm and emission 460 nm). Unconjugated 4-methylumbelliferone (free acid) was used as the quantitative standard.

4.3.11 Nano-Luc Luciferase Assay for Measuring Transfection Efficiency

NanoLuc luciferase activity in the transfected cells were measured using Nano-Glo® Luciferase Assay System (Promega, Madison, WI). Equal volumes (12.5 µl) of the

assay buffer and appropriately diluted cell culture media were combined in 384-well Lumitrac 200 white-bottom microtiter plates (Greiner) and incubated at 37°C temperature for 30 minutes. Luminescence of the secreted luciferase in the culture medium was measured at 460 nm by a Tecan M200Pro Plate Reader (83).

4.3.12 Cell Sorting by FACS

Adherent cells were washed twice with sterile PBS at 37°C, detached using Accutase (Invitrogen, Burlington, ON), collected in 50 ml falcon tubes, pelleted down by centrifuging at 500×g for 3 minutes, washed once with sterile PBS, followed by washing with sterile sort buffer (Ca^{++}/Mg^{++}-free Hank's Balanced Salt Solution (HBSS) with 25 mM HEPES (pH 7.4), 1% FBS (heat inactivated) and 1mM EDTA). Washed cell pellets were diluted with an appropriate volume of sort buffer and filtered through 40-micron cell strainer just before sorting. Green-fluorescent cells were sorted from non-fluorescent cells using a BD FACSAria III instrument with 488nm BLUE excitation laser, 515-545 nm detection filter, 100 µm nozzle, at 20 Psi and at 4°C, operated by FACSDiva software (version 8.02).

4.3.13 Measuring Mitochondrial Membrane Potential

4.3.13.1 Imaging Live Cells

Mitochondrial membrane potential was assessed in live cells by confocal fluorescence microscopy. U2OS (osteosarcoma) cells were seeded on 35 mm glass-bottom cell culture dishes (Ibidi, GmbH, Germany) at a density of 100,000 cells/dish and transiently transfected with cDNA constructs to co-express mClover (a green fluorescent protein expressed in the cytoplasm) and various versions of GBA2. At 48 hours post-transfection, the culture medium was replaced with FluoroBrite DMEM (Gibco, Grand

Island, NY) medium supplemented with 10% FBS and 200 µM L-glutamine. TMRM (Tetramethylrhodamine methyl ester), a red fluorescent dye sequestered by active mitochondria, was added to the culture medium to a final concentration of 25 nM, incubated for 15 minutes at 37° C and images were captured immediately using eiss LSM 510 meta confocal microscope. Parallel set of cells were combinedly treated with 10 µM FCCP (mitochondrial membrane depolarizer) and 25 nM TMRM for 15 minutes at 37° C temperature.

4.3.13.2 Quantitative Image Analysis

ImageJ was used for quantification of fluorescent intensity of TMRM of transfected cells in captured images. Contours were drawn around individually selected images and integrated density was measured for each cell. Background integrated density was subtracted from the cellular integrated density for each field of analysis. Total 30 cells were quantified in this way for each condition (TMRM only, and TMRM in presence of FCCP) for each GBA2 construct and the differences were noted as the quantifications of mitochondrial membrane potentials.

4.3.14 Sample Preparation for Electron Microscopy

All steps of sample preparation were performed on ice and cells were treated as a monolayer until the dehydration step to retain the cellular features. Cells were briefly washed with 2% glutaraldehyde at 37°C temperature, fixed with cold 2% glutaraldehyde in sodium cacodylate buffer for one hour on ice, washed with ice-cold sodium cacodylate buffer (pH 7.4), followed by washing with 20 mM glycine in sodium cacodylate buffer. Cells were stained with freshly prepared staining mixture (0.5 mg/ml diaminobenzidine DAB and 0.03% H_2O_2) for 25 minutes. The DAB reaction mixture was carefully

aspirated and discarded into a bleach solution. Cells were washed twice with cacodylate buffer and incubated with freshly prepared 2% osmium tetroxide (OsO_4) for 30 minutes. OsO_4 was very carefully discarded into 0.5M sodium sulfite solution, cells were washed with ice-cold miliQ water and treated with 2% uranyl acetate overnight in the dark. Uranyl acetate was washed off with ice cold water and cells were gently scraped off, transferred to Eppendorf tubes and centrifuged at 5000×g for 15 minutes. The resulting pellet was dehydrated with a graduated series of acetone and embedded in Epon Araldite resin. The resin was cured at 60°C for 48 hours prior to sectioning. Thin sections were cut using Reichert-JungUltracut E Ultramicrotome with a diamond knife (100nm thick) and placed on 300 mesh copper grids which were then stained with 2% uranyl acetate and lead citrate. Samples were viewed using JEOL JEM 1230 Transmission Electron Microscope at 80kV and images were captured using a Hamamatsu ORCA-HR digital camera.

4.3.15 Quantitative Image Analysis for Co-Localization Assessment

ImageJ was used for determining the colocalization coefficient of WT and mutant forms of GBA2. Confocal fluorescence images captured by LSM510 or LSM510 meta microscope were opened in ImageJ, channels were split, a contour was drawn around the cell of interest in one channel and added to the other channel by region of interest (ROI) manager, then rest of the field of the image was cleared and Mander's overlap co-efficient (MOC) values were obtained by using the ImageJ JACoP plug-in.

4.4 Results

4.4.1 Expression of GBA2 Mutants

4.4.1.1 SPG46-Associated GBA2 Mutants Are Expressed at Different Levels

To characterize SPG46-associated *GBA2* mutations, I engineered ten mutations in the GBA2 cDNA. Five of the these were truncation mutants (Tyr121*, Trp173*, Arg234*, Arg340*, and Arg870*) having premature stop codons and five were point mutants (Phe419Val, Asp594His, Arg630Trp, Gly683Arg, and Arg873His) containing single-nucleotide changes. The cDNAs of WT and mutant GBA2s carried a C-terminal myc-FLAG tag, except Arg870*. I introduced the cDNAs of WT and mutant forms of GBA2 in COS-7 and HeLa cells by transient transfections and compared their levels of expression by western blot, which were quite variable (Figure 4.4.1.1). The shortest truncation mutant Tyr121* was expressed abundantly whereas the Trp173* mutant was expressed at a much lower level compared to WT GBA2 in both cell lines. The levels of expression of the Arg234* and Arg340* mutants varied in between the two cell lines. Both mutants were expressed at a higher level in COS-7 cells, but at a comparable level to WT GBA2 in HeLa cells. The longest truncation mutant Arg870* lacked only 58 amino acids from the C-terminus of WT GBA2 and was expressed at a moderately reduced level in both cell lines in comparison to WT GBA2. The point mutants followed similar patterns of expression in COS-7 and HeLa cells. All but the Arg630Trp mutant were expressed at a lower level in both cell lines. The expression level of Arg630Trp was comparable to that of WT GBA2, whereas the Gly683Arg, Phe419Val, Arg873His, and Asp594His mutants were detected at lower amounts.

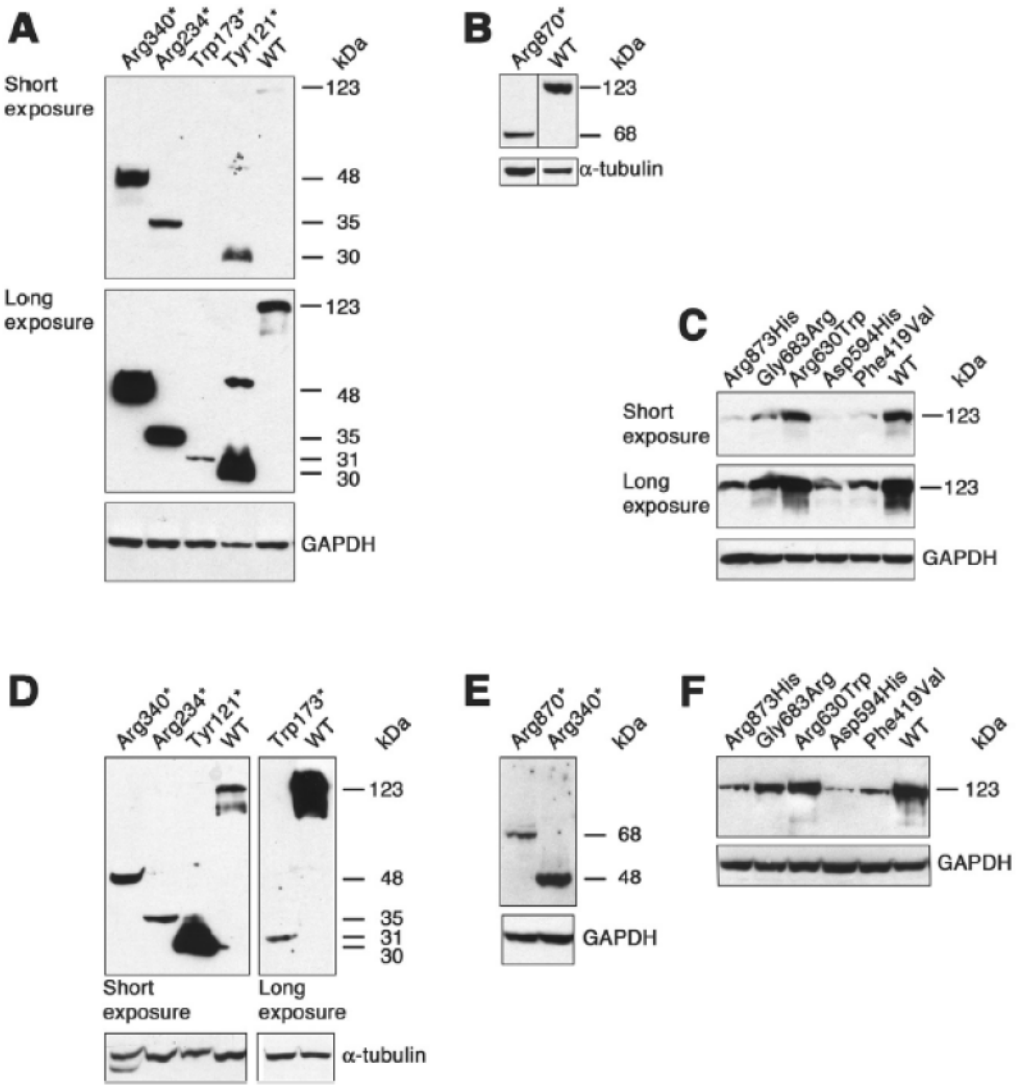

Figure 4.4.1.1. Expression of WT and mutant forms of GBA2 in COS-7 and HeLa cells. Western blot analysis of WT and mutant GBA2 expressed in COS-7 cells (A–C) and HeLa cells (D–F). (A) The truncation mutants Arg340*, Arg234*, Trp173*, and Tyr121* and WT GBA2 were expressed in COS-7 cells (anti-FLAG), the Trp173* mutant was detectable upon prolonged exposure due to its very low level of expression. (B) The Arg870* mutant and WT GBA2 was detected in COS-7 cells with an anti-GBA2 antibody. (C) The missense GBA2 mutants were expressed at variable levels in COS-7 cells (anti-FLAG antibody). The poorly expressed missense mutants were only seen after extended exposure. (D) The truncation mutants Arg340*, Arg234*, Trp173*, Tyr121*, and WT GBA2 were expressed in HeLa cells (anti-FLAG antibody). Trp173* was visible upon prolonged exposure. (E) Detection of the Arg340* and Arg870* mutant in HeLa cells by the anti-GBA2 antibody. (F) Variable levels of expressions of the missense GBA2 mutants in HeLa cells (anti-FLAG antibody). Typical results are shown based on multiple independent experiments [Figure source Sultana *et al.* (83)].

The apparent molecular weights of the truncation mutants varied from their expected molecular weights. The apparent molecular weight of the two shortest nonsense mutants, Tyr121* and Trp173*, were 30 and 31 kDa respectively (Figure 4.4.1.1), higher than their expected molecular weights of 16 and 22 kDa. The truncation mutants Arg234* and Arg340* migrated as 35 and 48 kDa proteins on SDS-PAGE respectively, close to their expected molecular weights of 30 and 41 kDa respectively. The largest truncation mutant Arg870* appeared as a 68 kDa protein on western blots which was much lower than its theoretical molecular weight of 98 kDa. WT GBA2 and the point mutations appeared as 123 kDa molecular weight forms in western blots, close to their expected molecular weight of 108 kDa. In all cases, I included the C-terminal myc-FLAG tags while calculating the expected molecular weights (83). The changes in the molecular weights indicated the possibility of post-translational modifications of overexpressed GBA2 mutants in cultured cells.

4.4.1.2 Transfection Efficiencies of the GBA2 Mutants Are Comparable to WT GBA2

To evaluate whether the variation in the level of expression of the mutant proteins was related to their transfection efficiencies, I used a luciferase reporter assay. HeLa and COS-7 cells were co-transfected with GBA2 cDNAs and an expression vector for the NanoLuc luciferase. The luminescence of the secreted luciferase was measured to quantify of the transfection efficiency. The luciferase activities of COS-7 cells co-expressing NanoLuc with WT or mutant GBA2 were similar to those of cells only expressing NanoLuc (Figure 4.4.1.2).

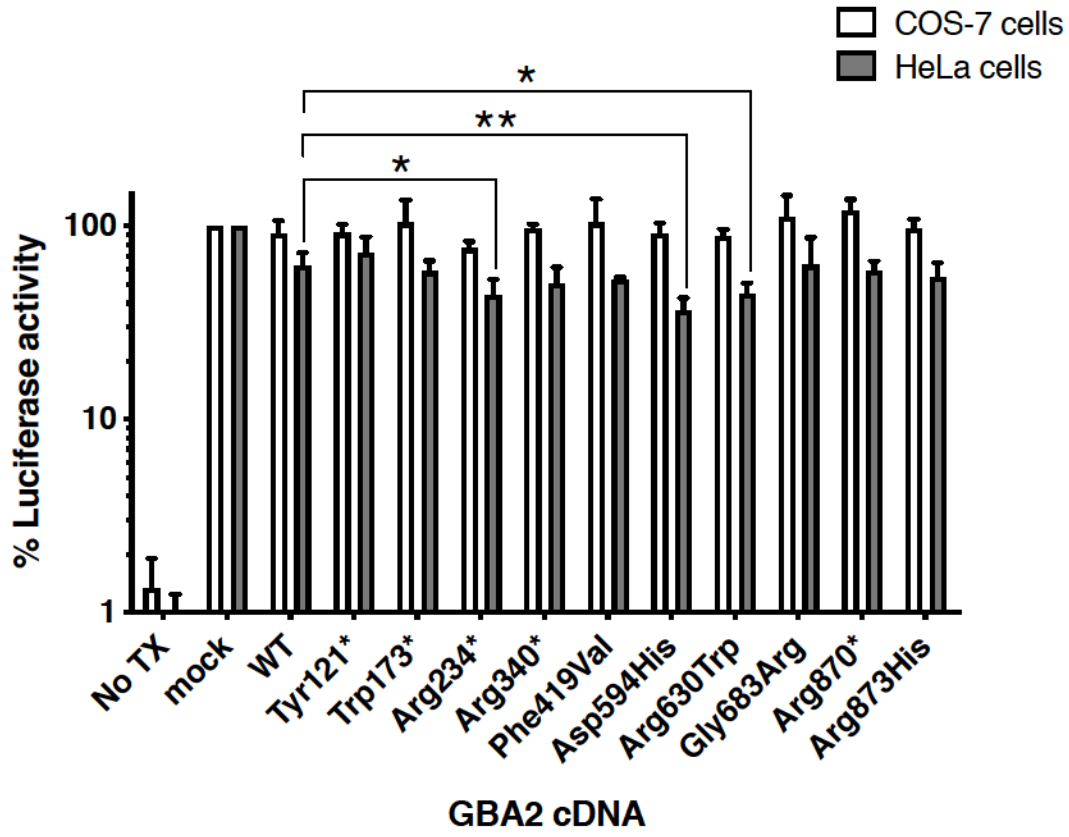

Figure 4.4.1.2. Transfection efficiencies of WT GBA2 and the mutant forms of GBA2 are comparable. Cells were transfected exclusively with the luciferase expression vector (mock), or in combination with various forms of GBA2. NanoLuc luciferase activities of co-transfected cells are presented as the percentage of the luciferase activity of mock-transfected cells. Luciferase activities of COS-7 cells expressing WT or mutant GBA2 were at the similar level of those of the mock-transfected COS-7 cells ($P > 0.35$). In HeLa cells, NanoLuc luciferase activities expressing WT or mutant GBA2 were lower compared to mock-transfected cells ($P \leq 0.0002$). However, luciferase activities of HeLa cells expressing mutant GBA2 were similar ($P > 0.2$) to cells expressing WT GBA2, except for cells expressing Arg234*, Asp594His, and Arg630Trp (*, $P < 0.05$; **, $P < 0.001$). Results presenting the average + SD of three individual experiments. Statistical significances were analyzed via one-way ANOVA. (Image source Sultana *et al.* (83)).

HeLa cells co-transfected with the cDNAs of WT or mutant GBA2 and NanoLuc had lower level of luciferase activity compared to the mock-transfected cells. The luciferase activities of cells expressing different forms of GBA2 ranged from 73% to 37% of total luciferase activity of mock-transfected cells. HeLa cells expressing Arg234*,

Asp594His, and Arg630Trp mutants had 75%, 64%, and 76% of luciferase activity, respectively, compared to the luciferase activity of cells expressing WT GBA2, although the expression of Arg630Trp was higher compared to WT GBA2 at protein level.

4.4.1.3 Mutant Forms of GBA2 Are Poorly Soluble

To assess whether WT and mutant forms of GBA2 were similarly soluble, I homogenized COS-7 cells expressing WT or mutant GBA2 in phosphate-buffered saline (PBS) in the absence of any detergent, centrifuged in at 21,000 × g for 30 minutes and resolved the soluble and insoluble fractions through SDS-PAGE. All but the Tyr121* truncation mutants and WT GBA2 were mostly present in the insoluble fractions (Figure 4.4.1.3). Tyr121* was highly soluble in PBS. Among the point mutants, Arg630Trp and Arg873His were scarcely present in the soluble fraction. Solubility of Asp594His and Gly683Arg was very comparable to that of WT GBA2.

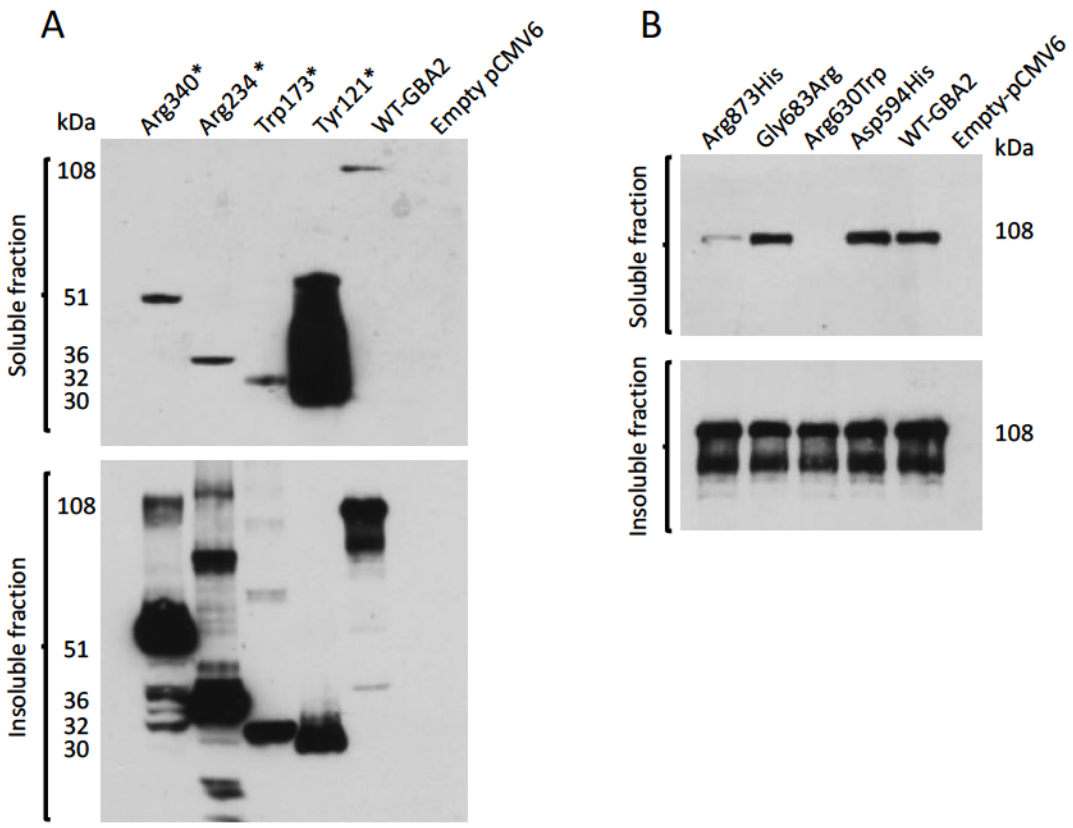

Figure 4.4.1.3. WT GBA2 and GBA2 mutants are poorly soluble in PBS. WT and mutant forms of GBA2 were overexpressed in COS-7 cells, homogenized in PBS and soluble and insoluble fractions were analysed by western blot (anti-FLAG). 10 μg of total protein was loaded per lane. (A) Solubility of truncated GBA2 mutants in PBS. The Tyr121* truncation mutant was mostly soluble. WT GBA2 and other nonsense mutants were predominantly present in the membrane-bound fractions. (B) Solubility of missense GBA2 mutants in PBS. Missense mutants were predominantly insoluble.

4.4.2 Enzymatic Activity of SPG46-Associated GBA2 Mutants

4.4.2.1 GBA2 Mutants Do Not Elevate GBA2 Activity in Cultured Cells

To assess whether the SPG46-associated GBA2 mutants are enzymatically active, I measured the GBA2 activity of COS-7 and HeLa cells overexpressing mutant forms of GBA2. Upon overexpression, GBA2 mutants did not elevate the overall β-glucosidase activity above the background, whereas WT GBA2 elevated the GBA2 activity by 88- and 66-fold in HeLa and COS-7 cells, respectively (Figure 4.4.2.1 A). The enzymatic

activities of all but Gly683Arg GBA2 mutants were similar when overexpressed in HeLa and COS-7 cells and comparable to the endogenous GBA2 activity of these cell lines (mock transfected cells). These enzyme activity data suggest that all pathogenic variants of GBA2 were enzymatically inactive. Overexpression of the Gly683Arg mutant elevated GBA2 activity slightly (1.5-fold) above the endogenous levels in COS-7 and HeLa cells (83). We got similar results when the GBA2 activity was measured in patients' lymphoblasts homozygous for the Arg340* truncation mutation and the Arg630Trp point mutation. In both cases, we were unable to detect any GBA2 activity (Figure 4.4.2.1 B).

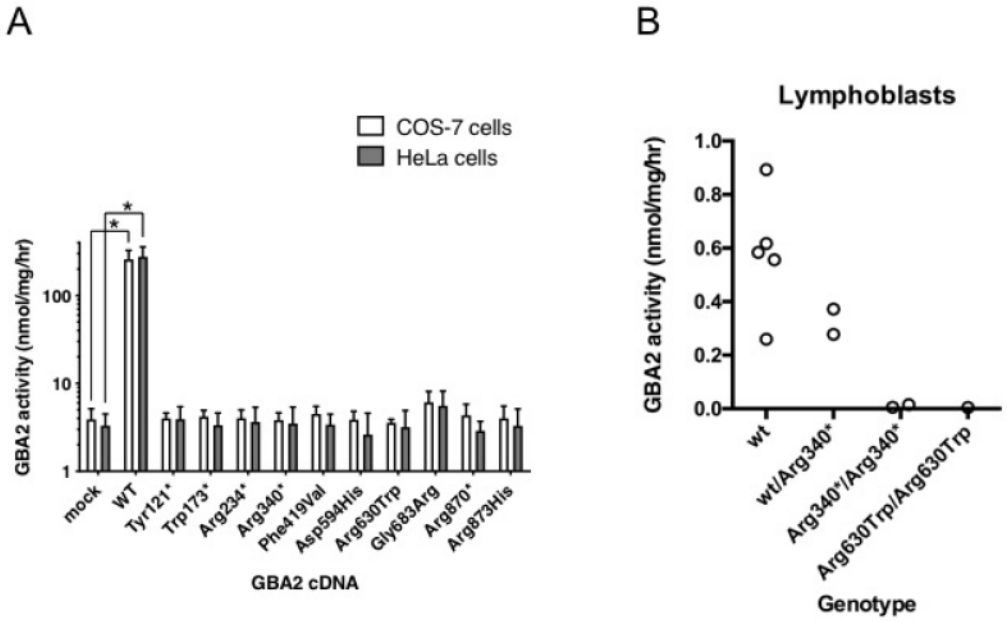

Figure 4.4.2.1. GBA2 activity of WT and SPG46-associated GBA2 mutants. (A) GBA2 activity of WT and ten GBA2 mutants in HeLa and COS-7 cells. Mock transfected cells were transfected with the empty pCMV6 vector. Overexpression of WT GBA2 elevated GBA2 activity above the endogenous enzyme activity in mock-transfected cells (*, $P < 0.0001$). In contrast, GBA2 activity was not increased above the background ($P \geq 0.999$) upon overexpression of nonsense and missense GBA2 mutants. GBA2 activities were quantified as average values + SD of three independent experiments and plotted on a logarithmic scale on the graph (Image source: Sultana *et al*. (83)). Statistical significances were analyzed via one-way ANOVA. (B) GBA2 activity of patient's lymphoblasts homozygous for Arg340* and Arg630Trp GBA2 mutations. Residual enzyme activity was nearly undetectable in homozygous mutant cells.

4.4.2.2 Co-Expression of GBA2 Mutants with WT or Active-Site Mutant of GBA2

To assess whether enzyme activity of SPG46-associated GBA2 mutants is affected by the presence of WT GBA2 or any non-pathogenic variant of GBA2, I co-expressed the pathogenic variants of GBA2 with WT GBA2 and Glu527Gln GBA2, an active-site mutant of GBA2. Glu527Gln is a full length and enzymatically inactive variant of GBA2 which has not been reported in SPG46 (80,86,181). During co-transfection, I used plasmid DNAs at a 1:1 ratio for each combination of plasmids, keeping the total DNA content constant. Upon co-expression of pathogenic variants of GBA2 either with WT GBA2 or Glu527Gln, total GBA2 activity was around 50% of the GBA2 activity of cells exclusively expressing WT GBA2 (Figure 4.4.2.2). This is due to the fact that I used half amount of WT GBA2 cDNA for the co-transfections to keep the total DNA amount constant during the transfection. When pathogenic variants of GBA2 were co-expressed with the active site mutant of GBA2 (Glu527Gln), no additional enzymatic activity was observed. In the co-transfected cells, the maximum amount of GBA2 activity was obtained when WT GBA2 was co-transfected with the Gly683Arg missense mutant (Figure 4.4.2.2). It should be noted here that, this GLy683Arg mutant is associated with milder phenotype in patients and showed some GBA2 activity in initial enzyme activity assays (Figure 4.4.2.1) and also formed a dimer like the WT-GBA2 under native conditions (Figure 4.4.4). These results suggest that WT or other non-pathogenic variant of GBA2 have no effect on the enzymatic activity of pathogenic variants of GBA2 when co-expressed (Figure 4.4.2.2). I have not assessed cellular expression levels of WT and mutant forms of GBA2 by western blot when co-expressed in cultured cells.

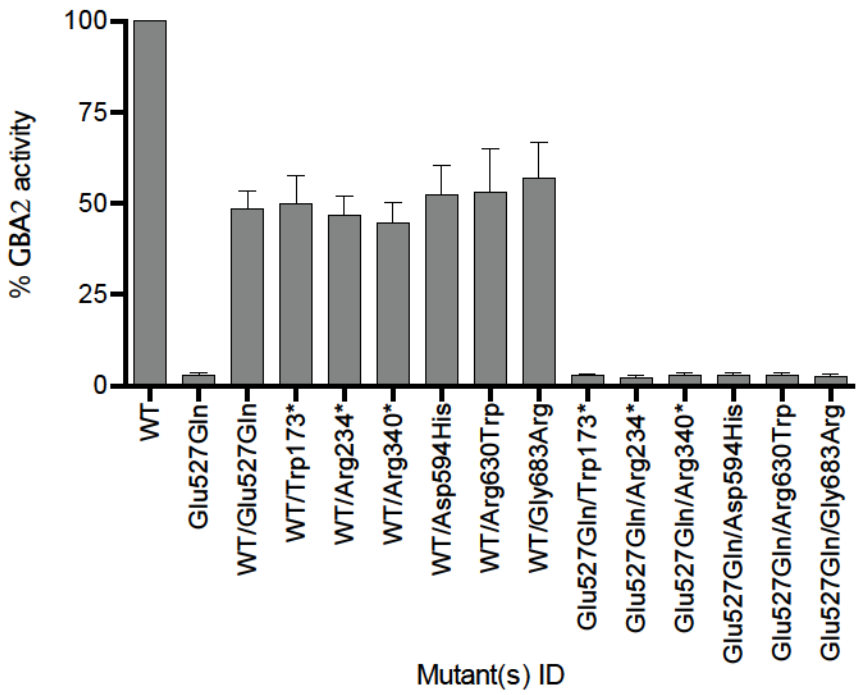

Figure 4.4.2.2. GBA2 activity of HeLa cells co-expressing pathogenic GBA2 mutants with WT or an active-site mutant of GBA2. GBA2 activity was measured in HeLa cells overexpressing WT GBA2, active-site mutant of GBA2, and co-expressing pathogenic variants of GBA2 with WT or active-site mutant of GBA2. GBA2 activity of cells co-expressing Gly683Arg mutant and WT GBA2 was 56.1% of the total GBA2 activity of cells expressing only WT GBA2; all other mutants showed less than 50% enzyme activity when co-expressed with WT GBA2. Data representing the average GBA2 activities +SD of three independent experiments and plotted as a percentage total GBA2 activity of cells overexpressing only WT GBA2.

4.4.3 GBA2 Mutants are Ubiquitinated and Undergo Proteasomal Degradation

4.4.3.1 MG-132 Treatment Recovers Poorly Expressed GBA2 Mutants

To assess whether the mutant forms of GBA2 were undergoing proteasomal degradation, I treated HeLa cells expressing WT and mutant versions of GBA2 with MG-132, a proteasomal degradation inhibitor (182,183), and compared the levels of expression of the proteins by western blot analysis. Four GBA2 mutants (Trp173*, Arg234*, Gly683Arg and Asp594His) were used in this experiment. Among those four GBA2 mutants, Arg234* had a higher level of expression and the other three had lower

levels of expression compared to WT GBA2 when their expression levels were initially assessed in COS-7 and HeLa cells (Figure 4.4.1.1). The Trp173* and Asp594His mutants were expressed at such a low level that the proteins were detectable on western blots only after very long exposures. Treatment with MG-132 increased the levels of expression of all four mutants whereas the level of expression of WT GBA2 remained comparable after treating with MG-132 (Figure 4.4.3.1). The Trp173* and Arg234* truncation mutants recovered highly upon treatment with MG-132 (Figure 4.4.3.1). At 3 μM, MG-132 elevated the levels of expression of Trp173* and Arg234* by 7.8- and 3.6-fold, respectively, while the Asp594His and Gly683Arg mutants were 2.6- and 1.5-fold increased, respectively. Less prominent results were obtained upon treatment with lactacystin, another proteasomal degradation inhibitor (184,185) (data not shown). These results suggest that SPG46-associated GBA2 mutants undergo proteasomal degradation, and the truncation mutants are more prone to degradation compared to the full-length point mutants.

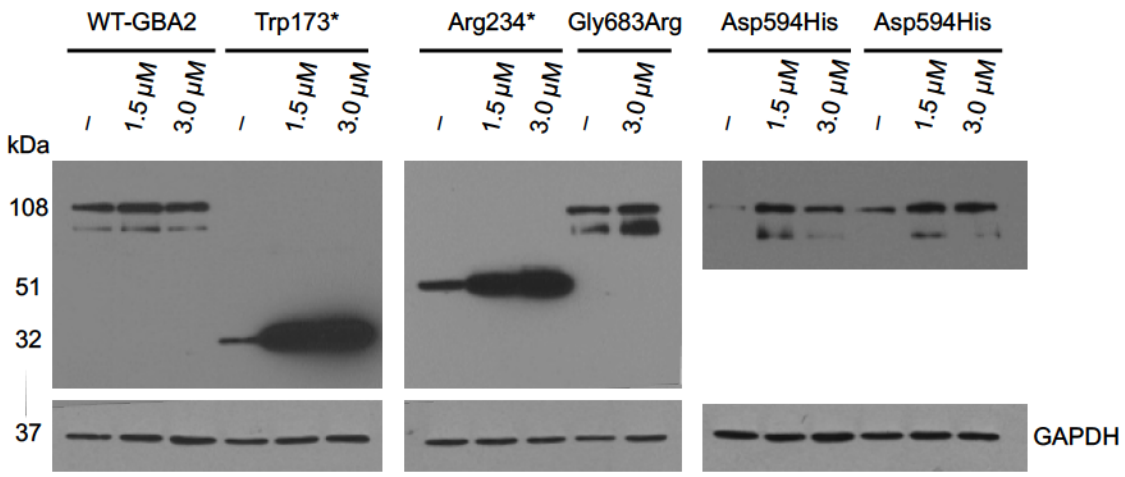

Figure 4.4.3.1. MG-132 recovers poorly expressed GBA2 mutants. Western blot analysis (anti-FLAG) of HeLa cells expressing WT and mutant forms of GBA2 treated with MG-132 for 24 hours 24 hours post-transfection. Protein levels of Trp173*, Arg234*, Gly683Arg and Asp594His increased upon treatment with MG-132.

4.4.3.2 MG-132 Treatment Increases the Levels of Ubiquitinated Proteins

As GBA2 mutants underwent proteasomal degradation in cultured cells, it was likely that the mutant proteins were post-translationally modified, leading to their proteasomal degradations. One of the most common intracellular protein degradation pathways is the ubiquitin-proteasome pathway. Ubiquitin, a small 8.6 kDa protein acts as a molecular marker for the recognition of misfolded, aggregation-prone or damaged proteins (186,187). The Proteasome is a protease complex that hydrolyses proteins in a very selective and processive manner (188-190). To assess whether GBA2 mutants were ubiquitinated, I re-probed the blots prepared with the MG-132-treated HeLa cells with an anti-ubiquitin antibody. The blots showed enhanced signals of ubiquitinated proteins at the same positions where the mutant proteins were expected (Figure 4.4.3.2).

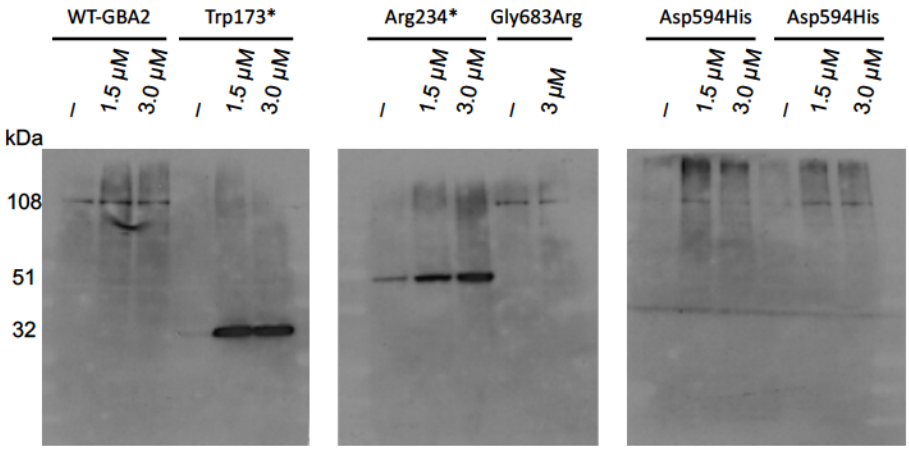

Figure 4.4.3.2. GBA2 mutants are ubiquitinated. WT and mutant forms of GBA2 were expressed in HeLa cells, treated with MG-132, and analyzed by western blot (anti-ubiquitin). The Trp173* and Arg234* mutants showed distinct increases in ubiquitination upon treatment with MG-132, while the Asp594His mutant was moderately ubiquitinated.

These data indicate that some of the GBA2 mutants are likely to be ubiquitinated and degraded through the ubiquitin-proteasome pathway. Complementary experimental approaches are required to confirm the ubiquitination of GBA2 mutants.

4.4.4 Native Structures of GBA2 Mutants

To assess whether the native conformations of GBA2 mutants were different from that of WT GBA2, I analyzed HeLa cells expressing WT and mutant versions of GBA2 by blue-native polyacrylamide gel electrophoresis. Under native conditions, WT GBA2 formed a discrete band corresponding to a molecular weight of 240 kDa, which was twice its molecular weight of 120 kDa under denaturing conditions. This result indicates the possibility of WT GBA2 forming a dimer in native state (Figure 4.4.4). In contrast, all SPG46-associated GBA2 mutants appeared as high-molecular weight streaks on native gel. None of the GBA2 mutants exhibited a defined molecular mass. The only exception was the Gly683Arg missense mutant that was also present as the 240 kDa form like WT GBA2, along with a high molecular weight complex.

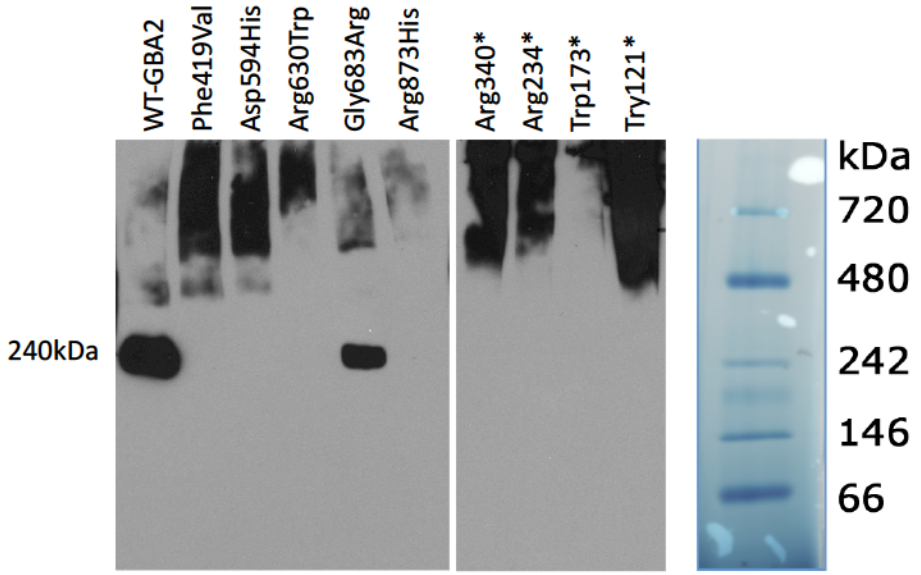

Figure 4.4.4. Native conformations of WT and mutant forms of GBA2. HeLa cells were transfected with WT and mutant forms of GBA2, homogenized in lysis buffer containing 5% digitonin, resolved by 4-16% bis-tris native gels and analysed by western blot (anti-FLAG). WT GBA2 and the Gly683Arg mutant migrated as a 240 kDa dimer. The other mutants were present as high molecular weight complexes (molecular mass of 500 kDa and above).

4.4.5 Cellular Localization of Nonsense GBA2 Mutants

Human GBA2 and zebrafish gba2 were expressed at the plasma membrane of SH-SY5Y cells (Figure 4.4.5.1) (191). WT GBA2 showed a similar pattern in COS-7 and HeLa cells (Figure 4.4.5.2). However, the expression patterns of the truncation mutants were different. All but Arg870* truncation mutants showed a punctate expression pattern. The sizes of the puncta were variable, ranging from small, compact ones to larger, globular shapes. A minor number of cells expressing the truncation mutants showed a combination of punctate and overall expression pattern (Figure 4.4.5.2). The cellular expression patterns of the missense mutants were similar to the expression pattern of WT GBA2 (Figure 4.4.5.1).

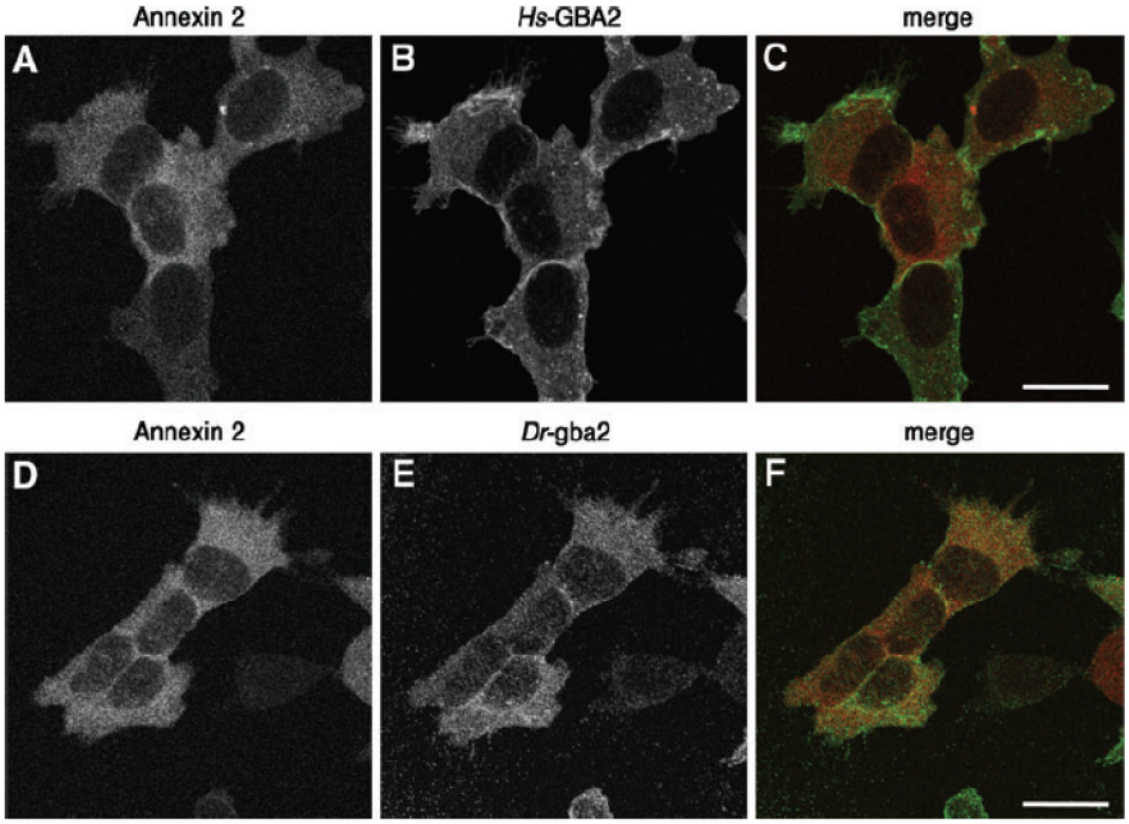

Figure: 4.4.5.1. Immunolocalization of human and zebrafish GBA2. SH-SY5Y cells stably expressing FLAG-tagged human GBA2 (Hs-GBA2) (A–C) and FLAG-tagged zebrafish gba2 (Dr-gba2) (C, D, F) were stained for annexin II, a plasma membrane protein (A, D; red in C, F) and the FLAG/ DYK epitope (B, E; green in C, F). Scale bar, 20 μm. [image source: Sultana ***et al***. (191)].

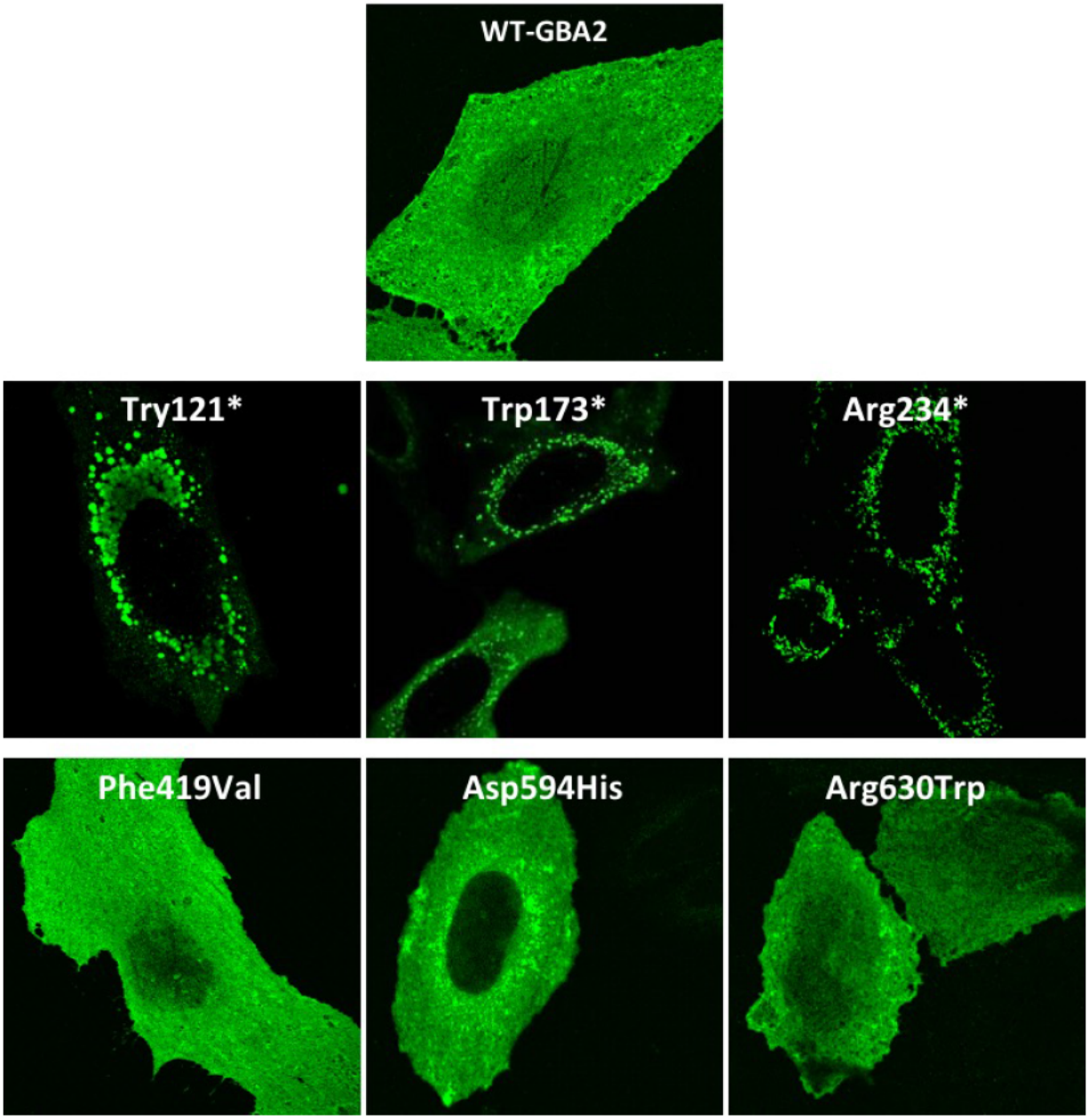

Figure 4.4.5.1. Expression patterns of WT and mutant forms of GBA2 in HeLa cells. WT and mutant forms of GBA2 were overexpressed and immunostained using an anti-DYK antibody. Representative images for WT GBA2, three nonsense mutants (Tyr121*, Trp173* and Arg234*) and three missense mutants (Phe419Val, Asp594His and Arg630Trp) are shown here.

4.4.6 Truncated GBA2 Mutants and Mitochondria

4.4.6.1 Truncated GBA2 Mutants Cause Mitochondrial Fragmentation and Colocalize with Fragmented Mitochondria

To further investigate the cellular localization of the GBA2 mutants, I co-stained HeLa cells expressing WT or mutant versions of GBA2 with anti-FLAG/anti-DYK (for GBA2) antibodies and different organelle markers (anti-calreticulin for endoplasmic reticulum, anti-GM130 for the Golgi, anti-annexin II for the plasma membrane, anti-LAMP1 for lysosomes, anti-EEA1 for endosomes, anti-LC3B for autophagosomes, and anti-cytochrome c for mitochondria). Organelle staining revealed that cells expressing WT GBA2 had regular mitochondria, whereas cells expressing the truncated GBA2 mutants had fragmented mitochondria. In addition, the GBA2 truncation mutants colocalized with the fragmented mitochondria (Figure 4.4.6.1.1 and Figure 4.4.6.1.2). Staining with COX IV and TOMM20, two other mitochondrial markers, confirmed the observations obtained with anti-cytochrome c (image not shown). These observations (fragmented mitochondria in cells overexpressing the truncated mutants and mitochondrial localization of the truncated mutants) were also made in COS-7 (monkey kidney cells), SH-SY5Y (human neuroblastoma), IMR-32 (human neuroblast), Neuro-2A (mouse neuroblast), CHO-K1 (Chinese hamster ovary), 293T (human kidney), U2OS (osteosarcoma) and primary neuronal cells (rat hippocampal neurons, Figure 4.4.6.1.3), indicating that the effects caused by the truncated GBA2 mutants are not restricted to one cell type.

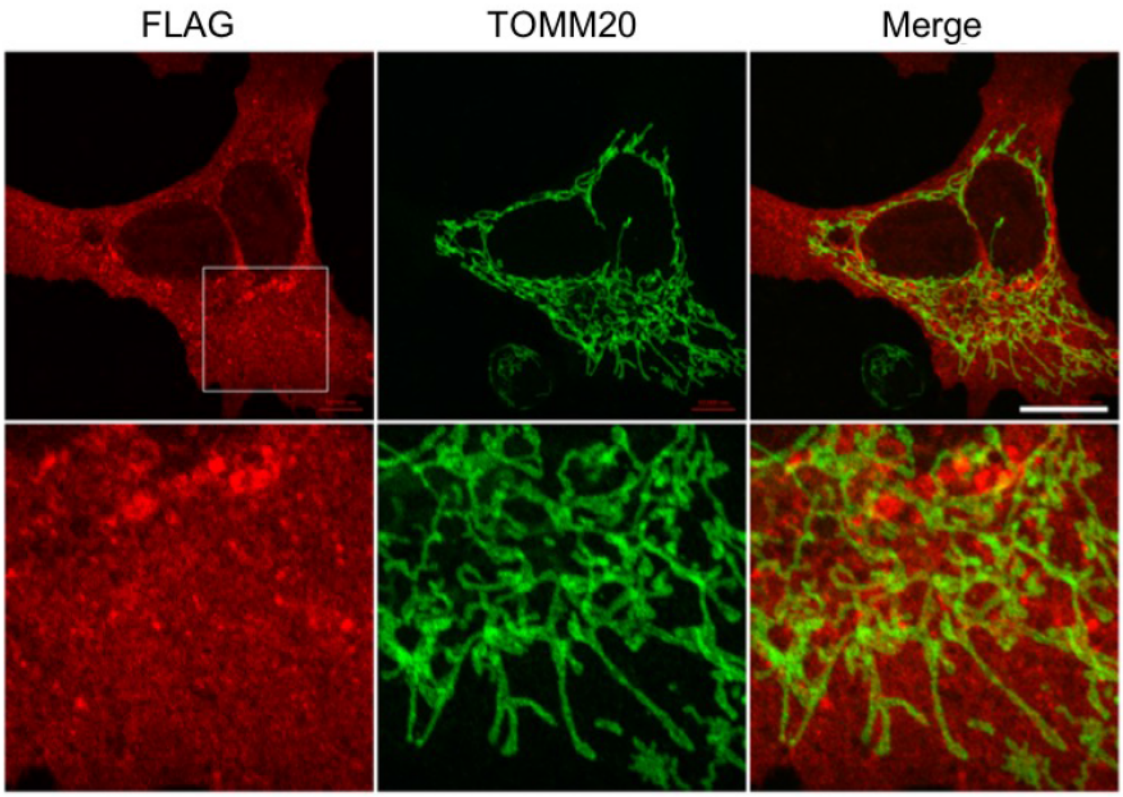

Figure 4.4.6.1.1. WT GBA2 does not cause mitochondrial fragmentation.
Osteosarcoma (U2OS) cells were transiently transfected with the cDNA of WT GBA2 and immunostained against anti-FLAG (red channel) and anti-TOMM20 (green channel) at 48 hours of post-transfection. Scale bar 20 μm.

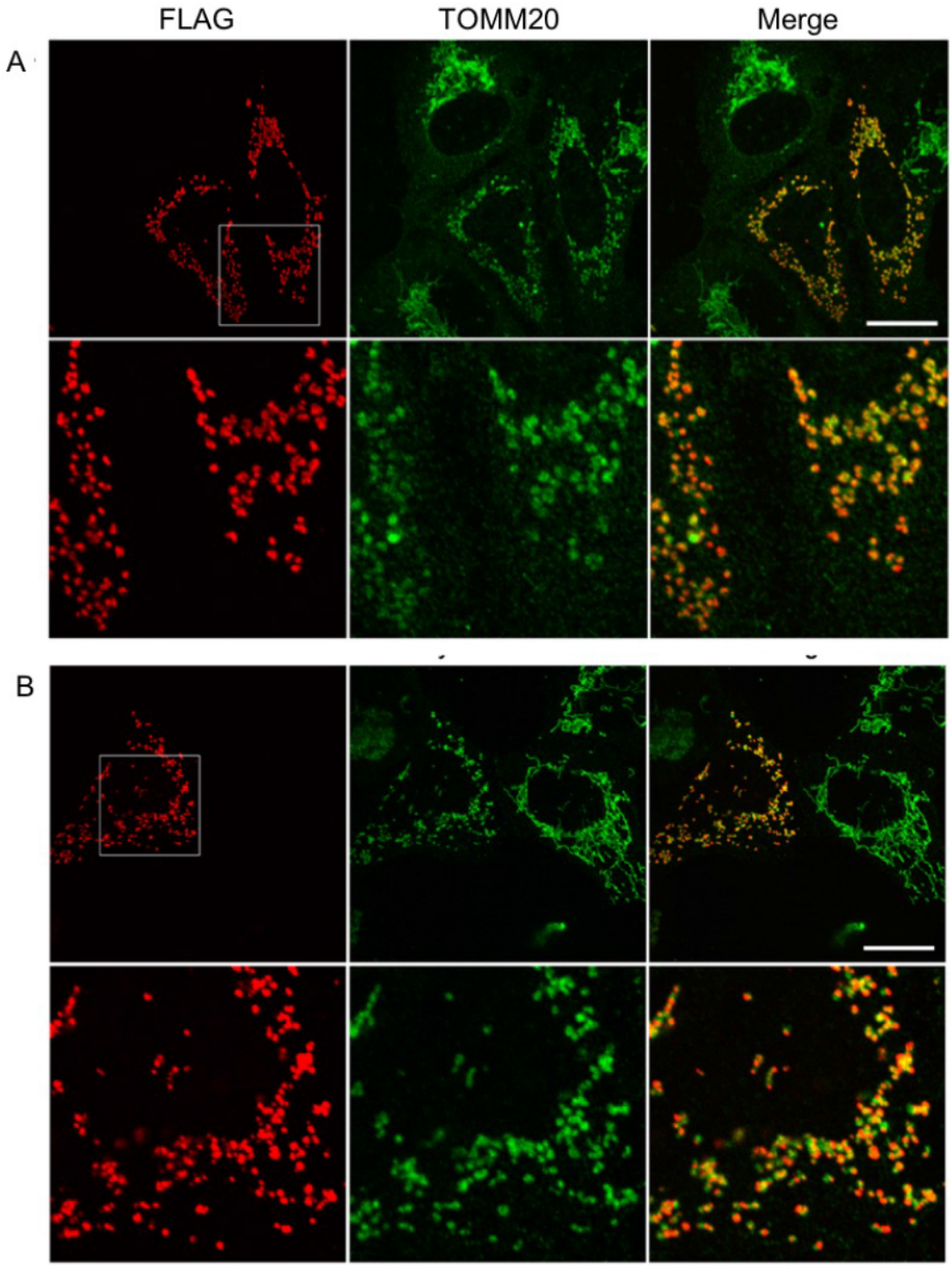

Figure 4.4.6.1.2. Truncated GBA2 mutants cause mitochondrial fragmentation. Osteosarcoma (U2OS) cells were transiently transfected with the cDNA of (A) Arg234*-GBA2 and (B) Arg340*-GBA2 and immunostained with anti-FLAG (red channel) and anti-TOMM20 (green channel) at 48 hours of post-transfection. Scale bar, 20 μm.

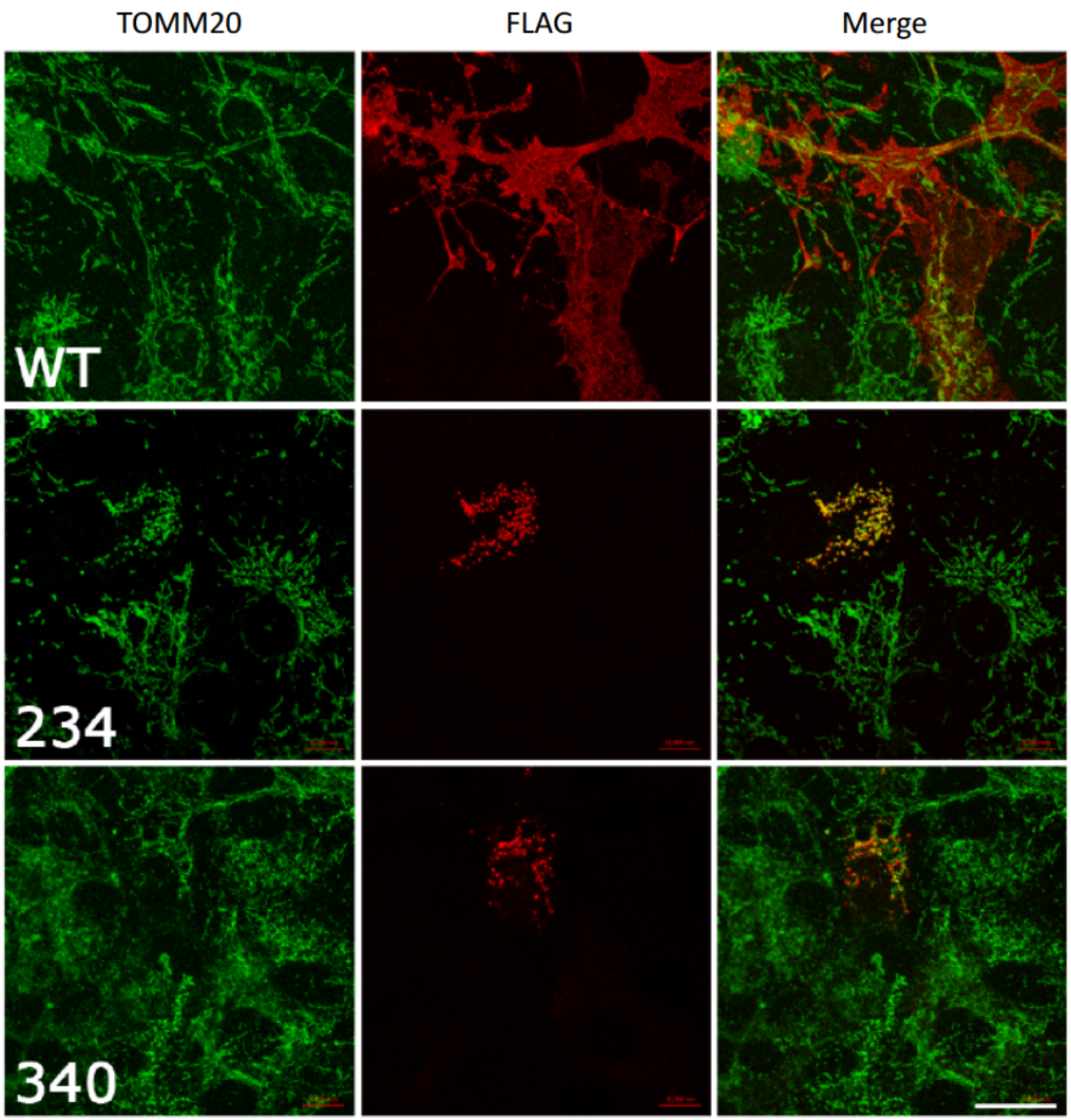

Figure 4.4.6.1.3. Expression of WT GBA2, Arg234* and Arg340* truncation mutants in rat hippocampal neurons. Rat hippocampal cells were transiently transfected with the cDNA of WT GBA2, Arg234*-GBA2 and Arg340*-GBA2 and immunostained with anti-FLAG (red channel) and anti-TOMM20 (green channel) at 48 hours of post-transfection. Scale bar, 20 μm.

4.4.6.2 Frameshift Mutation and Gluco-Hydrolase Domain Mutations Are Not Associated with Mitochondrial Abnormalities

A frameshift mutation in *GBA2* (Met510Valfs*17) has been reported in Marinesco-Sjögren-like Syndrome, a movement disorder having close clinical resemblance with SPG46 (119). It was of interest to examine the effect of this frameshift GBA2 mutant on the mitochondrial morphology. To examine the effect of non-SPG46-associated GBA2 truncation mutants on mitochondrial morphology of cultured cells, our lab generated two truncated variants of GBA2. The mutants contained stop codons after amino acids 471 or 501. The cDNAs of these three mutants, Met510Valfs*17, GBA2-Ser471, and GBA2-Ser501, contained an N-terminal streptactin tag (Figure 4.4.6.2.1A). The N-terminal TST tag was added to these constructs with the purpose of tandem affinity purification of these mutant proteins for further analysis. All three mutants were well detected in U2OS cells (Figure 4.4.6.2.1B) and did not cause any abnormal mitochondrial features (Figure 4.4.6.2.2).

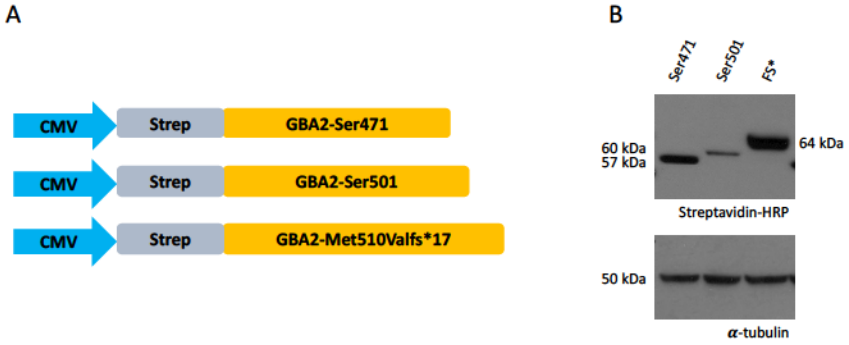

Figure 4.4.6.2.1. Glycohydrolase domain mutants and a frameshift mutant of GBA2. (A) Schematic presentation of the glycohydrolase domain mutants, GBA2-Ser471 and GBA2-Ser50, and the frameshift mutant GBA2-Met510Valfs*17; all mutants contained an N-terminal streptactin tag and were expressed under the strong CMV promoter. (B) Western blot analysis of osteosarcoma cells expressing the frameshift and domain mutants. FS* = frameshift mutation (GBA2-Met510Valfs*17). Blots were developed against streptavidin-HRP.

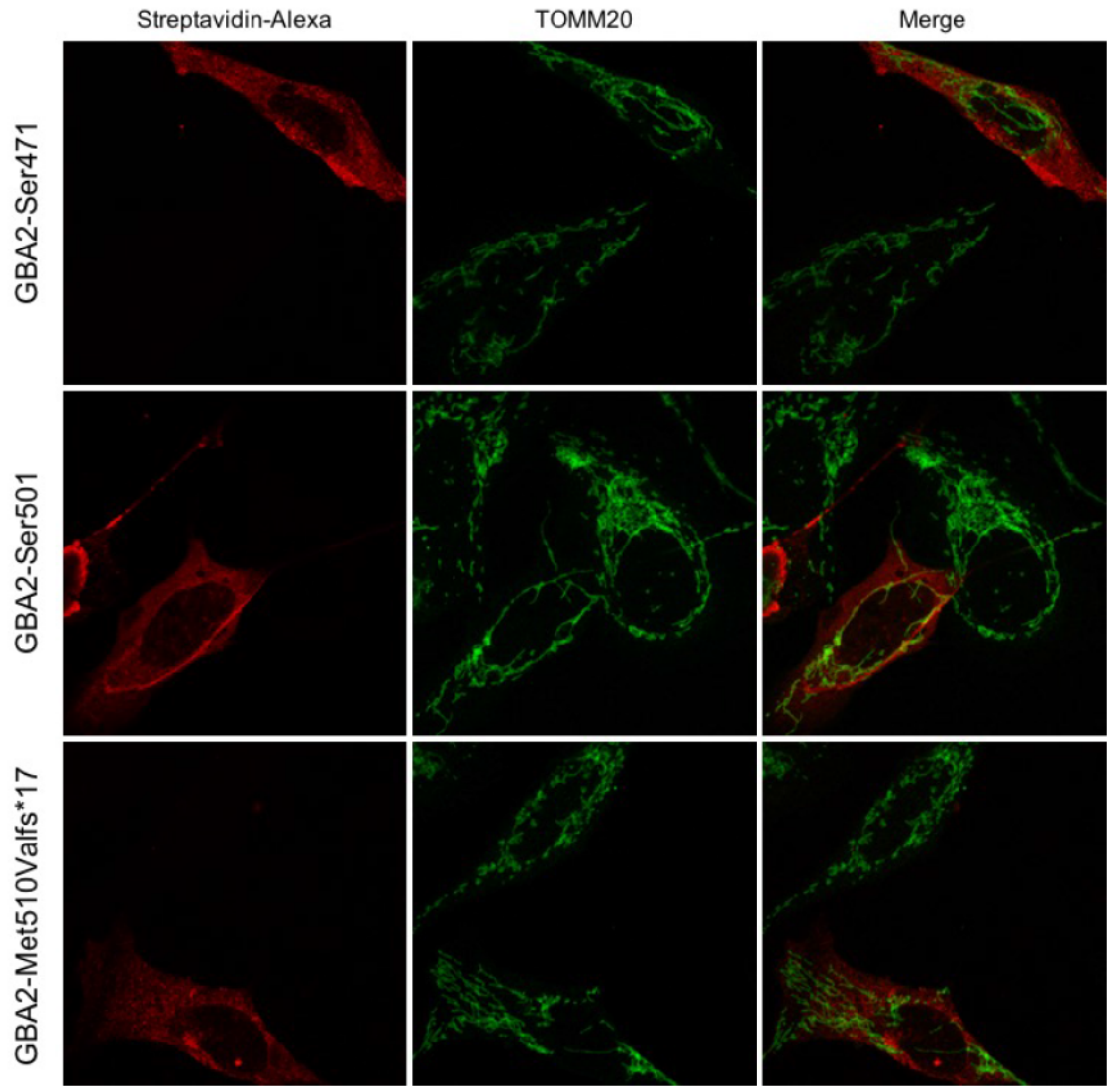

Figure 4.4.6.2.2. Glycohydrolase domain mutants and a frameshift mutant of GBA2 do not cause mitochondrial fragmentation. GBA2-Ser471, GBA2-Ser501 and GBA2-Met510Valfs*17 expressed in osteosarcoma cells were stained with Streptavidin-Alexa594 (red, GBA2) and anti-TOMM20 (green, mitochondria).

4.4.6.3 Quantification of Mitochondrial Localization

I quantified the extent of mitochondrial co-localization of WT GBA2 and truncation mutants Arg234* and Arg340* by determining Mander's overlap coefficient (MOC). I determined the extent of red fluorophore (anti-FLAG antibody for GBA2, Alexa 594 secondary antibody) overlapping with the green fluorophore (anti-TOMM20

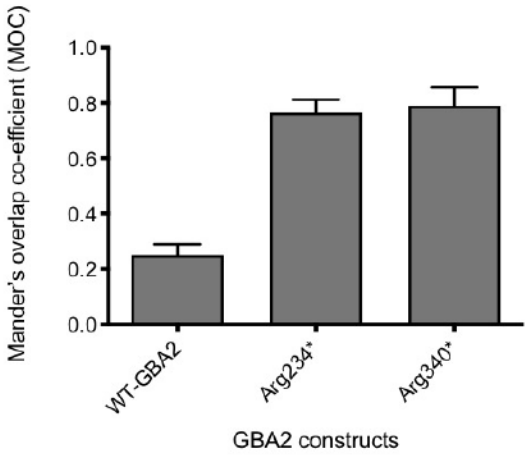

Figure 4.4.6.3. Mander's overlap co-efficient (MOC) values for different GBA2 constructs. Average MOC value for WT GBA2 was 0.251 whereas average MOC values for Arg234* and Arg340* were 0.77 and 0.79 respectively. Data representing average MOC values for three independent experiments +SD for each GBA2 variant; 10 cells were analyzed for each variant, per experiment.

antibody for mitochondria, Alexa 488 secondary antibody) using the JACoP plugin of ImageJ. MOC values of the truncation mutants were almost three times higher than the MOC values of WT GBA2 (Figure 4.4.6.3). These data support my observation of mitochondrial co-localization of the truncated GBA2 mutants.

4.4.6.4 Kinetics of Mitochondrial Fragmentation

To determine at what time after transfection mitochondrial fragmentation starts in cells expressing the truncation mutants, I performed a time-course study. I observed the mitochondrial morphology of HeLa cells expressing Arg234* mutant at 4, 8, 16, 20, 36, 68 and 96 hours of post-transfection. Mitochondrial fragmentation started at 20 hours of post-transfection and continued until at least 96 hours of post-transfection. In fact, proteins were not expressed properly before 20 hours of post-transfection, and after 96 hours of transfection, very few viable cells were present in culture dishes (not shown).

4.4.6.5 Effect of Expression Levels of the Truncated GBA2 Mutants on Mitochondrial Morphology

I investigated whether mitochondrial fragmentation caused by the truncated GBA2 mutants was an artifact due to overexpression of the mutant proteins. One of the approaches to assess the effect of overexpression on mitochondrial phenotype was to express the mutant proteins under a weaker promoter. I subcloned the GBA2 truncation mutants Arg234* and Arg340* in the pMSCV vector, which has a retroviral 5′- LTR as weak promoter. The levels of expression of WT GBA2, Arg234*-GBA2 and Arg340*-GBA2 were 2.2-times, 8.7-times and 8.3-times less, respectively, in the pMSCV vector compared to their levels of expression in the pCMV6 vector (Figure 4.4.6.5.1). Immunofluorescence staining revealed that both truncation mutants exhibited a similar kind of punctate expression pattern and co-localized with fragmented mitochondria as previously observed when expressed under the strong CMV promoter (Figure 4.4.6.5.2).

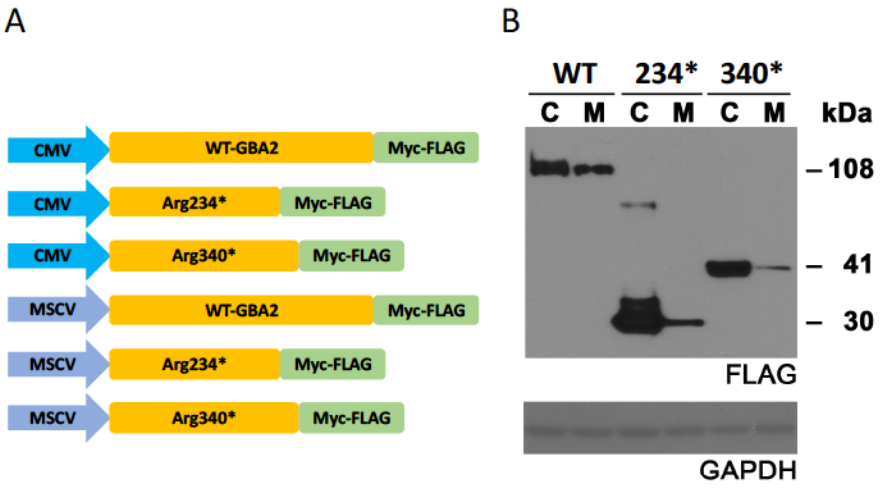

Figure 4.4.6.5.1. WT GBA2 and truncated GBA2 mutants under strong and weak promoters. (A) Schematic representation of WT GBA2, Arg234* and Arg340* truncation mutations in pCMV6 and pMSCV vectors. All constructs had a Myc-FLAG tag at the C-terminus. (B) Western blot analysis of U20S cells expressing WT GBA2, Arg234*, and Arg340* mutants under weak and strong promoters (anti-FLAG). C= CMV, M=MSCV.

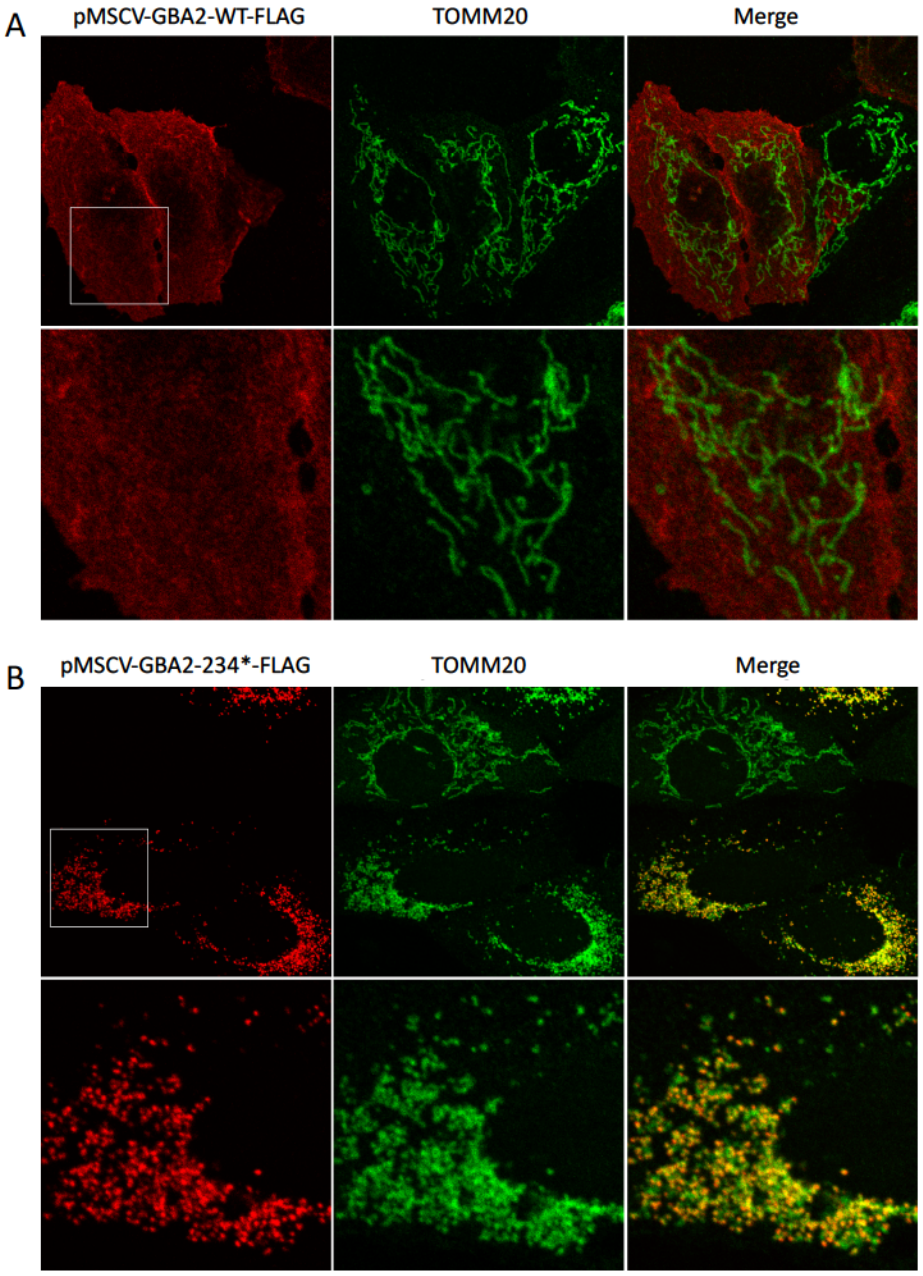

Figure 4.4.6.5.2. Expression pattern and cellular localization of WT GBA2 and the Arg234* mutant expressed in the pMSCV vector. U2OS cells expressing (A) WT GBA2 and (B) Arg234*-GBA2 encoded in pMSCV vector were immunostained with anti-FLAG (red) and anti-TOMM20 (green) antibody at 48 hours of post-transfection.

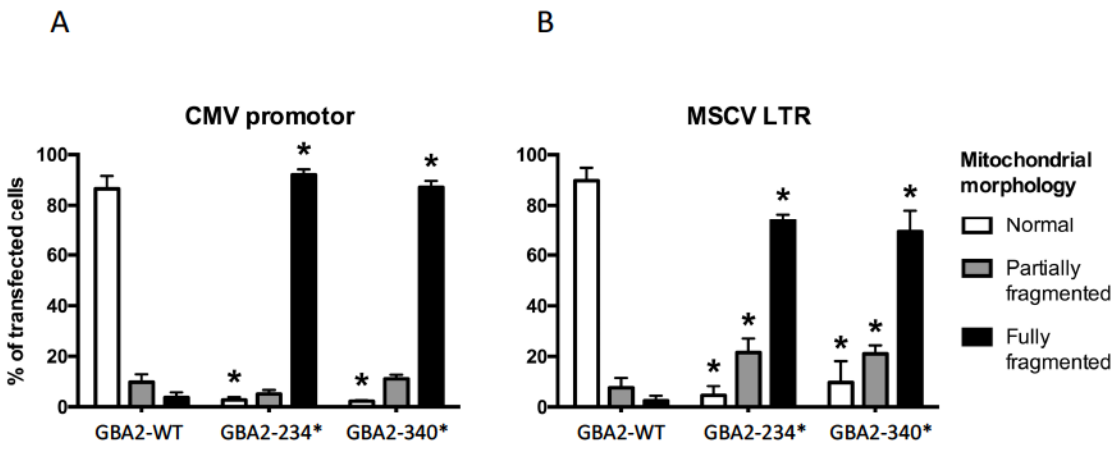

Figure 4.4.6.5.3. Quantification of mitochondrial morphology of cells expressing WT and truncation GBA2 mutants in U20S cells. Mitochondrial morphology of U2OS cells expressing WT and truncated GBA2 mutants encoded in the (A) pCMV6 vector and (B) in pMSCV vector. Data are presented as average values +SD for three individual experiments. 250 transfected cells were counted for each GBA2 construct per experiment. Asterisks indicate mitochondrial morphology of cells expressing truncated mutants which are statistically different from mitochondrial morphology of cells expressing WT GBA2. Statistical significances were analyzed via one-way ANOVA.

To quantify the observed effects, I scored cells expressing WT GBA2 and the truncation mutants based on their mitochondrial phenotype. More than 85% of the cells expressing WT GBA2 had normal, elongated mitochondria, encoded either in pCMV6 or pMSCV vector. For Arg234* and Arg340* mutants, more than 85% and 72% cells had fully fragmented mitochondria when expressed under CMV and MSCV promoter respectively (Figure 4.4.6.5.3).

Another approach to verify that mitochondrial fragmentation was not an overexpression artifact was to transfect cells using lower amounts of DNA. I transfected HeLa cells using 2-, 4-, 8-, and 16-times less plasmid DNA encoding Arg234* and Arg340*, compared to the recommended amount. Both mutants caused mitochondrial fragmentation even when transfected with 16-times less DNA (Figure 4.4.6.5.4).

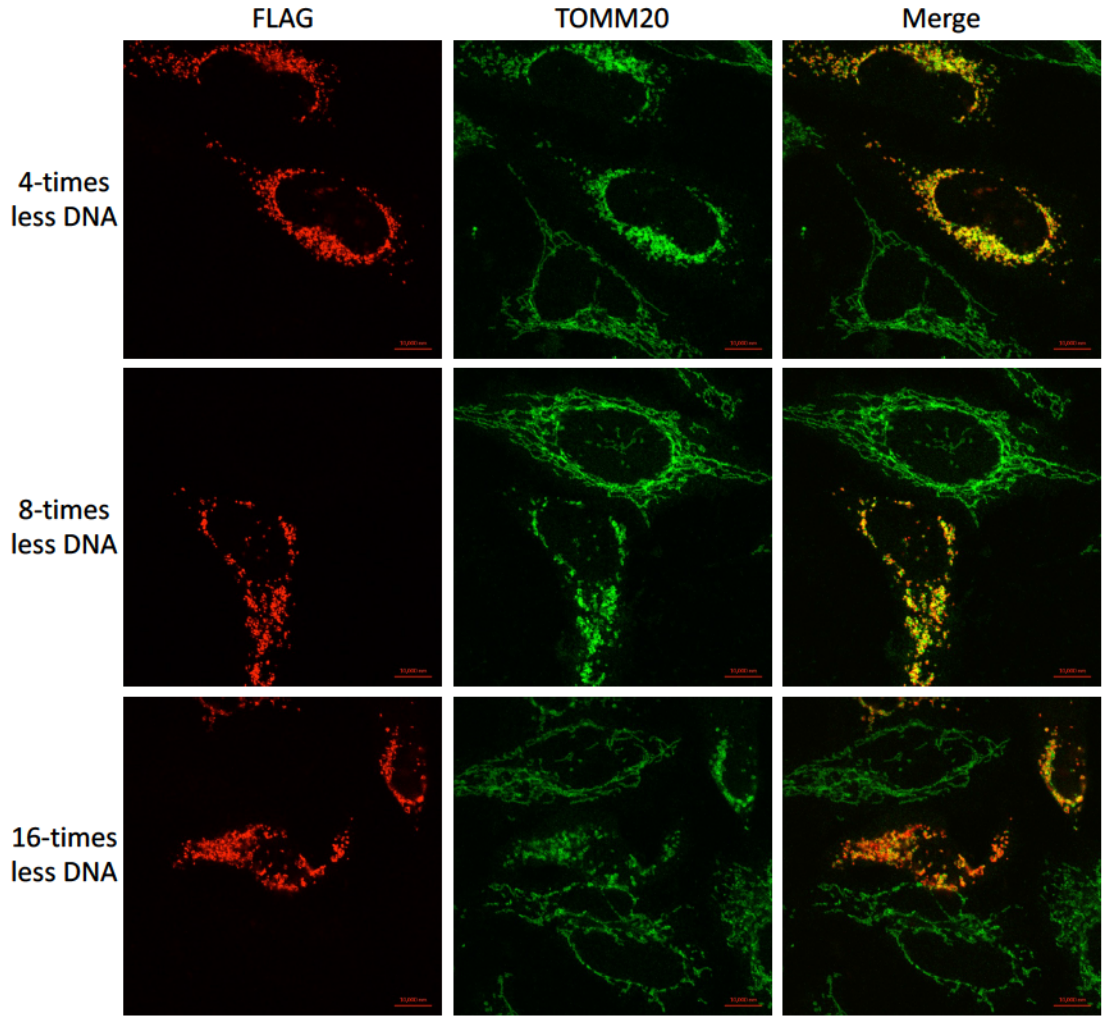

Figure 4.4.6.5.4. Mitochondrial fragmentation caused by Arg234* mutant in HeLa cells transfected with lower amounts of DNA. Hela cells transfected with 4-, 8-, and 16-times less DNA were immunostained with TOMM20 (green) and anti-FLAG antibody (red) at 48 hours of post-transfection.

4.4.6.6 Truncated GBA2 Mutants Are Present in the Mitochondrial Matrix

To analyze the mitochondria of cells expressing WT GBA2 and truncated GBA2 mutants in greater detail, I used electron microscopy. I generated GBA2 cDNAs carrying a C-terminal APEX2-tag, which is a monomeric peroxidase derived from soybean ascorbate peroxidase (192). APEX2 is a mutant of APEX that is more sensitive to

peroxide (192,193). In presence of hydrogen peroxide, APEX2 catalyzes the polymerization of diaminobenzidine (DAB) close to the APEX/APEX2-tagged protein, promoting the deposition of electron-dense osmium, which creates contrast for electron microscopy (Figure 4.4.6.6.1) (194).

Figure 4.4.6.6.1. Schematic of APEX as a reporter generating EM contrast. In the presence of hydrogen peroxide, APEX oxidizes DAB, which polymerizes and precipitates in the proximity of the APEX tag, attracting electron-dense osmium (Figure source: Lam *et al.*, (192)).

As a starting point of working with APEX2-tagged proteins, I generated cDNAs of WT GBA2 containing the APEX2 tag either at the C-terminus or at the N-terminus of the GBA2 cDNA. N-terminally APEX2-tagged GBA2 contained a C-terminal FLAG tag and the C-terminally APEX2-tagged GBA2 contained an additional HA-tag next to the APEX2 tag (Figure 4.4.6.6.2 A). Enzyme activity assays of osteosarcoma cells expressing APEX2-tagged WT GBA2 showed that both versions were enzymatically active (Figure 4.4.6.6.2 B). Both versions of APEX2-tagged GBA2 biotinylated neighboring proteins in presence of biotin-phenol at similar levels, activated by hydrogen peroxide (Figure 4.4.6.6.2 C). As the C-terminally APEX2-tagged WT GBA2 had slightly higher β-glucosidase activity than the N-terminally-tagged form, I decided to generate C-terminally APEX2-tagged versions of the truncation mutants Arg234* and Arg340* (Figure 4.4.6.6.2 A).

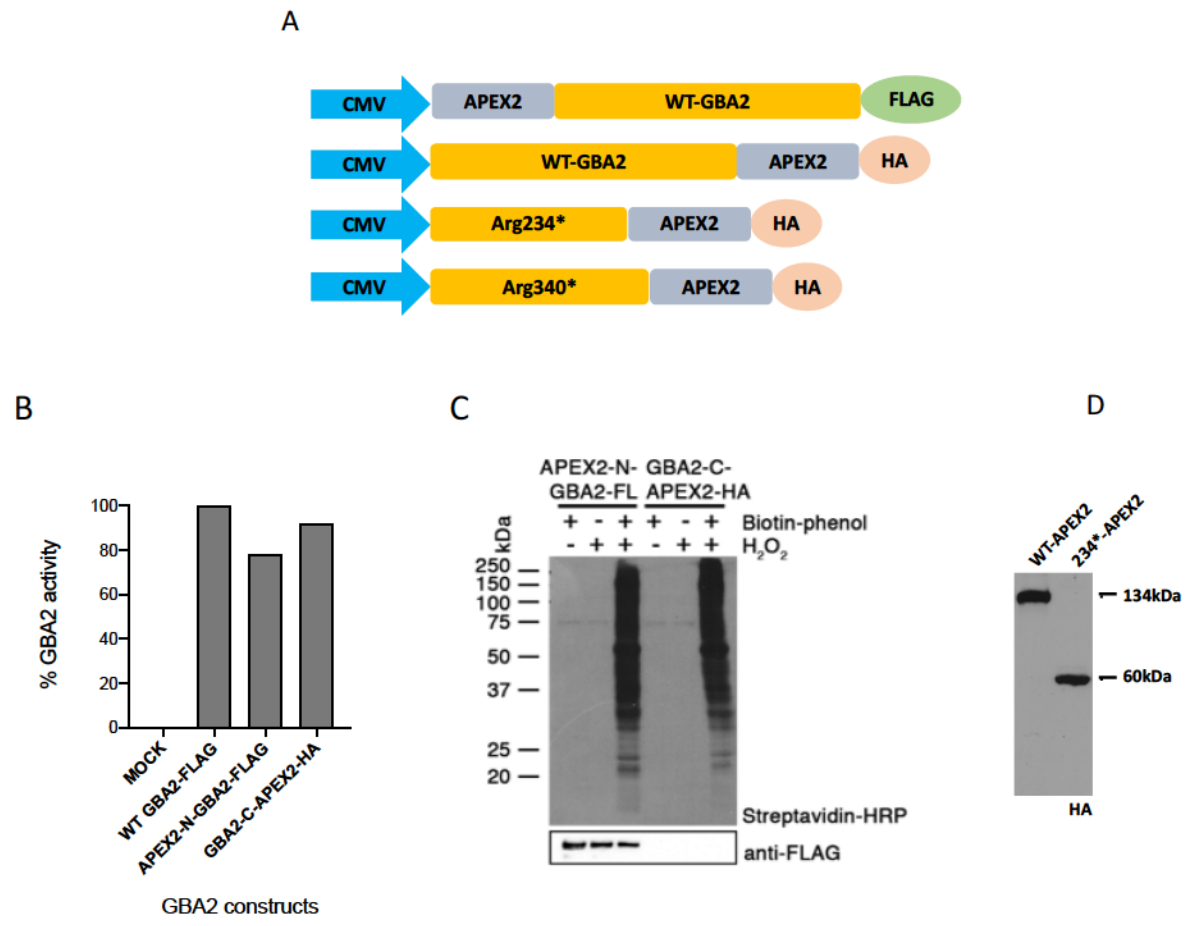

Figure 4.4.6.6.2. Schematic presentation and validation of APEX2-tagged GBA2. (A) Schematic presentation of N- and C-terminal-APEX2-tagged WT-GBA2, Arg234* and Arg340*. cDNAs were cloned in pCMV6 vector. (B) GBA2 activities of WT GBA2 carrying N- and C-terminal APEX2 expressed in HEK293 cells. Results are shown as a percentage of total GBA2 activity exerted by the FLAG-tagged WT GBA2 for a single experiment. (C) Proximity biotinylation in presence of APEX2-tag. C- and N-terminal APEX2-tagged WT GBA2 were expressed in HEK293 cells, treated with 0.5 mM biotin-phenol, in presence of 1 mM hydrogen peroxide for one minute. Biotinylated proteins were detected by western blot analysis (streptavidin-HRP). (D) Expression of WT GBA2 and Arg234* mutant containing C-terminal APEX2 and HA tag, expressed in U2OS cells. WT-GBA2-APEX2 and Arg234* appeared as 134 kDa and 60 kDa proteins, respectively.

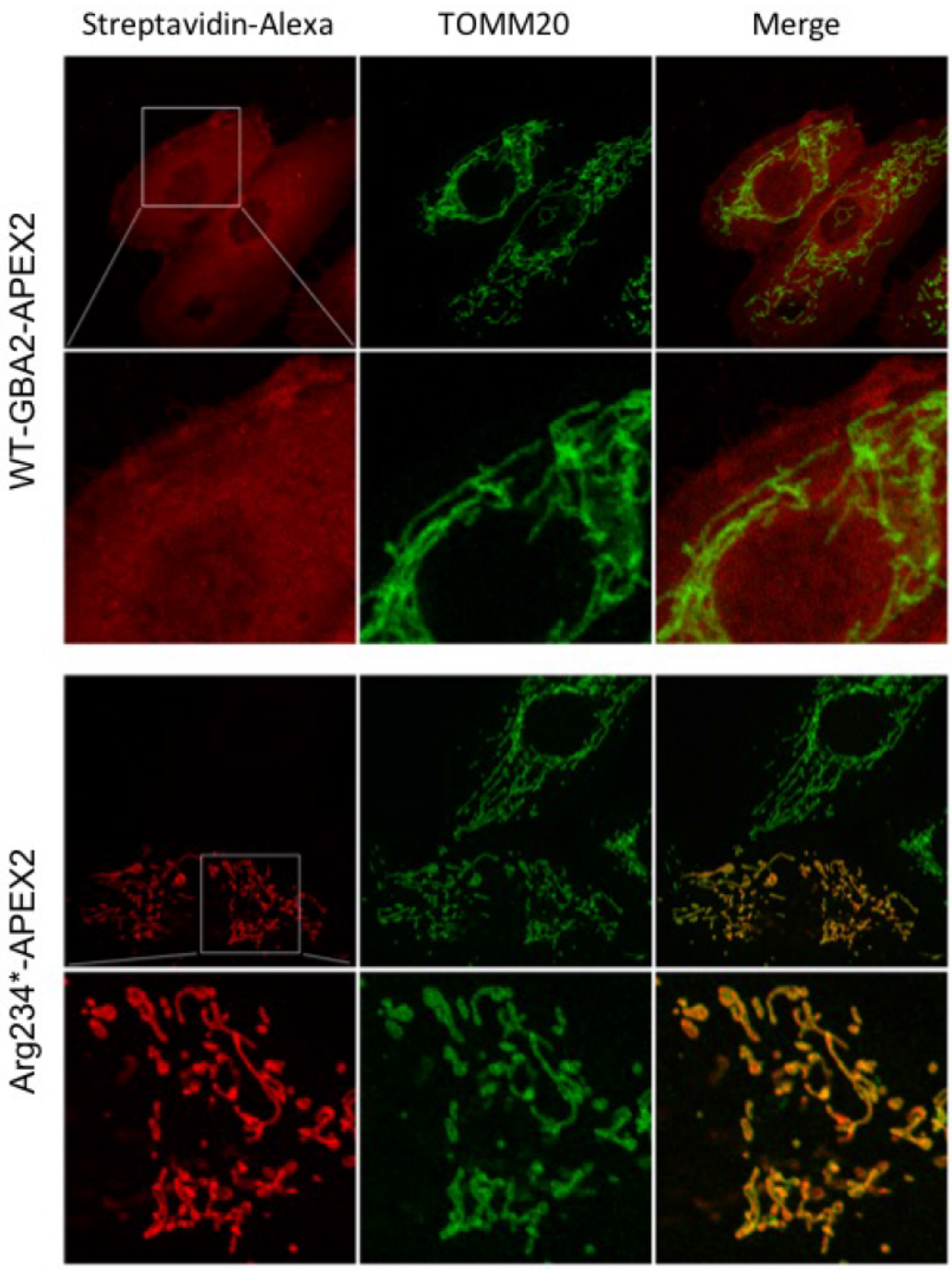

Figure 4.4.6.6.3. Proximal protein biotinylation by APEX2-tagged WT GBA2 and Arg234*. Osteosarcoma cells expressing WT GBA2-APEX2 and Arg234*-APEX2 were stained with Alexa594-streptavidin (red) and anti-TOMM20 (green) at 48 hours of post-transfection.

I examined the cellular localization of APEX2-tagged WT GBA2 and the Arg234* mutant by fluorescence staining. Cells were treated with biotin-phenol in presence of hydrogen peroxide and stained with fluorescently-labelled streptavidin to assess for biotinylation of proteins. Biotinylated WT GBA2 was present at the plasma membrane and biotinylated Arg234* was localized in the mitochondria (Figure 4.4.6.6.3).

Having validated the proximity-biotinylating activity and localization of APEX2-tagged forms of GBA2, I examined U20S cells expressing APEX2-tagged WT, Arg234*, and Arg340* GBA2 through electron microscopy. In the majority of the cells, WT GBA2 stained the plasma membrane (Figure 4.4.6.6.4 A), whereas the truncation mutants stained the mitochondrial matrix (Figure 4.4.6.6.4 B and C). This observation further supported the mitochondrial localization of truncation GBA2 mutants observed in the confocal microscopy images. Surprisingly, in a minority of cells, APEX2-tagged WT GBA2 stained both the plasma membrane and the mitochondrial matrix (Figure 4.4.6.6.4 A). Being observed that, it is also important to confirm that mitochondrial localization of the WT GBA2 is not an artifact due to a certain cell cycle phase. Synchronizing cells to bring them to the same phase and then assessing the cellular localization of GBA2 would be good way to assess that. Another alternative approach would be isolating mitochondria from cultured cells overexpressing WT GBA2 and detecting the presence of WT GBA2 my western blot analysis.

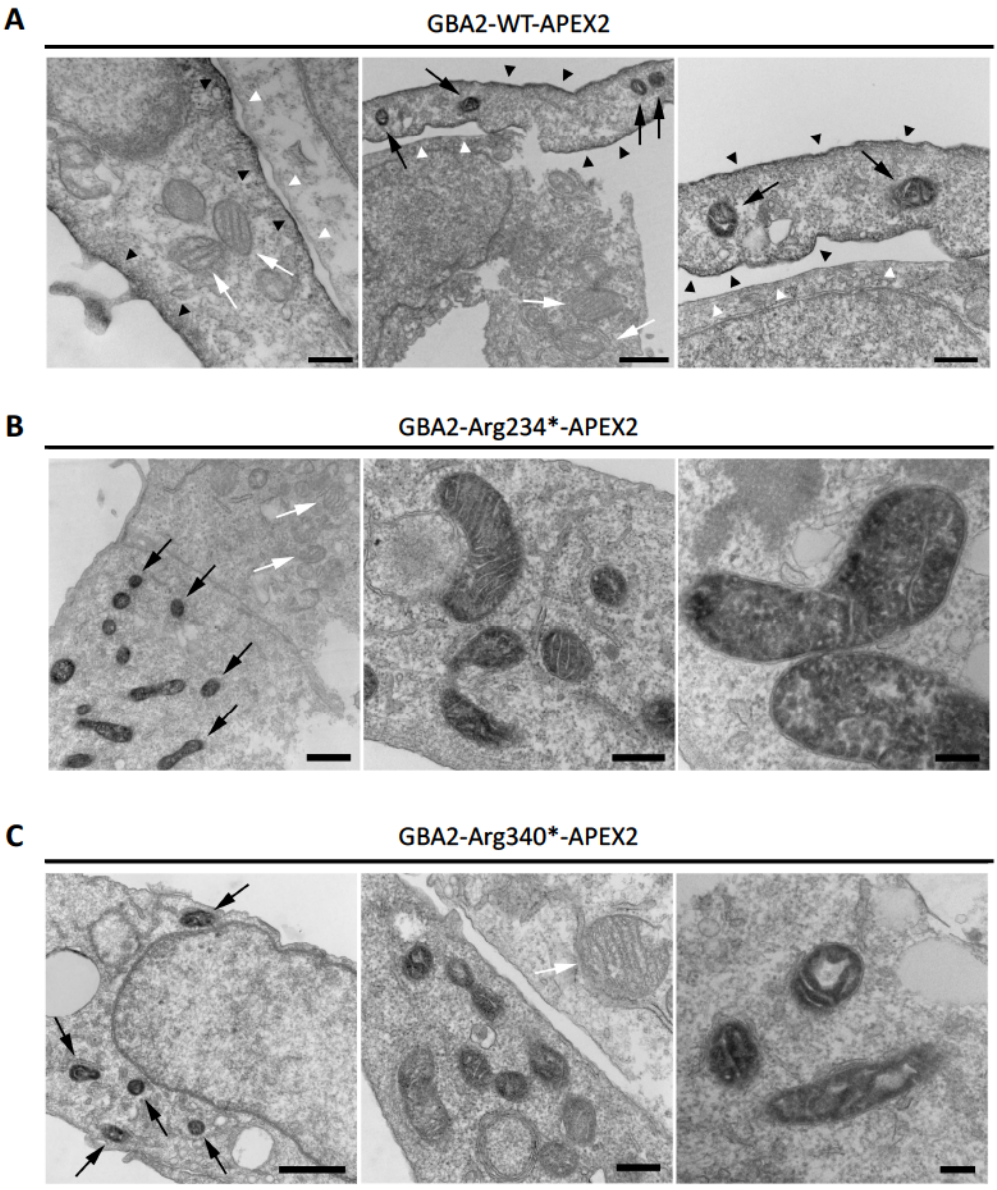

Figure 4.4.6.6.4. Ultrastructural localization of WT and mutant forms of GBA2 in U2OS cells. (A) WT-GBA2-APEX2 stained the plasma membrane (left image) or both the plasma membrane and the mitochondrial matrix (middle and right images). (B) and (C) GBA2-Arg234*-APEX2 and GBA2-Arg340*-APEX2 were present in the mitochondria. Higher magnification images show the presence of the mutants in the mitochondrial matrix. White arrows and white arrow heads point to unstained mitochondria and unstained plasma membrane respectively. Black arrows and black arrow heads point to stained mitochondria and stained plasma membrane respectively.

4.4.6.7 Truncated GBA2 Mutants Cause Loss of Mitochondrial Membrane Potential

To assess whether the truncation mutations affect mitochondrial function, I measured the mitochondrial membrane potential using the fluorescent dye tetramethylrhodamine methyl ester (TMRM). The fluorescence intensity of mitochondria was measured in the presence of TMRM only, and in the presence of TMRM combined with FCCP (carbonyl cyanide-4-phenylhydrazone), a mitochondrial membrane depolarizer. As not all cells are transfected in transient transfections, I co-expressed mClover, a green fluorescent protein, in the cytoplasm as a transfection marker (Figure 4.4.6.7.1 A). In cells expressing WT GBA2, mitochondria incorporated TMRM, revealing mitochondrial structure (Figure 4.4.6.7.2 A). In presence of FCCP, mitochondria did not incorporate TMRM and were barely visible (Figure 4.4.6.7.2 B). In cells expressing the Arg234* truncation mutant, mitochondria did not incorporate TMRM and were not visible (Figure 4.4.6.7.3 A). Presence of FCCP did not make any difference for these cells (Figure 4.4.6.7.3 B), indicating that the mitochondria of cells expressing the truncation GBA2 mutants were depolarized.

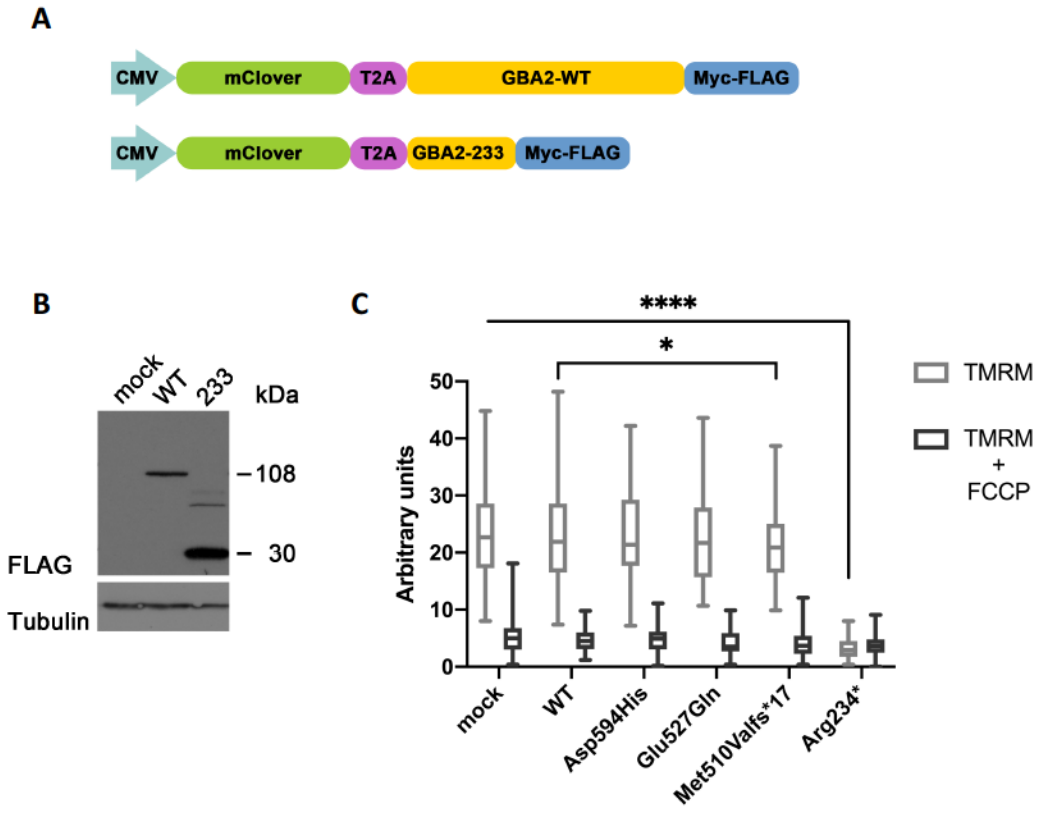

Figure 4.4.6.7.1. The GBA2 Arg234* mutant causes almost a complete loss of mitochondrial membrane potential. (A) Schematic presentation of constructs expressing GBA2 in tandem with mClover. mClover and GBA2 were separated by the ribosome-skipping peptide T2A, allowing co-expression of multiple proteins from a single cDNA. WT and mutant GBA2 had C-terminal Myc-FLAG tag. (B) Western blot showing the expression of WT GBA2 and the Arg234* mutant in U2OS cells (anti-FLAG) using the constructs depicted in panel (A). (C) Box-and-whiskers representation of TMRM fluorescence intensities of control and transfected cells expressing WT and mutant forms of GBA2. Asterisks indicate significant difference between TMRM fluorescence intensities; ****, $P < 0.0001$; *, $P = 0.0488$. The experiment was done in triplicate, 25 cells were analysed per GBA2 construct for each experimental condition. Statistical analysis was performed by one-way nested ANOVA using Prism v. 8.2.1.

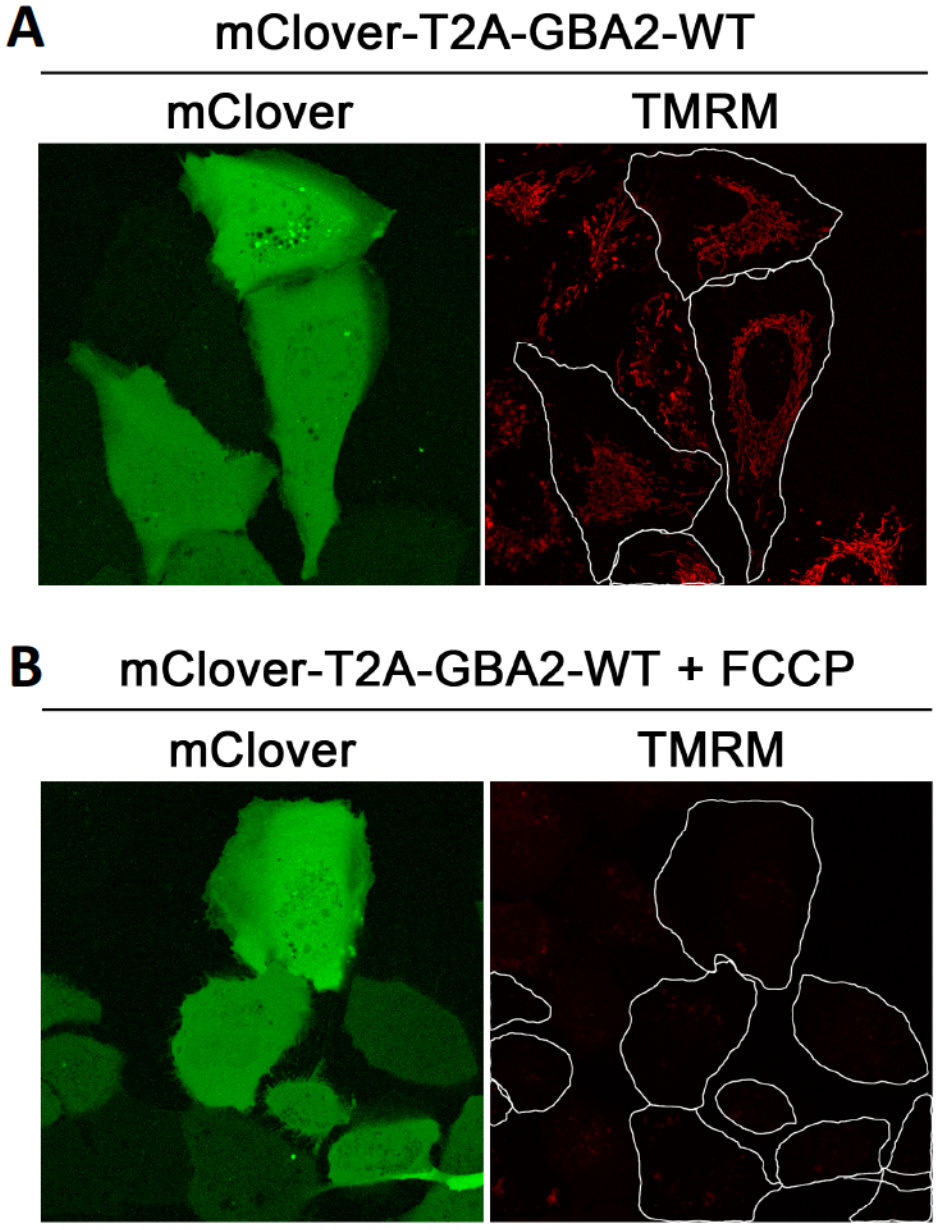

Figure 4.4.6.7.2. In cells expressing WT GBA2, FCCP blocks mitochondrial TMRM fluorescence. Transfected cells expressed mClover (green), allowing a contour to be drawn around each cell and to determine its area and integrated fluorescence intensity. Images in (A) show the cells upon addition of TMRM and images in (B) show the cells upon addition of FCCP along with TMRM.

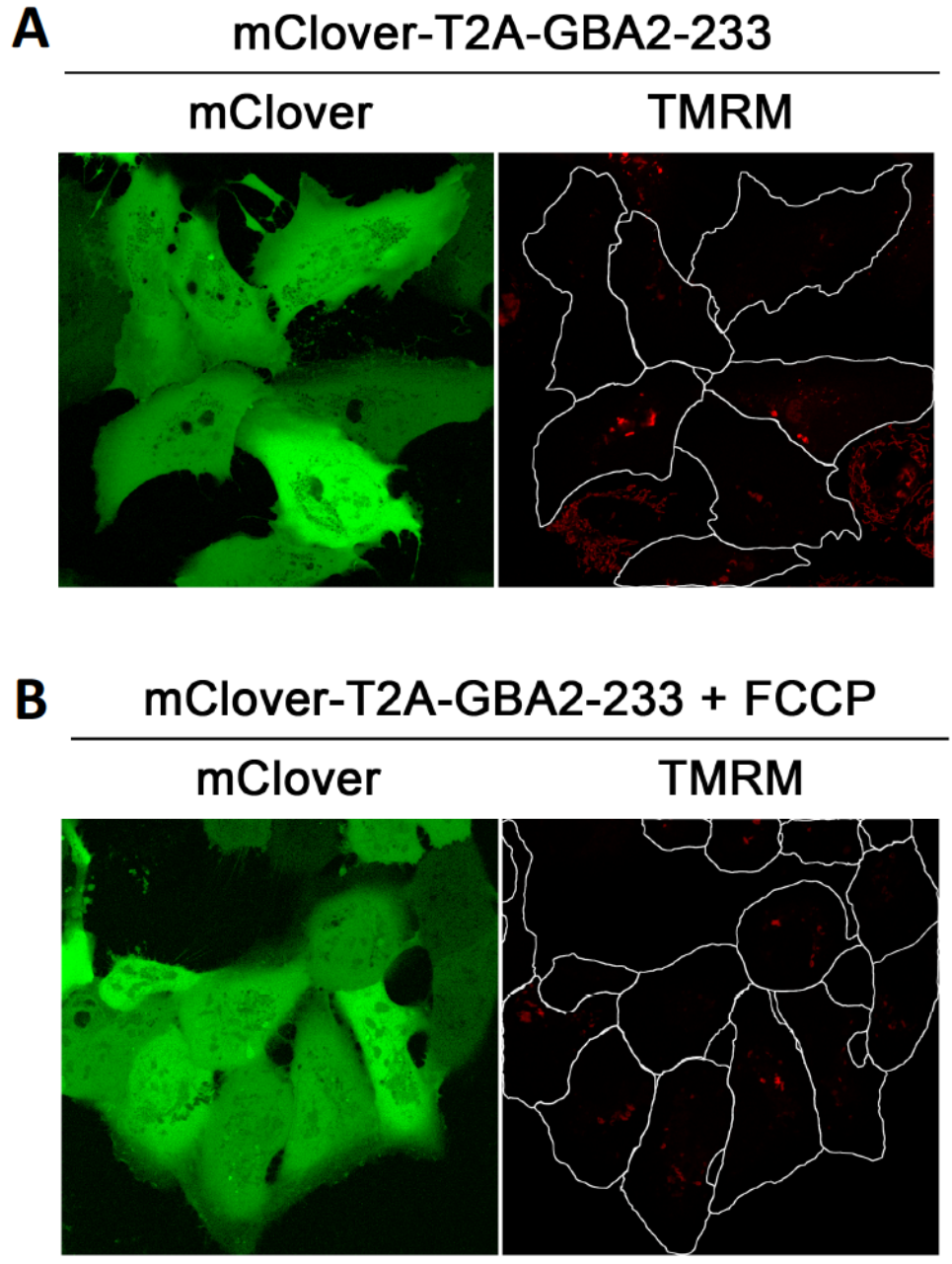

Figure 4.4.6.7.3. In cells expressing Arg 233-GBA2, mitochondrial TMRM fluorescence was not detectable. Transfected cells expressed mClover (green), allowing a contour to be drawn around each cell and to determine its area and integrated fluorescence intensity. Images in (A) show the cells upon addition of TMRM and images in (B) show the cells upon addition of FCCP along with TMRM.

4.4.6.8 Truncated GBA2 Mutants Promote the Import of Full-Length Forms of GBA2 Into Mitochondria

GBA2 is self-associates (195) and native gel electrophoresis showed that WT GBA2 dimerizes (Figure 4.4.4). To assess whether the truncated forms of GBA2 associate with full-length forms of GBA2 (WT or mutant), I co-expressed the truncation mutants with WT GBA2, point mutants and the active-site mutant. For these experiments, I made new constructs where WT GBA2 or full-length mutants were linked with the truncation mutants through the T2A peptide. To identify different versions GBA2 co-expressed in the same cell, Arg234* had a C-terminal Myc-FLAG tag while WT GBA2 had an N-terminal TST (twin-strep-tag) and a C-terminal HA tag (Figure 4.4.6.8.1 A). Full-length GBA2 mutants only carried a C-terminal HA tag. Upon overexpression of the new constructs in U2OS cells, the mitochondria of the transfected cells were fragmented. Strikingly, not only was the Arg234* mutant present in the fragmented mitochondria, but also WT GBA2 and the full-length mutants (Figure 4.4.6.8.2 and Figure 4.4.6.8.3).

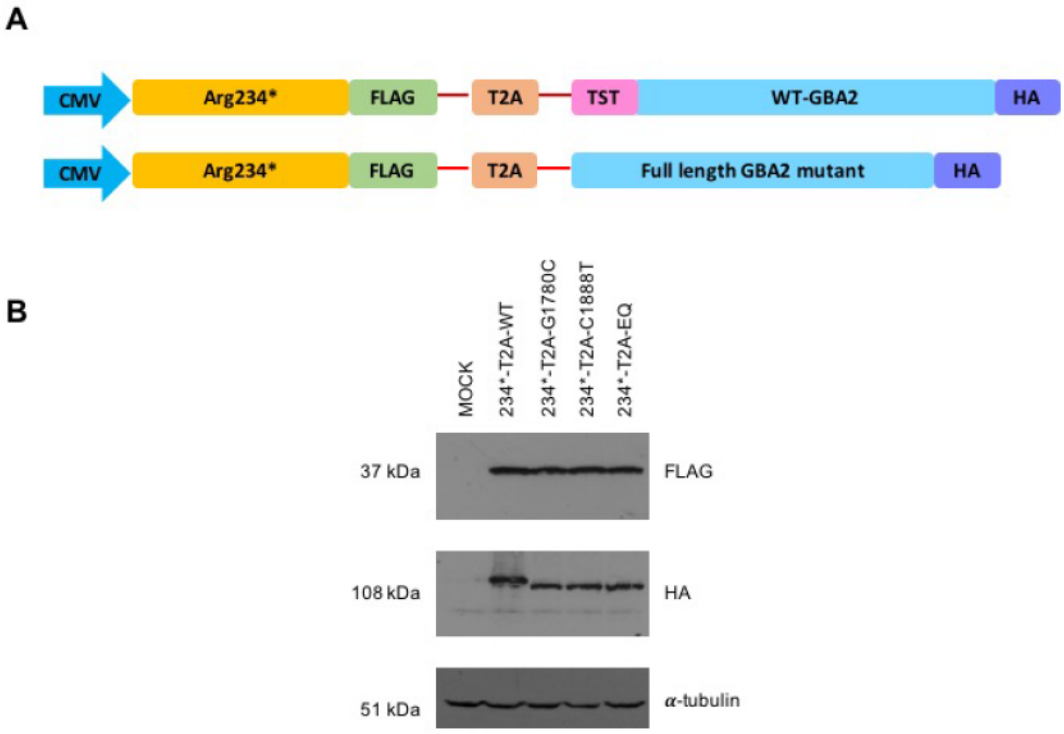

Figure 4.4.6.8.1. Co-expression of different forms of GBA2. (A) Schematic presentation of constructs for expression of the Arg234* mutant in tandem with WT GBA2 or full-length GBA2 mutants. (B) Western blot analysis of U2OS cells co-expressing Arg234* and other full-length forms of GBA2. The top panel shows the expression of Arg234* (anti-FLAG), and the middle panel shows the expression of full-length forms of GBA2 (anti-HA). EQ, active-site mutant (Glu527Gln); G1780C, Asp594His; C1888T, Arg630Trp.

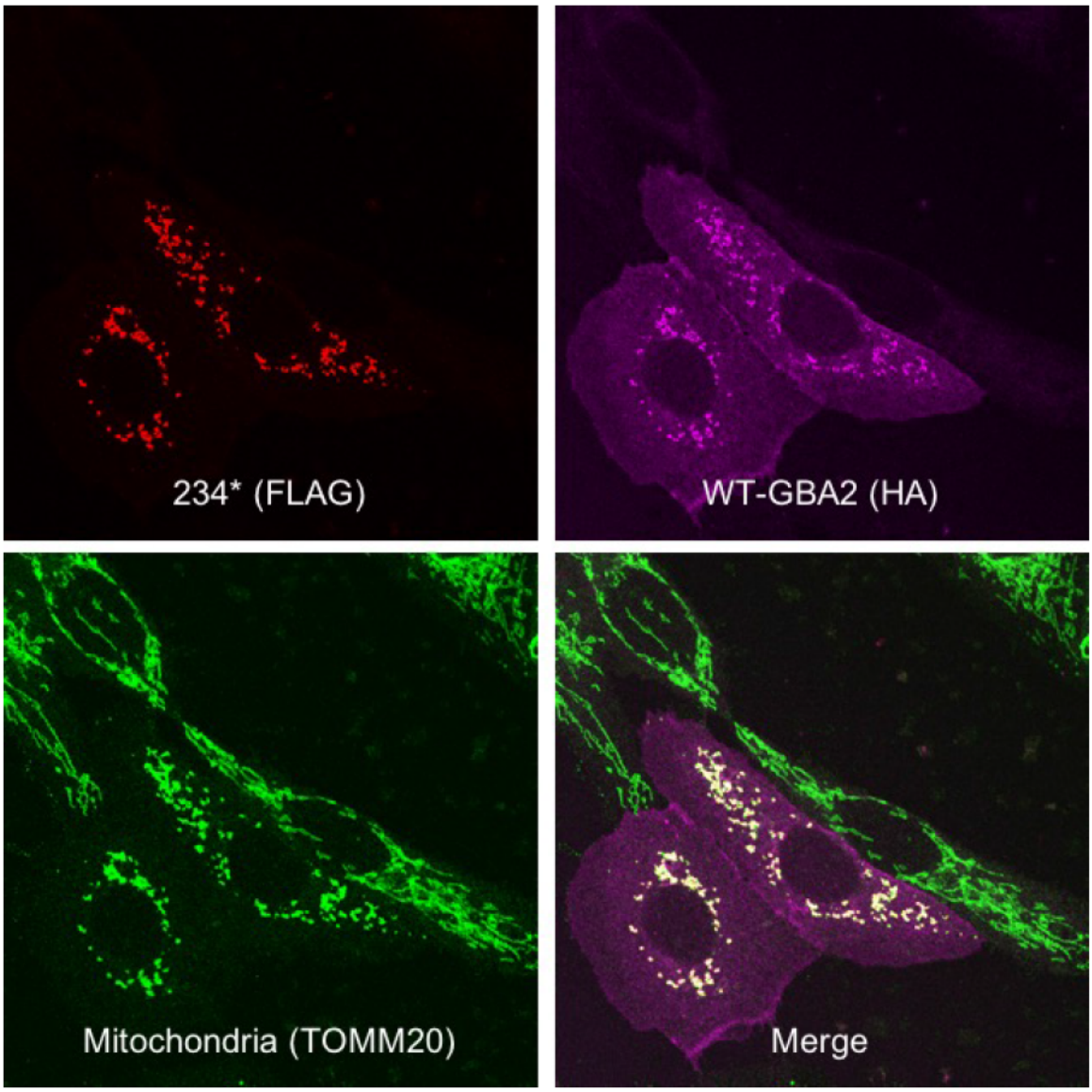

Figure 4.4.6.8.2. WT GBA2 colocalizes with fragmented mitochondria in cells co-expressing the Arg234* mutant. U2OS cells co-expressing WT GBA2 with a C-terminal HA tag and Arg234*-GBA2 with a C-terminal FLAG tag were immunostained with anti-HA (purple), anti-FLAG (red), and anti-TOMM20 (green) antibody. Images were taken at 63X magnification.

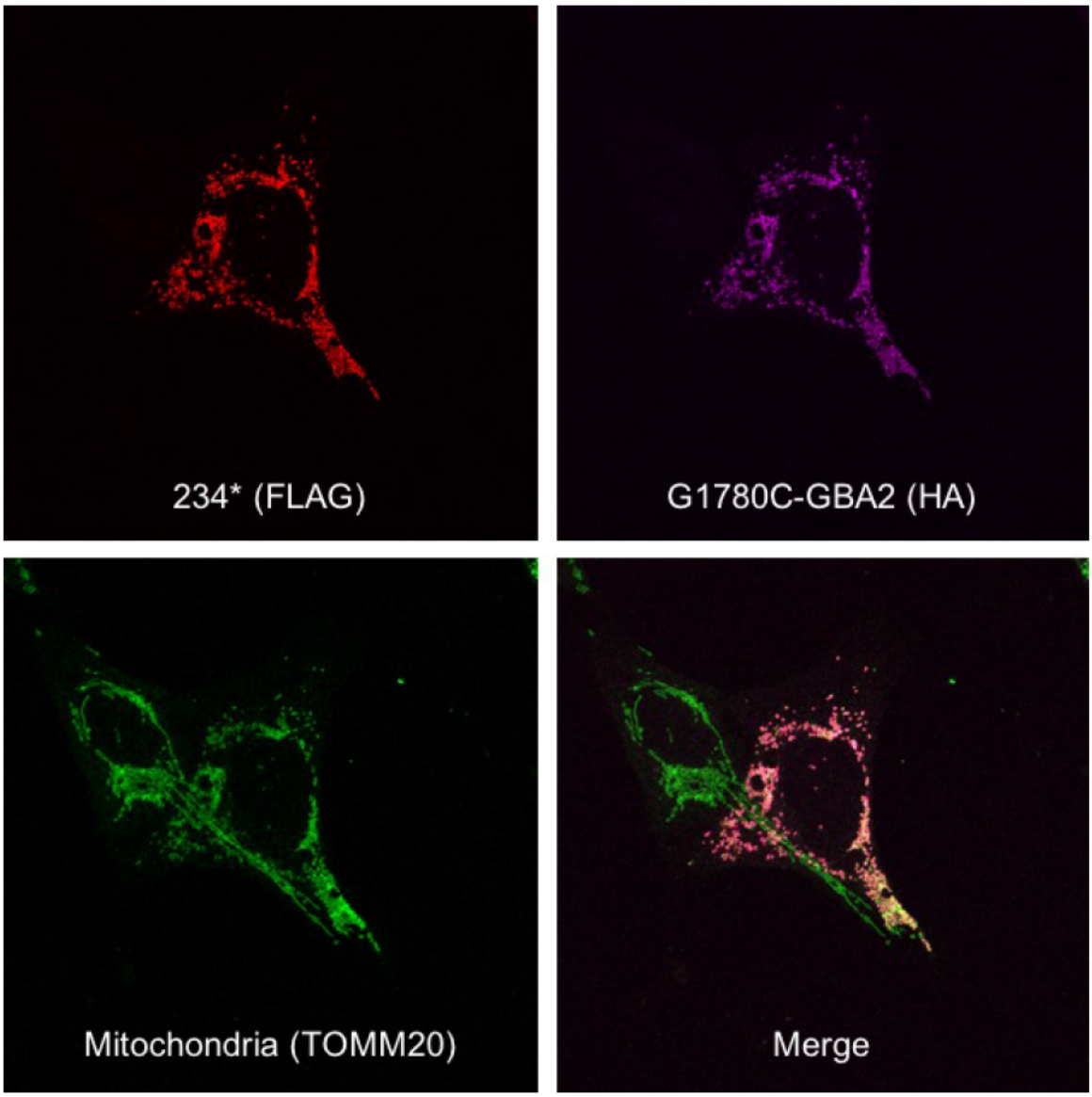

Figure 4.4.6.8.3. **The G1780T-GBA2 mutant colocalizes with fragmented mitochondria in cells co-expressing the Arg234* mutant**. U2OS cells co-expressing Arg234*-GBA2 with a C-terminal FLAG tag and the point mutant G1780T with a C-terminal HA tag were immunostained with anti-HA (purple), anti-FLAG (red), and anti-TOMM20 (green) antibody. Images were taken at 63X magnification.

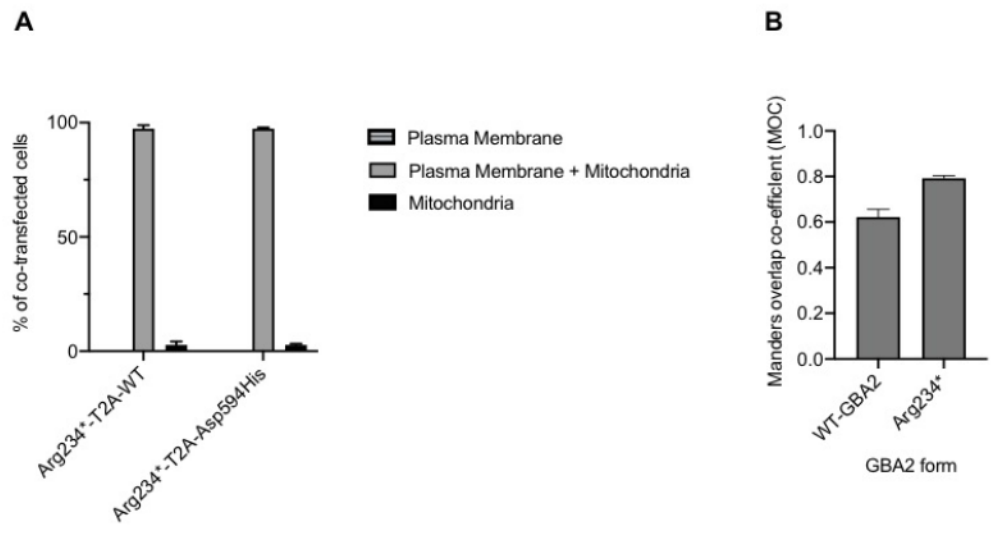

Figure 4.4.6.8.4. Mitochondrial localization of WT and full length GBA2 mutants in cells co-expressing Arg234*. (A) Quantification of cellular distribution of WT GBA2 and the Asp594His mutant when co-expressed with the Arg234* mutant. Data are presented as average values +SD for three individual experiments; at least 100 transfected cells were counted in each experiment. (B) Mander's overlap co-efficient (MOC) values for WT GBA2 and Arg234* overlapping mitochondria in cells co-expressing these forms of GBA2. Results showing the average MOC values +SD for three individual experiments, ten transfected cells were analysed in each experiment.

In more than 95% of transfected cells, full length GBA2 was present both at the plasma membrane and in mitochondria (Figure 4.4.6.8.4). In very few cells full-length GBA2 was exclusively present in mitochondria (Figure 4.4.6.8.3). Exclusive plasma membrane localization of full-length forms of GBA2 was not seen in any of the co-transfected cells. In co-transfected cells, Mander's overlap coefficient (MOC) for WT GBA2 and mitochondria was 0.621, which was almost 2.5 times higher than its value (0.251) in cells only expressing WT GBA2 (Figure 4.4.6.8.4 B). MOC for Arg234* and mitochondria in the co-transfected cells was slightly higher (0.792) than previously obtained (0.766) in cells singly transfected with Arg234* (Figure 4.4.6.8.4 B). These data indicate that co-expression of Arg234* facilitates the mitochondrial import of WT and full-length GBA2 mutants.

4.4.6.9 Truncated GBA2 Mutant Interferes with OPA1 Processing

As GBA2 truncation mutants resided in the mitochondrial matrix and caused mitochondrial fragmentation, it was of interest to see whether these mutants affected any of the mitochondrial fission or fusion factors. I co-expressed mClover (a green fluorescent protein expressed in the cytoplasm) and WT/mutant GBA2 in U2OS cells and separated fluorescently labeled transfected cells from non-transfected cells by flow cytometry. The sorted cells exclusively expressing WT or mutant forms of GBA2 were analysed by western blot to determine the levels of DRP1 (mitochondrial fission protein) and OPA1 (mitochondrial fusion protein). No form of GBA2 affected the level of DRP1, but the Arg234* mutant affected the processing of OPA1, depleting the higher-molecular weight OPA1 isoforms and the lower-molecular weight isoforms to a lesser extent (Figure 4.4.6.9).

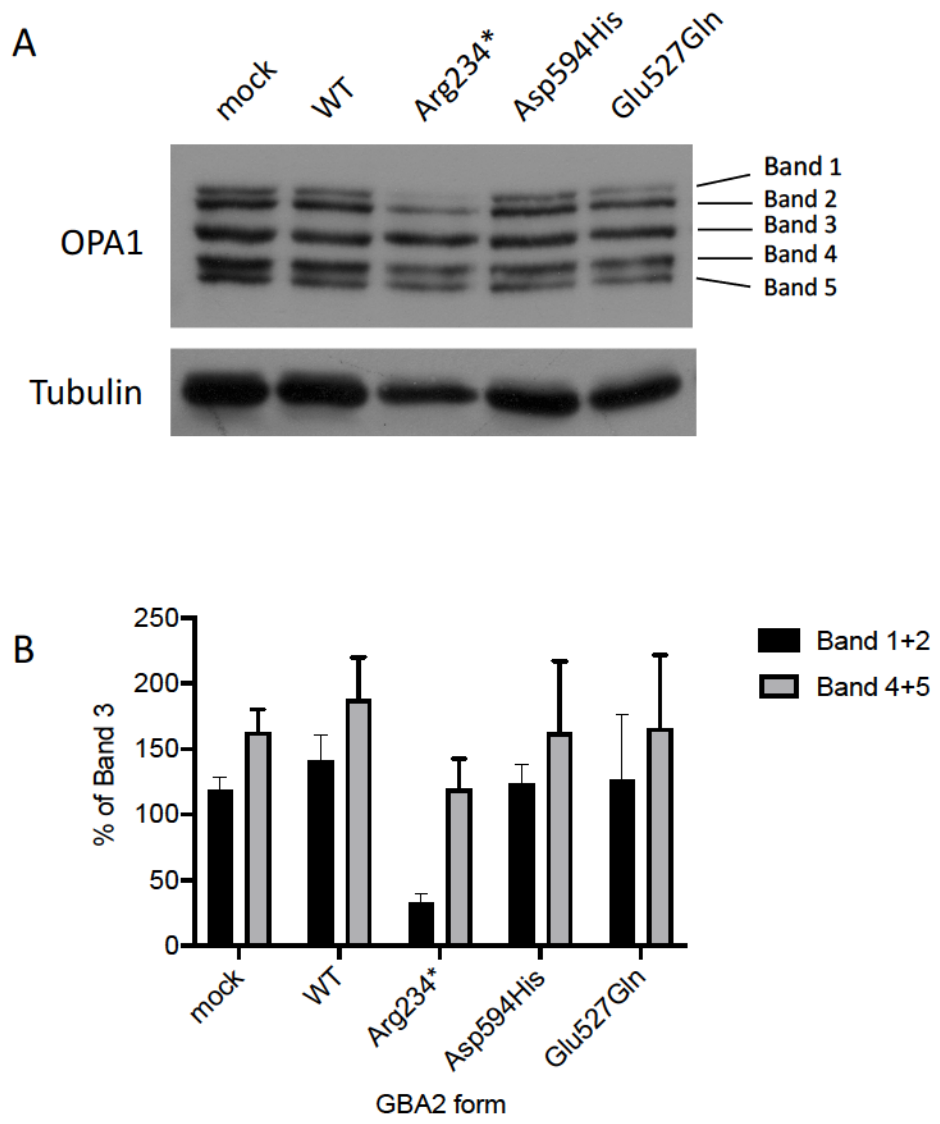

Figure 4.4.6.9. GBA2-Arg234* interferes with OPA1 processing. (A) U2OS cells co-expressing WT, Arg234*, Asp594His, or Glu527Gln GBA2 with mClover were isolated via flow cytometry and analyzed by western blot (anti-OPA1). Cells lysates were resolved by 8% polyacrylamide gel. Expression of Arg234* caused depletion of higher-molecular weight isoforms of OPA1 (band 1 and 2). (B) Densitometry analysis of different isoforms of OPA1 in cells expressing different forms of GBA2, normalized to the intensity of the middle band (#3). For cells expressing Arg234*, the combined band densities of bands 1 and 2 was 32.7%, whereas these densities were above 100% for all other forms of GBA2. The combined band densities of bands 4 and 5 for Arg234* were 119.8% whereas it was above 150% for other forms of GBA2. Data presented as an average +SD of two individual experiments.

4.4.7 Potential Mitochondria-Targeting Sequence in GBA2

My previous observations indicated that the four SPG46-associated truncation mutants of GBA2 co-localized with mitochondria and caused mitochondrial localization full-length forms of GBA2. So, I hypothesized that GBA2 may contain a mitochondria-targeting sequence within the first 340 amino acids from its N-terminus. The shortest truncation mutant that showed the mitochondrial localization was Tyr121*. So, I hypothesized that a mitochondrial targeting sequence must be present within the first 121 amino acids of GBA2. In an attempt to identify the potential mitochondrial targeting sequence within the first 121 amino acids of GBA2, I generated cDNA constructs encoding shorter fragments of the first 121 amino acids of GBA2, either 40 or 60 amino acids in length (Figure 4.4.7.1). However, these fragments were not detected in transfected U2OS cells using western blot or immunostaining.

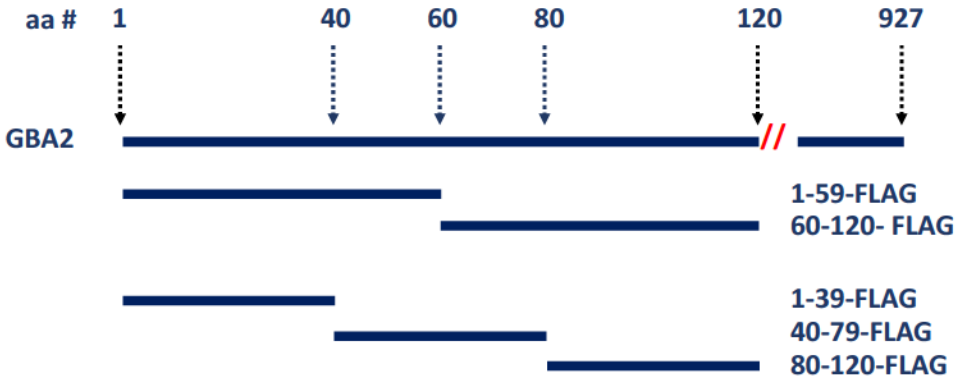

Figure 4.4.7.1. Schematic of short fragments of the first 121 amino acids of GBA2.

As an alternative approach, I made several deletion mutants, focusing on the first 233 amino acids of the GBA2-339 mutant. These mutants lacked 40, 80, 120, 160, 200, or 233 amino acids from the N- terminus of GBA2-339 or carried internal deletions of 40, 80, 120, 160, or 200 amino acids ending at amino acid 234 of GBA2-339 (Figure 4.4.7.2). When these deletion mutants were expressed in U2OS cells, the internal deletions did not cause any mitochondrial fragmentation, but the N-terminal deletions caused mitochondrial fragmentation when up to the first 160 amino acids were missing (Figure 4.4.7.3).

The first four N-terminally deleted mutants of GBA2-Arg340*, from GBA2-41-339 to GBA2-161-339, displayed punctate staining patterns and co-localized with fragmented mitochondria (Figure 4.4.7.3), comparable to the Arg234* and Arg340* truncation mutants associated with SPG46. This scenario changed when 200 amino acids were removed from the N-terminus of GBA2-Arg340*. Deletion mutants GBA2-201-339 and GBA2-234-339 were present at the plasma membrane and did not perturb mitochondria (Figure 4.4.7.4). These results indicate that GBA2 has another potential mitochondrial targeting sequence located in between GBA2 amino acids 160 and 200, other than the hypothetical mitochondrial targeting sequence within the first 121 amino acids. Fully fragmented mitochondria were the predominant mitochondrial phenotype when the first 160 amino acids were deleted from the N-terminus of GBA2-339, but when first 200 amino acids were missing, mitochondrial phenotype changed from fully fragmented to partially fragmented and normal mitochondria (Figure 4.4.7.5). For the cells expressing GBA2-234-339 deletion mutant, only 3.6% had fully fragmented mitochondria, and 85.7% of the cells had normal mitochondria.

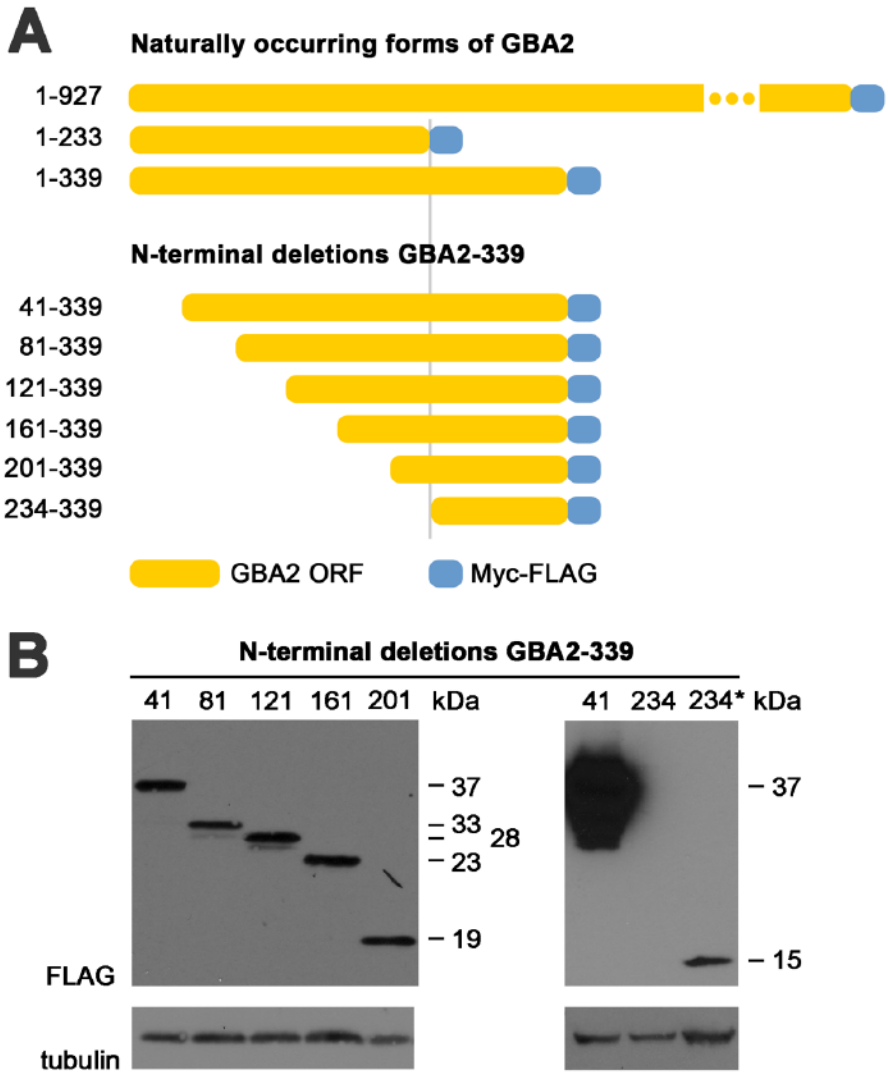

Figure 4.4.7.2. N-terminal deletion mutants of GBA2-339. (A) Schematic of the deletion mutants in comparison to WT GBA2. The open reading frame of all deletion mutants contained C-terminal myc-FLAG tag. (B) Western blot analysis of N-terminal deletion mutants expressed in osteosarcoma cells (anti-FLAG). The left-hand blot was obtained from 8% polyacrylamide gel and each lane contained 12 μg of total protein. The molecular weight of the shortest deletion mutant, N-234-339 was 15 kDa, it was resolved by 12.5% gel (right-hand blot) and it required 45 μg of total protein to obtain signal for this shortest deletion mutant.

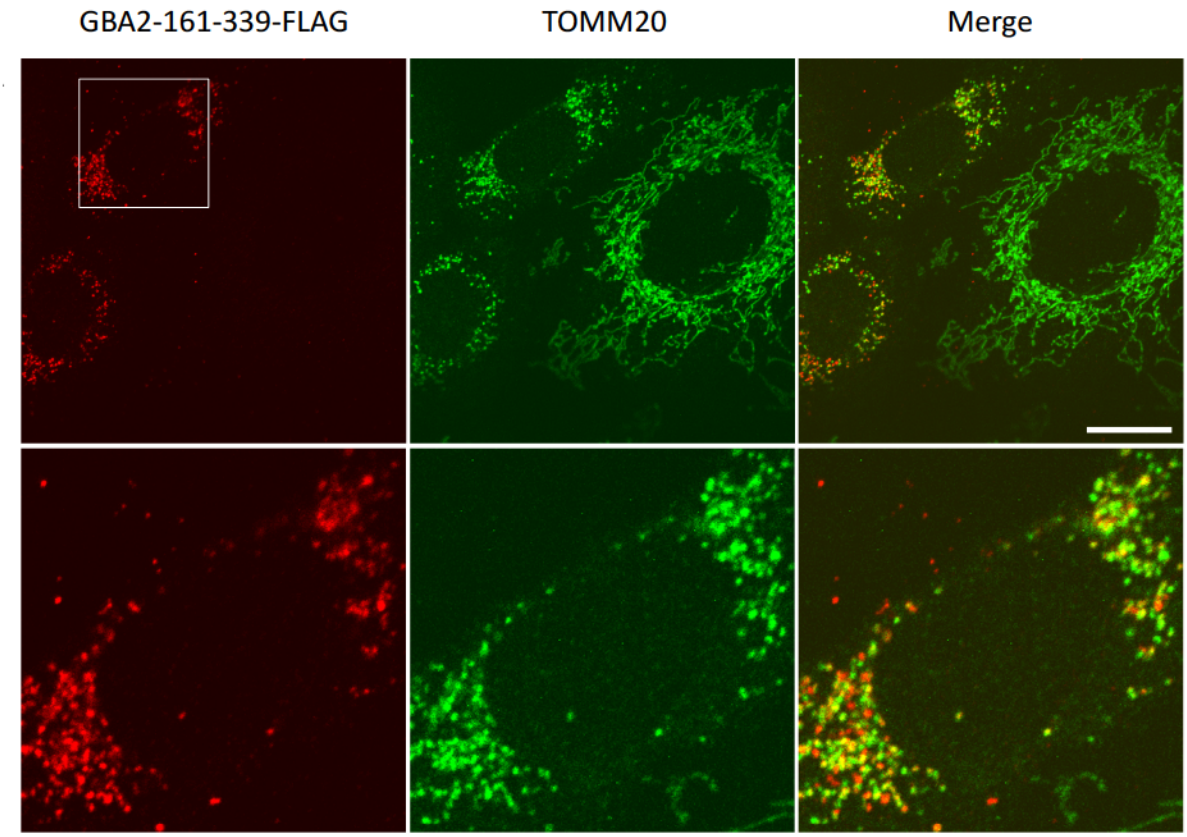

Figure 4.4.7.3. GBA2-161-339 causes mitochondrial fragmentation. U2OS cells expressing the GBA2-161-339 mutant were immunostained with anti-FLAG (red) and anti-TOMM20 (green) antibody at 48 hours of post-transfection. Scale bar, 20 μm.

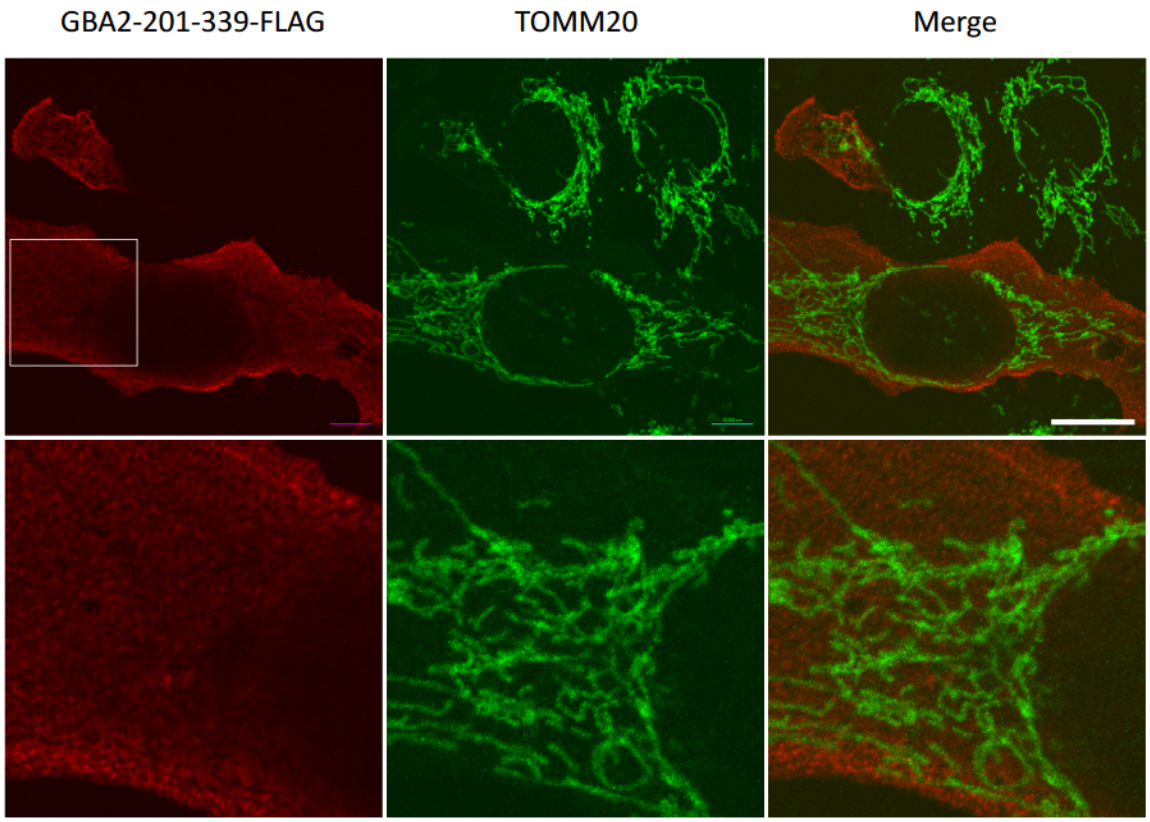

Figure 4.4.7.4. GBA2-201-339 does not cause mitochondrial fragmentation. U2OS cells expressing the GBA2-161-339 mutant were immunostained with anti-FLAG (red) and anti-TOMM20 (green) antibody at 48 hours of post-transfection. Scale bar, 20 μm.

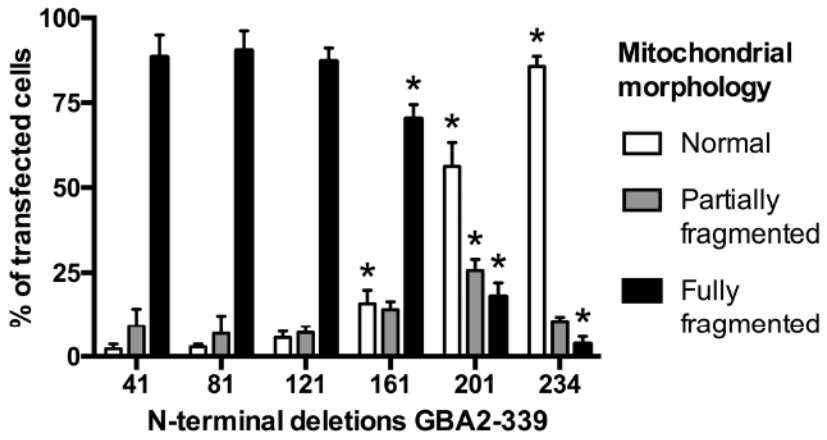

Figure 4.4.7.5. Mitochondrial morphology of U2OS cells expressing N-terminal deletion mutants of GBA2-339 (Arg340* mutant). U2OS cells expressing different N-terminal deletion mutants of GBA2-339 were scored based on their mitochondrial morphology. Asterisks indicate mitochondrial phenotypes of cells expressing Ndel-161, Ndel-201 and Ndel-234 which are statistically different from the mitochondrial phenotypes of cells expressing Ndel-41. At least 250 transfected cells were counted for each mutant. Data representing the average + SD of three individual experiments. Statistical analysis was done by one-way nested ANOVA.

4.4.8 GBA2 Expression Is Not Associated with Apoptosis

The GBA2 mutants Arg234* and Arg340* caused mitochondrial fragmentation and loss of mitochondrial transmembrane potential, both known to be important events in apoptotic process (196). So, it was of interest to see whether these proteins triggered apoptosis. To assess the effect of GBA2 mutation on apoptosis, I overexpressed WT GBA2, Arg234* truncation mutant, Asp594His point mutant, Glu527Gln active site mutant and Met510Valfs*17 frameshift mutant in tandem with mClover (a cytosolic green fluorescence protein) and isolated the transfected cells by flow cytometry, and analyzed the expression of apoptotic proteins Caspase 3, Caspase 7, and Caspase 9 by western blot.

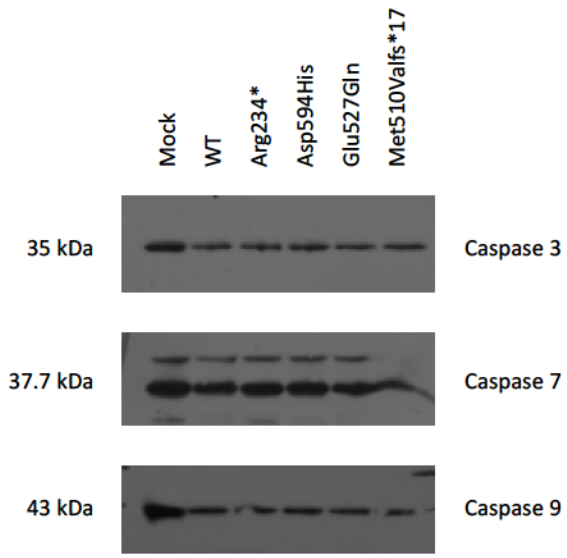

Figure 4.4.8. WT and mutant forms of GBA2 do not activate apoptotic pathway. Western blot analysis of FACS-sorted U2OS cells expressing WT or mutant forms of GBA2. Four different kinds of GBA2 mutants were expressed, truncation (Arg234*), missense (Asp594His), active-site (Glu527Gln) and frameshift (Met510Valfs*17). Neither WT nor the mutant versions of GBA2 affected the level of expression or processing pattern of caspase 3, caspase 7 and caspase 9.

Caspase 3, caspase 7, and caspase 9 are important proteins involved in the apoptotic pathway (197,198). Caspase 3 is known as an "executioner" that causes the activation of cascade of caspases responsible for apoptosis execution and activates caspase 7 and 9. Caspase 7 is directly involved in the execution of apoptosis, and Caspase 9 is an "instigator" (197,198). Western blot analysis of the cells expressing different forms of GBA2 did not show evidence of caspase activation (Figure 4.4.8). Furthermore, the nuclei of cells overexpressing WT or mutant forms of GBA2 did not look apoptotic (not shown). Nuclear condensation and fragmentation are important morphological features of apoptotic cells (199,200). Additionally, mitochondria of cells expressing different forms of GBA2 did not release cytochrome c, observed by fluorescence microscopy. Release of cytochrome c from mitochondria into the cytosol is

one of the events in the apoptotic cascade (196-198). These results indicate that short-term expression of GBA2 is not associated with apoptosis.

4.4.9 GBA2 Has No Effect on Some Mitochondria-Interactive Proteins

Western blot analysis of FACS-sorted cells expressing WT or truncation mutant of GBA2 showed that GBA2 had no effect on the processing or expression pattern of a few proteins found in the mitochondria, LONP1 (Lon Protease 1), HSP 60 (Heat Shock Protein 60), CLPP (Caseinolytic Mitochondrial Matrix Peptidase Proteolytic Subunit) and (AFG3 Like Matrix AAA Peptidase Subunit 2). LONP1 is an ATP-dependent protease (AAA+ protease) residing in the mitochondrial matrix. It causes selective degradation of misfolded, unassembled or oxidatively damaged polypeptides in the mitochondrial matrix (201). LONP1 has been reported to have a decreased gene expression in patients with hereditary spastic paraplegia (202,203). HSP60 is a mitochondrial chaperone that causes transportation and refolding of proteins from cytoplasm to mitochondrial matrix (204). CLPP is also a mitochondrial protease involved the quality control of mitochondrial proteins. CLPP defects has been associated in neurodegenerative disorders (205). Expression of WT GBA2 or the Arg234* truncation mutation did not have any effect on the expression of LONP1, HSP60 or CLPP (Figure 4.4.9.1).

AFG3L2 is the catalytic subunit of the m-AAA protease, an ATP-dependent proteolytic complex of the mitochondrial inner membrane that degrades misfolded proteins and regulates ribosome assembly (206,207). I also assessed the level of AFG3L2 in cells expressing WT and a range of GBA2 mutants. No form of GBA2 affected the level of AFG3L2 (Figure 4.4.9.2). Effect of GBA2 expression on the activation of AFG3L2 is yet to be done.

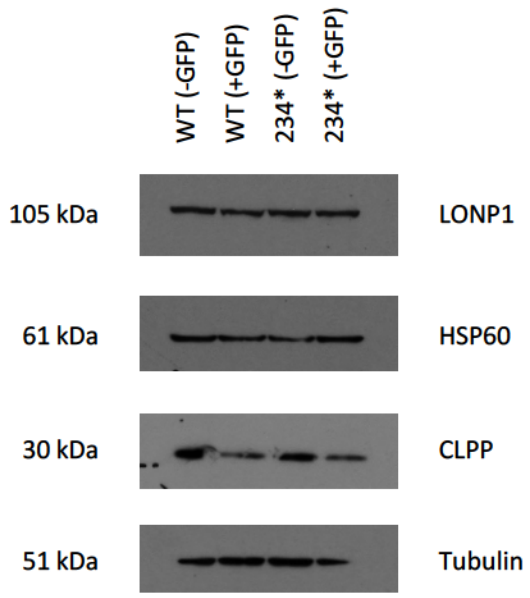

Figure 4.4.9.1. WT GBA2 and the Arg234* mutant do not change the levels of LONP1, HSP60, and CLPP. WT GBA2 and the Arg234* mutant were expressed in U2OS cells in tandem with mClover, and transfected cells were isolated by flow cytometry. Cell lysates were resolved by 12.5% polyacrylamide gel. (-GFP): non-transfected cells; (+GFP), transfected cells.

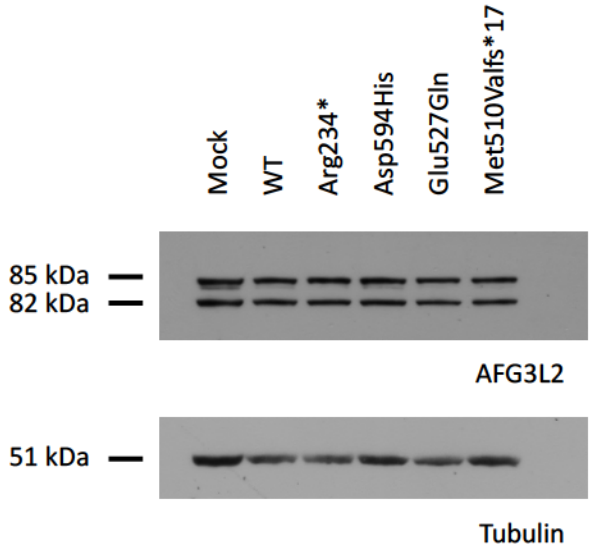

Figure 4.4.9.2. GBA2 expression has no effect on the level of AFG3L2. Transfected U2OS cells were analyzed by western blot (anti-AFG3L2). Levels of AFG3L2 were comparable for all forms of GBA2.

4.4.10 Long-Term Expression of GBA2 Mutants Is Not Well Tolerated in Cells

All previous experiments of this project were performed using transiently transfected cells. To further characterize the SPG46-associated GBA2 mutants, I needed more refined cellular models. So, I sought to generate cells lines stably expressing WT GBA2 and the Arg234* mutant via genome editing. GBA2 genes were inserted into the AAVS1-safe harbour locus of U2OS cells. The cells survived well all the initial steps of transfection, antibiotic treatment, dilution, colony picking and expansion, and I was able to select and grow ten individual colonies for each GBA2 construct, WT and Arg234*. By genomic PCR, the repair template was successfully integrated in most of the selected clones (Figure 4.4.10). I further verified the expression of WT GBA2 and Arg234* in cells where these proteins were stably transfected. Within three weeks of the initial transfection, I was able to detect WT and Arg234* GBA2 in some of the cell lines by western blot. By contrast, after 6 weeks of the transfection, none of the clones showed any sign of protein in western blot and immunofluorescence staining. This happened for both WT and Arg234* GBA2, indicating that long term-expression of GBA2 is not well tolerated in U2OS cells. It should be noted here that our lab previously generated stably transfected lines of SH-SY5Y cells for human and zebrafish GBA2 which were well tolerated (191).

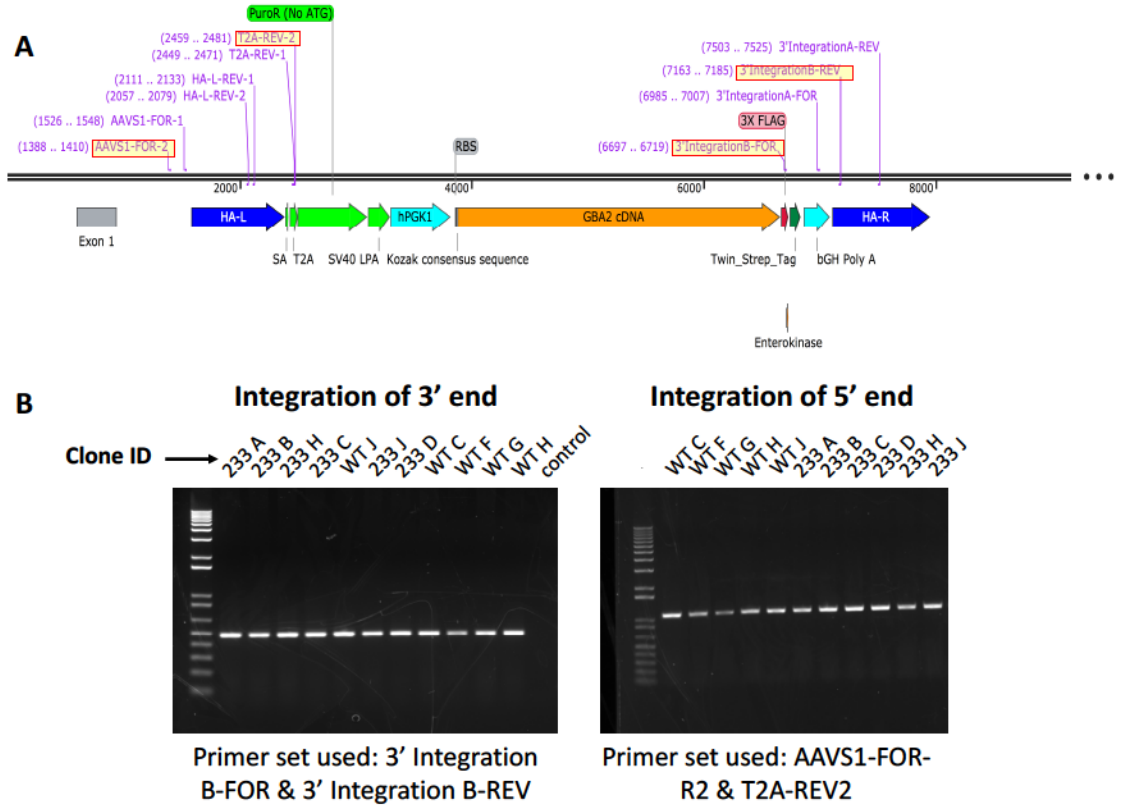

Figure 4.4.10. Genomic PCR results for selected clones of WT and Arg234* GBA2. CRISPR was used for genomic knock-in in the AAVS1 locus of osteosarcoma cells. (A) Schematic of AAVS1 safe harbor locus after integration of repair template using CRISPR/Cas9. Purple arrows and letters indicate the genomic primers available for PCR to confirm the genomic integration in selected clones; primers enclosed in red rectangles were used for the genomic PCR shown in this image (B) Results of genomic PCR to check for integration of cDNA, selected clones were coded with English alphabets.

4.5 Discussions

4.5.1 Protein-Protein Association Is Important for Enzyme Activity of GBA2

Mutations have been identified in *GBA2* in patients presenting with a combination of cerebellar ataxia and spastic paraplegia (SPG46) and with Marinesco-Sjögren-like syndrome. I have investigated the biochemical and cell biological consequences of ten SPG46-associated GBA2 mutants, five of which are nonsense mutants (Tyr121*, Trp173*, Arg234*, Arg340*, and Arg870*) and five are missense mutants (Phe419Val,

Asp594His, Arg630Trp, Gly683Arg, or Arg873His). Overexpression of WT GBA2 elevated the GBA2 activity in HeLa and COS-7 cells whereas none of the pathogenic variants of GBA2 raised the GBA2 enzyme activity. The lack of enzyme activity is expected for the first four truncation mutants (Tyr121*, Trp173*, Arg234*, Arg340*) as they lack the active site residues Glu527 and Asp677 (86). But the reason of enzyme inefficiency of the longest truncation mutant Arg870* which lacks only 57 amino acids from the C-terminus of the WT GBA2 or the mutants with single amino acid substitution is not understood. In transfected cells, the levels of expression of mutant proteins were variable (confirmed by western blot) but the transfection efficiencies were comparable. Furthermore, I assessed if there was any quantitative deficit in the mutant proteins caused by poor protein stability by investigating whether the proteins were being degraded by the ubiquitin-proteasome system. The truncation mutants (Trp173* and Arg234*) were noticeably subjected to proteasomal degradation and potential to ubiquitination. The point mutants Gly683Arg and Asp594His underwent proteasomal degradation, but at much lesser extent.

Via blue-native gel electrophoresis, I observed that the WT GBA2 forms a dimer under native conditions. By contrast, all but Gly683Arg GBA2 mutants formed high-molecular weight complexes. Gly683Arg formed a dimer as well as high-molecular weight complexes. This specific mutant was also exceptional in terms of GBA2 activity. Overexpression of Gly683Arg caused a slight elevation of GBA2 activity above the endogenous GBA2 activity in HeLa and COS-7 cells. Minor elevation of GBA2 activity was also observed when Gly683Arg was co-expressed with the enzymatically inactive Glu527Gln active site mutant. Considering all the exceptions associated the Gly683Arg

mutant, it can be speculated that the presence of the dimeric form is important for enzyme activity of GBA2. GBA2 has been reported as a self-associating protein (195). High throughput interactome studies have identified a number of proteins as binding partners of WT GBA2 (Table 1, chapter 1) and one of the binding partners of GBA2 is GBA2 itself. Our results suggest that this self-association of GBA2 is required for its enzymatic activity. It is not clear at this point why the truncation mutants or the other point mutants fail to form a dimer. For the truncation mutations, it is understandable that their three-dimensional structures are different as they lack a major part of GBA2. But, for the point mutations, it would be interesting to investigate how a single amino acid change affects the three-dimensional structure and dimerization of GBA2. X-ray crystallography or NMR spectroscopy would provide valuable information regarding the structure of GBA2 mutants.

4.5.2 Lack of GBA2 Dimer Is Associated with the Disease Severity of SPG46

SPG46 is a neurodegenerative disorder associated with mutations in *GBA2*. Some common clinical features of SPG46 are spasticity of upper and lower limbs, cerebellar ataxia, cognitive impairment and thin corpus callosum (83,118,208). Severity of disease is variable among patients carrying different mutations of *GBA2*. Patients carrying the Gly683Arg mutation have a less severe phenotype compared to patients carrying other *GBA2* mutations (208). The family carrying the Gly683Arg mutation includes three siblings, a pair of dizygotic twins, and a third sibling, and all of them inherited the homozygous mutation from their parents (Figure 4.5.2.1). These three siblings presented with spasticity, cerebellar signs and eyelid ptosis, although the degree of disease severity is higher in case of one sibling who suffers from severe spasticity with impaired gait. For

other two siblings, the disease is at subclinical levels, evident only at neurological examinations (208). In my project, the Gly683Arg mutation behaved differently than other SPG46-associated GBA2 mutations in terms of enzyme activity and dimerization. In conclusion, it seems that the presence of GBA2 dimer is associated with a milder phenotype in SPG46 patients. In other words, the lack of GBA2 dimer is related to the pathophysiology of SPG46.

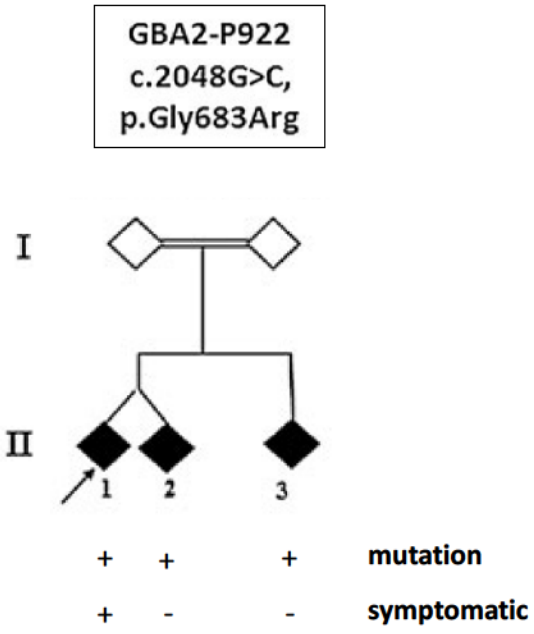

Figure 4.5.2.1. The Pedigree of the familial case carrying Gly683Arg GBA2 mutation. Diamond symbols indicate anonymous persons; white and black symbols indicate healthy and affected individuals, respectively. The arrow indicates the proband. All three siblings carry the mutation, but only one of them are symptomatic. [Image source: Citterio, *et al*. (208)].

4.5.3 GBA2 Has Multiple Mitochondrial Targeting Sites

Four of the SPG46-associated GBA2 truncation mutants (Tyr121*, Trp173*, Arg234* and Arg340*) caused mitochondrial fragmentation and were co-localized with fragmented mitochondria when overexpressed in multiple cell lines. The truncation mutants also promoted mitochondrial import of WT GBA2 and full-length GBA2 mutants. Electron microscopy further confirmed that the truncation mutants were present in the mitochondrial matrix. Additionally, WT GBA2 was also present in the mitochondrial matrix in a small number of cells. These data suggest that GBA2 has a mitochondria-targeting motif that is exposed in certain conditions, for example in the N-terminal fragments ending after amino acids 233 and 339 encoded by nonsense mutations. The mitochondria-targeting sequence of GBA2 might also be activated in full-length GBA2 in those rare cells where we observed WT GBA2 in mitochondria by electron microscopy. As the shortest truncation mutant that was localized in the mitochondria was the Tyr121*, there is likely a mitochondria-targeting sequence within the first 121 N-terminal amino acids of GBA2. My attempt of identifying the more precise location of this sequence was not successful because of lack of expression of shorter peptide fragments of the first 121 amino acids. I also focused on the first 233 amino acids of the GBA2-339 mutant to identify a mitochondria-targeting sequence within the first 233 amino acids of GBA2. I made few truncation mutants that lacked 40, 80, 120, 160, 200, or 233 amino acids from the N- terminus of GBA2-339 or carried internal deletions of 40, 80, 120, 160, or 200 amino acids ending at amino acid 234 of GBA2-339 (Figure 4.5.3.1). The internal deletions did not cause any mitochondrial fragmentation, but the N-terminal deletions caused mitochondrial fragmentation until the

first 160 amino acids were missing. When the first 200 amino acids were missed from the N-terminus of GBA2-339, the mutant proteins remained in the cytoplasmic compartment without affecting the mitochondria. This result points towards the presence of a potential mitochondrial targeting sequence within amino acids 160-200 of GBA2. It is intriguing that the potential mitochondrial targeting sequence that I have identified (160-200 amino acids) is also present in one of the internal deletion mutants, but I did not see any mitochondrial localization of the mutant protein in case of that mutant. So, it is not only the presence of a potential targeting sequence, but the sequence following the target sequence is also important for import of GBA2 into mitochondria. At this point I can conclude that it is likely that GBA2 has multiple mitochondrial targeting sequences.

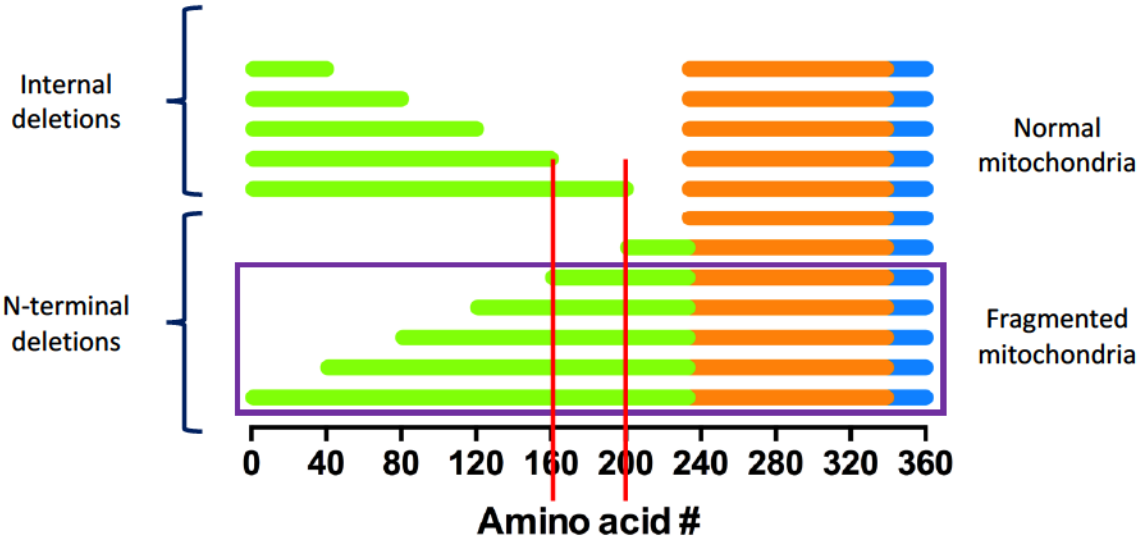

Figure 4.5.3.1. Schematic of internal deletion mutants and N-terminal deletion mutants targeting the first 233 amino acids of GBA2-339. Internal deletions did not cause mitochondrial fragmentation. N-terminal deletions caused mitochondrial fragmentation until the first 160 amino acids were missing (mutants present within the purple box). Potential mitochondrial targeting sequence resides within the 160 and 200 amino acids of GBA2 (the region between two red lines). Green lines: amino acid 1 – 234, orange line: amino acids 235-340, blue line: c-terminal FLAG-tag.

4.5.4 Expression of GBA2 Mutants and Apoptosis

Expression of truncated GBA2 mutants caused mitochondrial fragmentation and complete loss of mitochondrial membrane potential. These incidents are known as pro-apoptotic stimuli that trigger the cascade of apoptotic cell death (209-211). To confirm whether the overexpression of the GBA2 mutants activate the apoptotic pathway, I assessed the levels of expression and processing patterns of caspase 3, caspase 7 and caspase 9 in cells exclusively expressing different mutant forms of GBA2. None of the GBA2 mutants activated the above-mentioned caspases. Also, apoptotic nuclei were not seen in cells expressing any form of GBA2. Condensed or fragmented nuclei are morphological features of apoptotic cell (199,200). Additionally, when I used anti-cytochrome c antibody as a mitochondrial marker for immunofluorescence staining of cells expressing different forms of GBA2, cytochrome c was contained inside mitochondria, irrespective of mitochondrial morphology. Release of cytochrome c from mitochondria into cytosol is one of the early incidents in the apoptotic cascade (196-198). Containment of cytochrome c in the mitochondria indicated that the cells were not apoptotic upon overexpression of WT or mutant GBA2. But there were two important limitations of these studies. The first one is, all of my observations were made at 48 hours of post-transfection. I did not examine the cells expressing GBA2 mutants for a longer period. It is not impossible that long-term expression of GBA2 mutants may lead to apoptosis. My unsuccessful attempt of generating stable cell lines expressing WT and Arg234* mutation of GBA2 supports this assumption. I experienced that long-term expression of GBA2 was not well tolerated in osteosarcoma cells and GBA2 could not be detected in cells after three weeks of transfection. Another limitation of my studies was

that most of the experiments were performed in osteosarcoma cells which are cancer cells. Cancer cells are anti-apoptotic by nature (212). So, use of osteosarcoma cells could be another reason that I was unable to detect any early apoptotic feature in cells expressing GBA2 mutants. Examination of non-cancerous cells expressing GBA2 mutants for a longer period would give better insights into their effects on apoptosis.

4.5.5 Truncated GBA2 Mutants are More Likely to Interfere with Mitochondrial Fusion

I have observed that the truncated GBA2 mutants caused mitochondrial fragmentation and co-localized with fragmented mitochondria whereas the missense mutants did not cause mitochondrial fragmentation and. So, it is obvious that the truncated GBA2 mutants either hinder mitochondrial fusion or accelerate mitochondrial fission, resulting in the formation of fragmented mitochondria. The truncation mutants were transported into the mitochondrial matrix, observed by electron microscopy. One of the key proteins regulating mitochondrial fusion, the GTPase OPA1, is anchored in the inner mitochondrial membrane and extends into the intermembrane space (213). Western blot analysis of transfected cells isolated by flow cytometry revealed that the Arg234* truncation mutant depleted the higher molecular weight OPA1 isoforms. This result further confirms that the truncated mutants interfere with the mitochondrial fusion process and lead to formation of fragmented mitochondria.

I also observed that the truncated GBA2 mutants caused an almost complete loss of mitochondrial membrane potential. There is a complex interplay between mitochondrial membrane potential and mitochondrial dynamics (214). In summary, there are four major observations related to overexpression of truncated GBA2 mutants and

mitochondrial dynamics –(i) import of truncated mutant into the mitochondria, (ii) mitochondrial fragmentation, (iii) loss of mitochondrial membrane potential and (iv) depletion of higher molecular weight OPA1 isoforms. But it was not clear how these events were linked to each other.

OPA1 has two cleavage sites, S1 and S2. Alternative proteolytic processing of OPA1 in these two sites generates different isoforms of OPA1 (215). The specific function of each OPA1 isoform has not been fully elucidated as yet, but it appears that the long isoforms are important for mitochondrial fusion (216). Two mitochondrial inner membrane proteases, OMA1 and YME1L1, regulate the balance between long and short OPA1 forms (217). YME1L1 is constitutively active, whereas OMA1 is activated when the mitochondrial membrane is depolarized (218,219).

The most two common isoforms of OPA1 are isoform 1 and 2 (Figure 4.5.5.1). Isoform 1 has cleavage site S1, and isoform 2 has cleavage sites S1 and S2. Isoform 1 can be cleaved only by OMA1, but isoform 2 can be cleaved by both proteases, OMA1 and YME1L1 (Figure 4.5.5.1). Alternative cleavages of Isoform 1 and 2 by OMA1 and YME1L1 produces total five isoforms of OPA1. The membrane-anchored, non-cleaved long forms of Isoform 1 and 2 have the molecular weights of 101.6 kDa and 105.8 kDa respectively. Cleavage of isoform 1 and 2 by activated OMA1 generates two short-chain soluble forms of OPA1 having the molecular masses of 89.1 kDa and 93.3 kDa respectively. In case of YMEIL1 activation, Isoform 2 is cleaved, producing another short-chain, soluble form of OPA1 (90.6 kDa) (145,220,221).

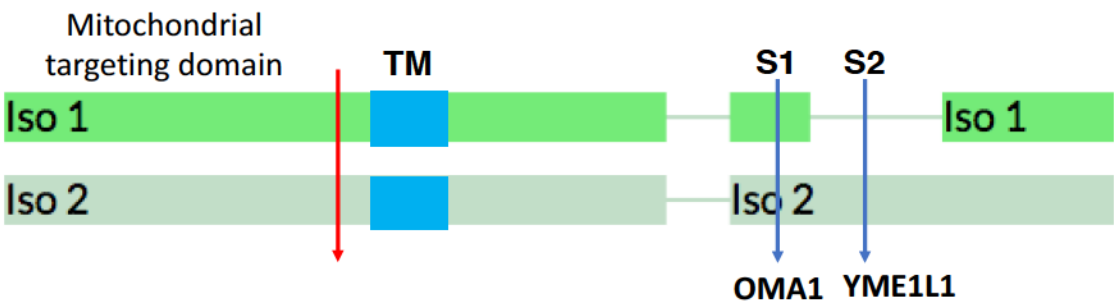

Figure 4.5.5.1. Common OPA1 isoforms. Schematic depiction of the two common isoforms of OPA1, Iso 1 and Iso 2, with the cleavage sites S1 and S2 and the mitochondrial targeting domain at the N-terminus, which is immediately followed by a transmembrane domain. OMA1 cleaves Iso 1 and 2 at S1 while YME1L1 only cleaves Iso 2 at S2. The red arrow indicates the cleavage site of mitochondrial targeting domain.

Taking together my observations and the literature, it can be speculated that expression of truncated GBA2 mutants and import into mitochondrial matrix caused depolarization of mitochondrial membrane. Loss of mitochondrial membrane potential might have activated OMA1, leading to cleavage of OPA1 by OMA1 and depletion of long isoforms of OPA1. As the long forms of OPA1 are important for the fusion process, lack of longer isoforms is likely to hamper the mitochondrial fusion process and promote mitochondrial fragmentation. The possible sequence of events in cells expressing truncated GBA2 mutants is outlined in Figure 4.5.5.1, which of course is a subject of further investigation.

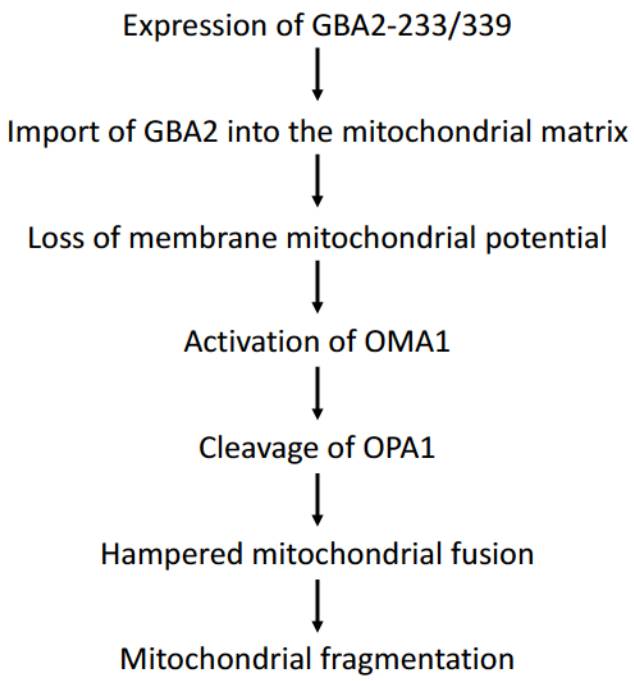

Figure 4.5.5.1. Hypothetical pathway for truncated GBA2 mutants leading to mitochondrial fragmentation.

4.5.6 SPG46 Is a Developmental Disorder

The goal of this project was to characterize various GBA2 mutants associated with SPG46. After investigating a number of biochemical and cell biological aspects of ten SPG46-associated GBA2 mutants, two common features were found, (i) enzymatic inactivity, and (ii) formation of high-molecular weight protein complexes.

Previously, no studies have reported any neurological symptoms associated with pharmacological or genetic inhibition of GBA2 in either human or mice. GBA2 knockout mice accumulates glucosylceramide in the brain and liver, but do not present any neurological symptoms or a reduced lifespan (82). Recently, it has been reported that *gba2*-knockout zebrafish do not display neurological symptoms (222). Moreover, GBA2 inhibition or silencing improved the neurological manifestations in a number of

conditions. Pharmacological inhibition of GBA2 by imino sugars in Niemann-Pick type C1 (NPC1) mouse models reduces the inflammation of central nervous system, delays the loss of motor coordination, and extends lifespan (223,224). Similarly, *Gba2* gene ablation in NPC1 mice delays the onset of motor deficits and loss of Purkinje cells (225). Disruption of *Gba2* in Type 1 Gaucher mouse models reduces disease severity (98) and Gaucher patients treated with miglustat for over ten years do not develop neurological symptoms (97). The identification of *GBA2* mutations in SPG46 was the first time GBA2 was reported to be involved in a neurodegenerative disorder.

Taking together all previous observations with GBA2 and my findings, two possible explanations can be put forward for the involvement of GBA2 in SPG46 and related motor neuron disorders. Patients affected with SPG46 inherit the mutated gene and grow up with forms of GBA2 that are functionally inactive and structurally aberrant. This makes the cases of SPG46 different from all other previous studies with GBA2. In case of pharmacological inhibition of GBA2 by miglustat or other inhibitors in either human or mice, fully functional GBA2 is being inactivated at a certain age to treat specific disease conditions. By the time GBA2 is being inactivated by drug administration, it must have performed its role during the developmental stage of the animal. So inhibiting GBA2 at that point without neurological symptoms does not provide any insight on the role of GBA2 during the developmental stage, especially on the development of the nervous system. On the other hand, *Gba2*-knockout mice do not produce the protein at all. Further, in a recent study (80), a number of SPG46-associated mutations were introduced into murine Gba2 and expressed in CHO cells, including all the five truncated GBA2 mutants that I have used in my study. None of the murine Gba2

mutants caused an abnormal mitochondrial phenotype, indicating a different role of mouse Gba2.

The pathophysiology associated with SPG46 seems be associated with the lack of enzyme activity of GBA2 which may change GSL profiles during human development. My study points towards the lack of GBA2 activity during development while other studies show that dysregulation of GSL homeostasis affects proper growth and functioning of the nervous system, including motor neurons functioning (32,33,37). In addition, it is increasingly evident that sphingolipids have functional roles in mitochondria, regulating the sensitivity of cells to apoptosis, mitophagy and stress signaling (226,227). In my study we have already observed truncated mutants are disrupting mitochondrial membrane potential and obstructing mitochondrial fission. It would be insightful to assess the GSL profiles of cellular or animal models carrying GBA2 mutations, with emphasis on the GSL profiles of mitochondria to understand the pathophysiology of SPG46.

I also found that GBA2 mutants form high molecular weight protein complexes under native conditions. High-throughput interactome studies have shown that GBA2 dimerizes and interacts with mitochondrial and other cellular proteins (100-102). The protein complexes formed by mutant forms of GBA2 could have aberrant activities and disrupt human development. SPG46 patients grow up with protein complexes formed by GBA2 mutants which may perturb important cellular processes. It is important to identify the composition of the protein complexes formed by mutant versions of GBA2 to understand the role of GBA2 on fundamental cellular processes and human development. It is also important to assess to what extent the truncated mutants are being expressed in

patients as there is a possibility of nonsense-mediated mRNA decay, a cellular surveillance mechanism for eliminating mRNAs harboring premature stop codons, preventing the production of truncated proteins (228,229).

For now, our findings indicate that SPG46 is a developmental disorder and that structural and functional deficiencies of GBA2 mutants are the bases of the development of complex neurological deficiencies in SPG46. Structural defects abolish the enzymatic activity of disease-associate mutants of GBA2 and change their protein-binding properties. Certain structural features (potential mitochondrial targeting sequences) also promote mislocalization of GBA2 from their usual cellular compartments (plasma membrane or ER) to mitochondria and impair mitochondrial dynamics and bioenergetics, which may also contribute to neurological symptoms in SPG46 (230-232).

Chapter 6: Conclusion

This thesis has attempted to understand the homeostatic regulation of glycosphingolipids (GSLs) in cultured cells by genetically or pharmacologically manipulating GSL biosynthesis and degradation. However, *in-vitro* studies on cellular models appeared not to be suited for achieving these aims. Animal models or more refined cellular models, such as stable cell lines or suspension cells, with careful consideration of experimental parameters are required to obtain reproducible and robust GSL profiles to understand how GSL homeostasis is maintained.

It has been relatively recent, about last 10 years, the effect of GBA2 on GSL metabolism has been identified (89,233,234), but the roles of GBA2 in human physiology have poorly been understood. This thesis took the opportunity to explore a number of biochemical and cell biological aspects of GBA2 mutations identified in SPG46 patients. This segment of my study has revealed some striking effects of GBA2 mutants on mitochondrial structure and functions which have not been previously reported. My study indicated that GBA2 has potential mitochondrial targeting sequences and that GBA2 can be conditionally imported into mitochondria. These are all preliminary data and further investigations are required to understand the conditions and exact mechanisms of mitochondrial import of GBA2 and its consequences. Apart from that, we also need to understand how do GBA2 mutations are leading to the complex pathophysiology involved in SPG46 and related motoneuron diseases. Mitochondrial impairment may be a part of the pathophysiology, but dysregulations of GSL homeostasis may likely lie at the core of the pathophysiology. Exploring the role of GBA2 on neuronal cells and animal models would be helpful in this context.

APPENDIX A. SUPPLEMENTARY MATERIALS

Table I. Pharmacological/ Chemical Compounds, Cell Culture Reagents, Dishes and Kits

Pharmacological/ chemical compounds, Kits, Reagents	Company	Catalogue number
Accutase	Thermo Fischer Scientific	00-4555-56
30% Acrylamide Bis Solution 29:1	Bio-Rad	161-0156
AG 3-X4A resin	Bio-Rad	1401341
Ammonium persulfate	Bio-Rad	161-0700
Amersham ECL Western Blotting Detection Reagent	GE Healthcare	RPN2106
Complete EDTA-free protease inhibitor cocktail tablets	Roche Diagnostics	04 693 132 001
Digitonin (5%)	Invitrogen	BN2006
Dithiothreitol	Bio-Rad	161-0611
Fetal bovine serum (FBS)	Sigma-Aldrich	F1051
FCCP	Sigma-Aldrich	C2920-10MG
FluoroBrite DMEM	Gibco by Life Technologies	A18967-01
GeneJET Plasmid Miniprep Kit	Fermentas	K0503
GeneJET Endo-free plasmid Maxiprep Kit	Fermentas	K0861
Ibidi cells in focus (glass bottom cell culture dishes	Ibidi GmbH	81158
Immobilon-P PVDF membranes	EMD Milipore corporation	IPVH00010
InnuPREP Gel Extraction Kit	Life Science unlimited/analyticjena	
Lactacystin	Toronto Research Chemicals Incorporation	L101000

Pharmacological/ chemical compounds, Kits, Reagents	**Company**	**Catalogue number**
Lipofectamine 2000	Invitrogen	11668-027
Mdivi-1	Enzo Life Sciences	BML-CM127-001
MG-132	Selleckchem.com	S2619
Native-PAGE G-250 Sample additive	Invitrogen	BN20042
Native-PAGE 4X sample buffer	Invitrogen	BN20032
Native-PAGE 20X Cathode Buffer Additive	Invitrogen	BN2002
Native-PAGE 20X Running Buffer	Invitrogen	BN2001
Native-PAGE™ 3-12% Bis-Tris Protein Gels	Invitrogen	BN1001BOX
*N*B-DGJ	Toronto Research Chemicals	B690500
NucleoSpin Gel and PCR Clean-up	Macherey-Nagel	740609.10
Octyl-Sepharose® CL-4B	Milipore Sigma	68652-09-5
Opti-MEM	Gibco	31985-070
Pierce BCA Protein Assay Reagent A	Thermo Scientific	23223
Pierce BCA Protein Assay Reagent B	Thermo Scientific	23224
Pierce Bovine Serum Albumin Standard Ampules, 2mg/ml	Thermo Scientific	P123209
Precision Plus Protein All Blue Standards	Bio-Rad	161-0373
Puromycin	Gibco by Life Technologies	A11138-03

Pharmacological/ chemical compounds, Kits, Reagents	Company	Catalogue number
QuickExtract DNA Extraction Solution	Epicentre (available through Lucigen)	QE09050
Restore Western blot stripping buffer	Thermo Fischer Scientific	21059
SeperSignal West Pico Chemiluminescent Substrate	Thermoscientific	32209
Sep-Pak C18 1 cc Vac Cartridge	Waters	WAT023590
SuperSignal West Pico PLUS Chemiluminescent Substrate	Thermoscientific	34577
Tetramethylethylenediamine	Bio-Rad	161-0800
Thin-layer chromatography (TLC) silica gel G	Analtech	5719800
TMRM	Invitrogen	134361
TransIT LT1	Mirus Biolynx	MIR 2300
TransIT 2020	Mirus Biolynx	MIR 5404
Trypsin (0.25%) with EDTA	Invitrogen	11900-073
TSKgel® Amide-80 HPLC Column	TOSOH Bioscience LLC	32110501
T4 DNA ligase buffer	Thermo Scientific	B69
Vectashield, Mounting Medium for Fluorescence	Vector Laboratoreis Incorporations	VECTH1200
Wizard Genomic DNA Purification Kit	Promega	A1120
X-ray films	Radiomat LS	XC6A2
1 Kb plus DNA ladder	Invitrogen	10787-018

Table II. Antibodies Information.

Antibodies	Company	Catalogue number
Anti-AFG3L2, rabbit polyclonal	Protientech	14631-1-AP
Alexa Fluor 488 goat anti-rabbit	Thermoscientific	A11034
Alexa Fluor 488 goat anti-rabbit	Thermoscientific	A11032
Alexa Fluro 645 mouse anti-cytochrome C (clone 6H2.B4)	BD Pharmigen/BD Bioscience	558709
Anti-alpha-tubulin, rabbit monoclonal	Cell Signaling	2125S
Anti-Calreticulin, rabbit polyclonal	Enzo Life Sciences	ADI-SPA-600-F
Anti-Caspase-3, rabbit monoclonal	Cell Signaling	9662
Anti-Caspse-7, mouse monoclonal	Cell Signaling	9494
Anti-Caspase-9, rabit monoclonal	Cell Signaling	9502
Anti-CLPP, rabbit monoclonal	Cell Signaling	14181S
Anti-COX IV, rabbit monoclonal	Cell Signaling	4850S
Anti-cytochrome c, mouse monoclonal	BD Bioscience	556432
Anti-ATF4, rabbit monoclonal	Cell Signaling	11815S
Anti-DRP1, rabbit monoclonal	Cell Signaling	8570S
Anti-DYKDDDDDK, rabbit monoclonal	Cell Signaling	2368S
Anti-FLAG M2, mouse monoclonal	Sigma	1002687-430
Anti-GAPDH (14C10), rabbit monoclonal	Cell Signaling	2118S
Anti-GBA2, mouse polyclonal	Abcam	ab69366
Anti-HA biotin, rat monoclonal	Roche	12158167001
Anti-LONP1/PRSS15 (clone D8W1J), rabbit monoclonal	Cell Signaling	28020S

Antibody	Company	Catalogue number
Anti-OPA1, mouse monoclonal	BD Transduction Laboratories	612606
Anti-TOM20, mouse monoclonal	BD Transduction Laboratories	612278
Anti-TOM20 (FL-145), rabbit polyclonal	Santa Cruz Biotechnology	Sc-11415
Anti-Ubiquitin, mouse monoclonal	Cell signaling	3936P
Peroxidase Affinity Pure Goat Anti-Rabbit IgG (H+L)	Jackson Immuno Research Laboratories	111-035-003
Peroxidase Affinity Pure Goat Anti-mouse IgG (H+L)	Jackson Immuno Research Laboratories	115-035-003
Streptavidin, Alexa Fluor 635 conjugate	Invitrogen	S32364
Streptavidin, Alexa Fluor 488 conjugate	Invitrogen	S11227

REFERENCES

1. Bielawski, J., Pierce, J. S., Snider, J., Rembiesa, B., Szulc, . M., and Bielawska, A. (2010) Sphingolipid analysis by high performance liquid chromatography-tandem mass spectrometry (HPLC-MS/MS). *Adv Exp Med Biol* **688**, 46-59

2. Quinn, P. J. (2013) Structure of sphingomyelin bilayers and complexes with cholesterol forming membrane rafts. *Langmuir* **29**, 9447-9456

3. Jana, A., and Pahan, K. (2010) Sphingolipids in multiple sclerosis. *Neuromolecular Med* **12**, 351-361

4. Olsen, A. S. B., and Færgeman, N. J. (2017) Sphingolipids: membrane microdomains in brain development, function and neurological diseases. *Open Biol* **7**

5. Platt, F. M., Jeyakumar, M., Andersson, U., Dwek, R. A., and Butters, T. D. (2005) New developments in treating glycosphingolipid storage diseases. *Adv Exp Med Biol* **564**, 117-126

6. Kolter, T., Proia, R. L., and Sandhoff, K. (2002) Combinatorial ganglioside biosynthesis. *J Biol Chem* **277**, 25859-25862

7. Barreto-Bergter, E., Pinto, M. R., and Rodrigues, M. L. (2004) Structure and biological functions of fungal cerebrosides. *Anais da Academia Brasileira de Ciências* **76**, 67-84

8. Labrada, M., Dorvignit, D., Hevia, G., Rodríguez- hurbenko, N., Hernández, A. M., Vázquez, A. M., and Fernández, L. E. (2018) GM3(Neu5Gc) ganglioside: an evolution fixed neoantigen for cancer immunotherapy. *Seminars in Oncology* **45**, 41-51

9. Yu, R. K., Tsai, Y. T., Ariga, T., and Yanagisawa, M. (2011) Structures, biosynthesis, and functions of gangliosides--an overview. *J Oleo Sci* **60**, 537-544

10. úñiga, M., Monedero, V., and Yebra, M. J. (2018) Utilization of Host-Derived Glycans by Intestinal Lactobacillus and Bifidobacterium Species. *Frontiers in Microbiology* **9**

11. Heald, P. J., and Robinson, M. A. (1961) The metabolism of sulphatides in cerebral tissues. *The Biochemical journal* **81**, 157-163

12. Tettamanti, G. (2004) Ganglioside/glycosphingolipid turnover: new concepts. *Glycoconj J* **20**, 301-317

13. Di Pardo, A., Basit, A., Armirotti, A., Amico, E., Castaldo, S., Pepe, G., Marracino, F., Buttari, F., Digilio, A. F., and Maglione, V. (2017) De novo Synthesis of Sphingolipids Is Defective in Experimental Models of Huntington's Disease. *Frontiers in Neuroscience* **11**

14. Bartke, N., and Hannun, Y. A. (2009) Bioactive sphingolipids: metabolism and function. *J Lipid Res* **50 Suppl**, S91-96

15. Levy, M., and Futerman, A. H. (2010) Mammalian ceramide synthases. *IUBMB Life* **62**, 347-356

16. D'Angelo, G., Polishchuk, E., Tullio, G. D., Santoro, M., Campli, A. D., Godi, A., West, G., Bielawski, J., Chuang, C.-C., van der Spoel, A. C., Platt, F. M., Hannun, Y. A., Polishchuk, R., Mattjus, P., and De Matteis, M. A. (2007) Glycosphingolipid synthesis requires FAPP2 transfer of glucosylceramide. *Nature* **449**, 62-67

17. D'Angelo, G., Rega, L. R., and De Matteis, M. A. (2012) Connecting vesicular transport with lipid synthesis: FAPP2. *Biochim Biophys Acta* **1821**, 1089-1095

18. D'Angelo, G., Capasso, S., Sticco, L., and Russo, D. (2013) Glycosphingolipids: synthesis and functions. *FEBS J* **280**, 6338-6353

19. Gault, C. R., Obeid, L. M., and Hannun, Y. A. (2010) An overview of sphingolipid metabolism: from synthesis to breakdown. *Adv Exp Med Biol* **688**, 1-23

20. Hanada, K., Kumagai, K., Yasuda, S., Miura, Y., Kawano, M., Fukasawa, M., and Nishijima, M. (2003) Molecular machinery for non-vesicular trafficking of ceramide. *Nature* **426**, 803-809

21. Sun, A. (2018) Lysosomal storage disease overview. *Ann Transl Med* **6**, 476-476

22. Iwamori, M., Shimomura, J., Tsuyuhara, S., and Nagai, Y. (1984) Gangliosides of Various Rat Tissues: Distribution of Ganglio-N-Tetraose-Containing Gangliosides and Tissue-Characteristic Composition of Gangliosides. *The Journal of Biochemistry* **95**, 761-770

23. Iwamori, M., Shimomura, J., Tsuyuhara, S., and Nagai, Y. (1984) Gangliosides of various rat tissues: distribution of ganglio-N-tetraose-containing gangliosides and tissue-characteristic composition of gangliosides. *J Biochem* **95**, 761-770

24. Schaeren-Wiemers, N., van der Bijl, P., and Schwab, M. E. (1995) The UDP-galactose:ceramide galactosyltransferase: expression pattern in oligodendrocytes and Schwann cells during myelination and substrate preference for hydroxyceramide. *J Neurochem* **65**, 2267-2278

25. Palmano, K., Rowan, A., Guillermo, R., Guan, J., and McJarrow, P. (2015) The role of gangliosides in neurodevelopment. *Nutrients* **7**, 3891-3913

26. Muthing, J., Maurer, U., Sostaric, K., Neumann, U., Brandt, H., Duvar, S., Peter-Katalinic, J., and Weber-Schurholz, S. (1994) Different distributions of glycosphingolipids in mouse and rabbit skeletal muscle demonstrated by biochemical and immunohistological analyses. *J Biochem* **115**, 248-256

27. Xu, Y.-H., Barnes, S., Sun, Y., and Grabowski, G. A. (2010) Multi-system disorders of glycosphingolipid and ganglioside metabolism. *Journal of lipid research* **51**, 1643-1675

28. Malisan, F., and Testi, R. (2002) GD3 ganglioside and apoptosis. *Biochim Biophys Acta* **1585**, 179-187

29. Dyatlovitskaya, E. V., Novikov, A. M., Gorkova, N. P., and Bergelson, L. D. (1976) Gangliosides of hepatoma 27, normal and regenerating rat liver. *Eur J Biochem* **63**, 357-364

30. hang, T., de Waard, A. A., Wuhrer, M., and Spaapen, R. M. (2019) The Role of Glycosphingolipids in Immune Cell Functions. *Frontiers in Immunology* **10**

31. Yamashita, T., Wada, R., Sasaki, T., Deng, C., Bierfreund, U., Sandhoff, K., and Proia, R. L. (1999) A vital role for glycosphingolipid synthesis during development and differentiation. *Proc Natl Acad Sci U S A* **96**, 9142-9147

32. Jennemann, R., Sandhoff, R., Wang, S., Kiss, E., Gretz, N., uliani, C., Martin-Villalba, A., Jager, R., Schorle, H., Kenzelmann, M., Bonrouhi, M., Wiegandt, H., and Grone, H. J. (2005) Cell-specific deletion of glucosylceramide synthase in brain leads to severe neural defects after birth. *Proc Natl Acad Sci U S A* **102**, 12459-12464

33. Wennekes, T., van den Berg, R. J., Boot, R. G., van der Marel, G. A., Overkleeft, H. S., and Aerts, J. M. (2009) Glycosphingolipids--nature, function, and pharmacological modulation. *Angew Chem Int Ed Engl* **48**, 8848-8869

34. Yamashita, T., Hashiramoto, A., Haluzik, M., Mizukami, H., Beck, S., Norton, A., Kono, M., Tsuji, S., Daniotti, J. L., Werth, N., Sandhoff, R., Sandhoff, K., and Proia, R. L. (2003) Enhanced insulin sensitivity in mice lacking ganglioside GM3. *Proc Natl Acad Sci U S A* **100**, 3445-3449

35. Takamiya, K., Yamamoto, A., Furukawa, K., hao, J., Fukumoto, S., Yamashiro, S., Okada, M., Haraguchi, M., Shin, M., Kishikawa, M., Shiku, H., Aizawa, S., and Furukawa, K. (1998) Complex gangliosides are essential in spermatogenesis of mice: possible roles in the transport of testosterone. *Proc Natl Acad Sci U S A* **95**, 12147-12152

36. Honke, K., Hirahara, Y., Dupree, J., Suzuki, K., Popko, B., Fukushima, K., Fukushima, J., Nagasawa, T., Yoshida, N., Wada, Y., and Taniguchi, N. (2002) Paranodal junction formation and spermatogenesis require sulfoglycolipids. *Proc Natl Acad Sci U S A* **99**, 4227-4232

37. Takamiya, K., Yamamoto, A., Furukawa, K., Yamashiro, S., Shin, M., Okada, M., Fukumoto, S., Haraguchi, M., Takeda, N., Fujimura, K., Sakae, M., Kishikawa, M., Shiku, H., Furukawa, K., and Aizawa, S. (1996) Mice with disrupted GM2/GD2 synthase gene lack complex gangliosides but exhibit only subtle defects in their nervous system. *Proc Natl Acad Sci U S A* **93**, 10662-10667

38. Coderch, L., López, O., de la Maza, A., and Parra, J. L. (2003) Ceramides and Skin Function. *American Journal of Clinical Dermatology* **4**, 107-129

39. Tybulewicz, V. L., Tremblay, M. L., LaMarca, M. E., Willemsen, R., Stubblefield, B. K., Winfield, S., ablocka, B., Sidransky, E., Martin, B. M., Huang, S. P., and et al. (1992) Animal model of Gaucher's disease from targeted disruption of the mouse glucocerebrosidase gene. *Nature* **357**, 407-410

40. Choi, M. J., and Maibach, H. I. (2005) Role of Ceramides in Barrier Function of Healthy and Diseased Skin. *American Journal of Clinical Dermatology* **6**, 215-223

41. Inoue, M., Fujii, Y., Furukawa, K., Okada, M., Okumura, K., Hayakawa, T., Furukawa, K., and Sugiura, Y. (2002) Refractory skin injury in complex knock-out mice expressing only the GM3 ganglioside. *J Biol Chem* **277**, 29881-29888

42. Platt, F. M. (2014) Sphingolipid lysosomal storage disorders. *Nature* **510**, 68-75

43. Schultz, M. L., Tecedor, L., Chang, M., and Davidson, B. L. (2011) Clarifying lysosomal storage diseases. *Trends Neurosci* **34**, 401-410

44. Meikle, P. J., Hopwood, J. J., Clague, A. E., and Carey, W. F. (1999) Prevalence of lysosomal storage disorders. *JAMA* **281**, 249-254

45. Schneider, J. S. (2014) Gangliosides and glycolipids in neurodegenerative disorders. *Adv Neurobiol* **9**, 449-461

46. Walkley, S. U. (2004) Secondary accumulation of gangliosides in lysosomal storage disorders. *Semin Cell Dev Biol* **15**, 433-444

47. ervas, M., Somers, K. L., Thrall, M. A., and Walkley, S. U. (2001) Critical role for glycosphingolipids in Niemann-Pick disease type C. *Curr Biol* **11**, 1283-1287

48. Abe, A., Gregory, S., Lee, L., Killen, P. D., Brady, R. O., Kulkarni, A., and Shayman, J. A. (2000) Reduction of globotriaosylceramide in Fabry disease mice by substrate deprivation. *The Journal of Clinical Investigation* **105**, 1563-1571

49. ervas, M., Dobrenis, K., and Walkley, S. U. (2001) Neurons in Niemann-Pick disease type C accumulate gangliosides as well as unesterified cholesterol and undergo dendritic and axonal alterations. *J Neuropathol Exp Neurol* **60**, 49-64

50. Fewou, S. N., Plomp, J. J., and Willison, H. J. (2014) The pre-synaptic motor nerve terminal as a site for antibody-mediated neurotoxicity in autoimmune neuropathies and synaptopathies. *J Anat* **224**, 36-44

51. Brennan, K. M., Galban-Horcajo, F., Rinaldi, S., O'Leary, C. P., Goodyear, C. S., Kalna, G., Arthur, A., Elliot, C., Barnett, S., Linington, C., Bennett, J. L., Owens, G. P., and Willison, H. J. (2011) Lipid arrays identify myelin-derived lipids and lipid complexes as prominent targets for oligoclonal band antibodies in multiple sclerosis. *J Neuroimmunol* **238**, 87-95

52. Rinaldi, S., Brennan, K. M., Kalna, G., Walgaard, C., van Doorn, P., Jacobs, B. C., Yu, R. K., Mansson, J. E., Goodyear, C. S., and Willison, H. J. (2013) Antibodies to heteromeric glycolipid complexes in guillain-barre syndrome. *PLoS One* **8**, e82337

53. Rinaldi, S., Brennan, K. M., and Willison, H. J. (2010) Heteromeric glycolipid complexes as modulators of autoantibody and lectin binding. *Prog Lipid Res* **49**, 87-95

54. Natoli, T. A., Smith, L. A., Rogers, K. A., Wang, B., Komarnitsky, S., Budman, Y., Belenky, A., Bukanov, N. O., Dackowski, W. R., Husson, H., Russo, R. J., Shayman, J. A., Ledbetter, S. R., Leonard, J. P., and Ibraghimov-Beskrovnaya, O. (2010) Inhibition of glucosylceramide accumulation results in effective blockade of polycystic kidney disease in mouse models. *Nat Med* **16**, 788-792

55. Hammer, M. B., Eleuch-Fayache, G., Schottlaender, L. V., Nehdi, H., Gibbs, J. R., Arepalli, S. K., Chong, S. B., Hernandez, D. G., Sailer, A., Liu, G., Mistry, P. K., Cai, H., Shrader, G., Sassi, C., Bouhlal, Y., Houlden, H., Hentati, F., Amouri, R., and Singleton, A. B. (2013) Mutations in GBA2 cause autosomal-recessive cerebellar ataxia with spasticity. *Am J Hum Genet* **92**, 245-251

56. Martin, E., Schule, R., Smets, K., Rastetter, A., Boukhris, A., Loureiro, J. L., Gonzalez, M. A., Mundwiller, E., Deconinck, T., Wessner, M., Jornea, L., Oteyza, A. C., Durr, A., Martin, J. J., Schols, L., Mhiri, C., Lamari, F., uchner, S., De Jonghe, P., Kabashi, E., Brice, A., and Stevanin, G. (2013) Loss of function of glucocerebrosidase GBA2 is responsible for motor neuron defects in hereditary spastic paraplegia. *Am J Hum Genet* **92**, 238-244

57. Harlalka, G. V., Lehman, A., Chioza, B., Baple, E. L., Maroofian, R., Cross, H., Sreekantan-Nair, A., Priestman, D. A., Al-Turki, S., McEntagart, M. E., Proukakis, C., Royle, L., Kozak, R. P., Bastaki, L., Patton, M., Wagner, K., Coblentz, R., Price, J., Mezei, M., Schlade-Bartusiak, K., Platt, F. M., Hurles, M. E., and Crosby, A. H. (2013) Mutations in B4GALNT1 (GM2 synthase) underlie a new disorder of ganglioside biosynthesis. *Brain* **136**, 3618-3624

58. Boukhris, A., Schule, R., Loureiro, J. L., Lourenco, C. M., Mundwiller, E., Gonzalez, M. A., Charles, P., Gauthier, J., Rekik, I., Acosta Lebrigio, R. F., Gaussen, M., Speziani, F., Ferbert, A., Feki, I., Caballero-Oteyza, A., Dionne-Laporte, A., Amri, M., Noreau, A., Forlani, S., Cruz, V. T., Mochel, F., Coutinho, P., Dion, P., Mhiri, C., Schols, L., Pouget, J., Darios, F., Rouleau, G. A., Marques, W., Jr., Brice, A., Durr, A., uchner, S., and Stevanin, G. (2013) Alteration of ganglioside biosynthesis responsible for complex hereditary spastic paraplegia. *Am J Hum Genet* **93**, 118-123

59. Votsi, C., amba-Papanicolaou, E., Middleton, L. T., Pantzaris, M., and Christodoulou, K. (2014) A novel GBA2 gene missense mutation in spastic ataxia. *Ann Hum Genet* **78**, 13-22

60. Wakil, S. M., Monies, D. M., Ramzan, K., Hagos, S., Bastaki, L., Meyer, B. F., and Bohlega, S. (2014) Novel B4GALNT1 mutations in a complicated form of hereditary spastic paraplegia. *Clin Genet* **86**, 500-501

61. Grimm, M. O., inser, E. G., Grosgen, S., Hundsdorfer, B., Rothhaar, T. L., Burg, V. K., Kaestner, L., Bayer, T. A., Lipp, P., Muller, U., Grimm, H. S., and Hartmann, T. (2012) Amyloid precursor protein (APP) mediated regulation of ganglioside homeostasis linking Alzheimer's disease pathology with ganglioside metabolism. *PLoS One* **7**, e34095

62. Mazzulli, J. R., Xu, Y. H., Sun, Y., Knight, A. L., McLean, P. J., Caldwell, G. A., Sidransky, E., Grabowski, G. A., and Krainc, D. (2011) Gaucher disease glucocerebrosidase and alpha-synuclein form a bidirectional pathogenic loop in synucleinopathies. *Cell* **146**, 37-52

63. Fantini, J., and Yahi, N. (2011) Molecular basis for the glycosphingolipid-binding specificity of alpha-synuclein: key role of tyrosine 39 in membrane insertion. *J Mol Biol* **408**, 654-669

64. Simpson, M. A., Cross, H., Proukakis, C., Priestman, D. A., Neville, D. C., Reinkensmeier, G., Wang, H., Wiznitzer, M., Gurtz, K., Verganelaki, A., Pryde, A., Patton, M. A., Dwek, R. A., Butters, T. D., Platt, F. M., and Crosby, A. H. (2004) Infantile-onset symptomatic epilepsy syndrome caused by a homozygous loss-of-function mutation of GM3 synthase. *Nat Genet* **36**, 1225-1229

65. Tallman, J. F., Johnson, W. G., and Brady, R. O. (1972) The metabolism of Tay-Sachs ganglioside: catabolic studies with lysosomal enzymes from normal and Tay-Sachs brain tissue. *The Journal of clinical investigation* **51**, 2339-2345

66. Ghauharali-van der Vlugt, K., Langeveld, M., Poppema, A., Kuiper, S., Hollak, C. E. M., Aerts, J. M., and Groener, J. E. M. (2008) Prominent increase in plasma ganglioside GM3 is associated with clinical manifestations of type I Gaucher disease. *Clinica Chimica Acta* **389**, 109-113

67. Fuller, M. (2010) Sphingolipids: the nexus between Gaucher disease and insulin resistance. *Lipids in Health and Disease* **9**, 113

68. Langeveld, M., Ghauharali, K. J. M., Sauerwein, H. P., Ackermans, M. T., Groener, J. E. M., Hollak, C. E. M., Aerts, J. M., and Serlie, M. J. (2008) Type I Gaucher Disease, a Glycosphingolipid Storage Disorder, Is Associated with Insulin Resistance. *The Journal of Clinical Endocrinology & Metabolism* **93**, 845-851

69. Berra, B., Brunngraber, E. G., Aguilar, V., Aro, A., and ambotti, V. (1973) Gangliosides, glycoproteins, and glycosaminoglycans in Krabbe's disease. *Clin Chim Acta* **47**, 325-328

70. Dodge, J. C. (2017) Lipid Involvement in Neurodegenerative Diseases of the Motor System: Insights from Lysosomal Storage Diseases. *Frontiers in Molecular Neuroscience* **10**

71. Brennan, P. J., Tatituri, R. V., Brigl, M., Kim, E. Y., Tuli, A., Sanderson, J. P., Gadola, S. D., Hsu, F. F., Besra, G. S., and Brenner, M. B. (2011) Invariant natural killer T cells recognize lipid self antigen induced by microbial danger signals. *Nat Immunol* **12**, 1202-1211

72. King, I. L., Fortier, A., Tighe, M., Dibble, J., Watts, G. F., Veerapen, N., Haberman, A. M., Besra, G. S., Mohrs, M., Brenner, M. B., and Leadbetter, E. A. (2011) Invariant natural killer T cells direct B cell responses to cognate lipid antigen in an IL-21-dependent manner. *Nat Immunol* **13**, 44-50

73. Degroote, S., Wolthoorn, J., and van Meer, G. (2004) The cell biology of glycosphingolipids. *Semin Cell Dev Biol* **15**, 375-387

74. Kim, S.-J., Chung, T.-W., Choi, H.-J., Jin, U.-H., Ha, K.-T., Lee, Y.-C., and Kim, C.-H. (2014) Monosialic ganglioside GM3 specifically suppresses the monocyte adhesion to endothelial cells for inflammation. *The International Journal of Biochemistry & Cell Biology* **46**, 32-38

75. Jennemann, R., and Grone, H. J. (2013) Cell-specific in vivo functions of glycosphingolipids: lessons from genetic deletions of enzymes involved in glycosphingolipid synthesis. *Prog Lipid Res* **52**, 231-248

76. Proia, R. L. (2003) Glycosphingolipid functions: insights from engineered mouse models. *Philos Trans R Soc Lond B Biol Sci* **358**, 879-883

77. Garcia-Ruiz, C., Morales, A., and Fernández-Checa, J. C. (2015) Glycosphingolipids and cell death: one aim, many ways. *Apoptosis* **20**, 607-620

78. Sorli, S. C., Colie, S., Albinet, V., Dubrac, A., Touriol, C., Guilbaud, N., Bedia, C., Fabrias, G., Casas, J., Segui, B., Levade, T., and Andrieu-Abadie, N. (2013) The nonlysosomal beta-glucosidase GBA2 promotes endoplasmic reticulum stress and impairs tumorigenicity of human melanoma cells. *FASEB J* **27**, 489-498

79. Körschen, H. G., Yildiz, Y., Raju, D. N., Schonauer, S., Bönigk, W., Jansen, V., Kremmer, E., Kaupp, U. B., and Wachten, D. (2013) The Non-lysosomal β-Glucosidase GBA2 Is a Non-integral Membrane-associated Protein at the Endoplasmic Reticulum (ER) and Golgi. *Journal of Biological Chemistry* **288**, 3381-3393

80. Woeste, M. A., Stern, S., Raju, D. N., Grahn, E., Dittmann, D., Gutbrod, K., Dormann, P., Hansen, J. N., Schonauer, S., Marx, C. E., Hamzeh, H., Korschen, H. G., Aerts, J., Bonigk, W., Endepols, H., Sandhoff, R., Geyer, M., Berger, T. K., Bradke, F., and Wachten, D. (2019) Species-specific differences in nonlysosomal glucosylceramidase GBA2 function underlie locomotor dysfunction arising from loss-of-function mutations. *J Biol Chem* **294**, 3853-3871

81. Boot, R. G., Verhoek, M., Donker-Koopman, W., Strijland, A., van Marle, J., Overkleeft, H. S., Wennekes, T., and Aerts, J. M. (2007) Identification of the non-lysosomal glucosylceramidase as beta-glucosidase 2. *J Biol Chem* **282**, 1305-1312

82. Yildiz, Y., Matern, H., Thompson, B., Allegood, J. C., Warren, R. L., Ramirez, D. M., Hammer, R. E., Hamra, F. K., Matern, S., and Russell, D. W. (2006) Mutation of beta-glucosidase 2 causes glycolipid storage disease and impaired male fertility. *J Clin Invest* **116**, 2985-2994

83. Sultana, S., Reichbauer, J., Schule, R., Mochel, F., Synofzik, M., and van der Spoel, A. C. (2015) Lack of enzyme activity in GBA2 mutants associated with hereditary spastic paraplegia/cerebellar ataxia (SPG46). *Biochem Biophys Res Commun* **465**, 35-40

84. Hayashi, Y., Okino, N., Kakuta, Y., Shikanai, T., Tani, M., Narimatsu, H., and Ito, M. (2007) Klotho-related protein is a novel cytosolic neutral beta-glycosylceramidase. *J Biol Chem* **282**, 30889-30900

85. Matern, H., Boermans, H., Lottspeich, F., and Matern, S. (2001) Molecular cloning and expression of human bile acid beta-glucosidase. *J Biol Chem* **276**, 37929-37933

86. Charoenwattanasatien, R., Pengthaisong, S., Breen, I., Mutoh, R., Sansenya, S., Hua, Y., Tankrathok, A., Wu, L., Songsiriritthigul, C., Tanaka, H., Williams, S. J., Davies, G. J., Kurisu, G., and Cairns, J. R. (2016) Bacterial beta-Glucosidase Reveals the Structural and Functional Basis of Genetic Defects in Human Glucocerebrosidase 2 (GBA2). *ACS Chem Biol* **11**, 1891-1900

87. Marques, A. R., Aten, J., Ottenhoff, R., van Roomen, C. P., Herrera Moro, D., Claessen, N., Vinueza Veloz, M. F., hou, K., Lin, ., Mirzaian, M., Boot, R. G., De eeuw, C. I., Overkleeft, H. S., Yildiz, Y., and Aerts, J. M. (2015) Reducing GBA2 Activity Ameliorates Neuropathology in Niemann-Pick Type C Mice. *PLoS One* **10**, e0135889

88. Hartz, P. A. GLUCOSIDASE, BETA, ACID 2; GBA2. 2005 Ed., Johns Hopkins University, OMIM®

89. Walden, C. M., Sandhoff, R., Chuang, C. C., Yildiz, Y., Butters, T. D., Dwek, R. A., Platt, F. M., and van der Spoel, A. C. (2007) Accumulation of glucosylceramide in murine testis, caused by inhibition of beta-glucosidase 2: implications for spermatogenesis. *J Biol Chem* **282**, 32655-32664

90. Bone, W., Walden, C. M., Fritsch, M., Voigtmann, U., Leifke, E., Gottwald, U., Boomkamp, S., Platt, F. M., and van der Spoel, A. C. (2007) The sensitivity of murine spermiogenesis to miglustat is a quantitative trait: a pharmacogenetic study. *Reprod Biol Endocrinol* **5**, 1

91. van der Spoel, A. C., Jeyakumar, M., Butters, T. D., Charlton, H. M., Moore, H. D., Dwek, R. A., and Platt, F. M. (2002) Reversible infertility in male mice after oral administration of alkylated imino sugars: a nonhormonal approach to male contraception. *Proc Natl Acad Sci U S A* **99**, 17173-17178

92. Woeste, M. A., and Wachten, D. (2017) The Enigmatic Role of GBA2 in Controlling Locomotor Function. *Frontiers in molecular neuroscience* **10**, 386-386

93. Ridley, C. M., Thur, K. E., Shanahan, J., Thillaiappan, N. B., Shen, A., Uhl, K., Walden, C. M., Rahim, A. A., Waddington, S. N., Platt, F. M., and van der Spoel, A. C. (2013) beta-Glucosidase 2 (GBA2) activity and imino sugar pharmacology. *J Biol Chem* **288**, 26052-26066

94. Xu, M., Motabar, O., Ferrer, M., Marugan, J. J., heng, W., and Ottinger, E. A. (2016) Disease models for the development of therapies for lysosomal storage diseases. *Ann N Y Acad Sci* **1371**, 15-29

95. Hollak, C. E., and Wijburg, F. A. (2014) Treatment of lysosomal storage disorders: successes and challenges. *J Inherit Metab Dis* **37**, 587-598

96. Pastores, G. M., Giraldo, P., Cherin, P., and Mehta, A. (2009) Goal-oriented therapy with miglustat in Gaucher disease. *Curr Med Res Opin* **25**, 23-37

97. Kuter, D. J., Mehta, A., Hollak, C. E., Giraldo, P., Hughes, D., Belmatoug, N., Brand, M., Muller, A., Schaaf, B., Giorgino, R., and imran, A. (2013) Miglustat therapy in type 1 Gaucher disease: clinical and safety outcomes in a multicenter retrospective cohort study. *Blood Cells Mol Dis* **51**, 116-124

98. Mistry, P. K., Liu, J., Sun, L., Chuang, W. L., Yuen, T., Yang, R., Lu, P., hang, K., Li, J., Keutzer, J., Stachnik, A., Mennone, A., Boyer, J. L., Jain, D., Brady, R. O., New, M. I., and aidi, M. (2014) Glucocerebrosidase 2 gene deletion rescues type 1 Gaucher disease. *Proc Natl Acad Sci U S A* **111**, 4934-4939

99. Overkleeft, H. S., Renkema, G. H., Neele, J., Vianello, P., Hung, I. O., Strijland, A., van der Burg, A. M., Koomen, G. J., Pandit, U. K., and Aerts, J. M. (1998) Generation of specific deoxynojirimycin-type inhibitors of the non-lysosomal glucosylceramidase. *J Biol Chem* **273**, 26522-26527

100. Hein, Marco Y., Hubner, Nina C., Poser, I., Cox, J., Nagaraj, N., Toyoda, Y., Gak, Igor A., Weisswange, I., Mansfeld, J., Buchholz, F., Hyman, Anthony A., and Mann, M. (2015) A Human Interactome in Three Quantitative Dimensions Organized by Stoichiometries and Abundances. *Cell* **163**, 712-723

101. Huttlin, E. L., Bruckner, R. J., Paulo, J. A., Cannon, J. R., Ting, L., Baltier, K., Colby, G., Gebreab, F., Gygi, M. P., Parzen, H., Szpyt, J., Tam, S., arraga, G., Pontano-Vaites, L., Swarup, S., White, A. E., Schweppe, D. K., Rad, R., Erickson, B. K., Obar, R. A., Guruharsha, K. G., Li, K., Artavanis-Tsakonas, S., Gygi, S. P., and Harper, J. W. (2017) Architecture of the human interactome defines protein communities and disease networks. *Nature* **545**, 505-509

102. Benleulmi-Chaachoua, A., Chen, L., Sokolina, K., Wong, V., Jurisica, I., Emerit, M. B., Darmon, M., Espin, A., Stagljar, I., Tafelmeyer, P., amponi, G. W., Delagrange, P., Maurice, P., and Jockers, R. (2016) Protein interactome mining defines melatonin MT1 receptors as integral component of presynaptic protein complexes of neurons. *J Pineal Res* **60**, 95-108

103. Feher, J. (2012) 4.1 - Organization of the Nervous System. in *Quantitative Human Physiology* (Feher, J. ed.), Academic Press, Boston. pp 297-306

104. Felten, D. L., O'Banion, M. K., and Maida, M. S. (2016) 1 - Neurons and Their Properties. in *Netter's Atlas of Neuroscience (Third Edition)* (Felten, D. L., O'Banion, M. K., and Maida, M. S. eds.), Elsevier, Philadelphia. pp 1-42

105. Feher, J. (2012) 4.5 - Balance and Control of Movement. in *Quantitative Human Physiology* (Feher, J. ed.), Academic Press, Boston. pp 341-353

106. Fallini, C., Donlin-Asp, P. G., Rouanet, J. P., Bassell, G. J., and Rossoll, W. (2016) Deficiency of the Survival of Motor Neuron Protein Impairs mRNA Localization and Local Translation in the Growth Cone of Motor Neurons. *The Journal of Neuroscience* **36**, 3811

107. Burke, R. E. (1987) Control of human voluntary movement: by John C. Rothwell, Croom Helm, 1987. £17.50 pbk/£35.00 hbk (xii + 325 pages) ISBN 0 7099 4229 X. *Trends in Neurosciences* **10**, 383

108. NATHAN, P. W., SMITH, M. C., and DEACON, P. (1990) THE CORTICOSPINAL TRACTS IN MAN: COURSE AND LOCATION OF FIBRES AT DIFFERENT SEGMENTAL LEVELS. *Brain* **113**, 303-324

109. Ivanenko, Y. P., Cappellini, G., Dominici, N., Poppele, R. E., and Lacquaniti, F. (2005) Coordination of Locomotion with Voluntary Movements in Humans. *The Journal of Neuroscience* **25**, 7238

110. Blackstone, C. (2012) Cellular pathways of hereditary spastic paraplegia. *Annu Rev Neurosci* **35**, 25-47

111. Spastic Paraplegia Foundation, I., https://sp-foundation.org

112. Spastic Paraplegia Foundation, I. PLS and HSP overview. 1605 Goularte Place Fremont, CA

113. Schuurs-Hoeijmakers, Janneke H. M., Geraghty, Michael T., Kamsteeg, E.-J., Ben-Salem, S., de Bot, Susanne T., Nijhof, B., van de Vondervoort, Ilse I. G. M., van der Graaf, M., Nobau, Anna C., Otte-Höller, I., Vermeer, S., Smith, Amanda C., Humphreys, P., Schwartzentruber, J., Ali, Bassam R., Al-Yahyaee, Saeed A., Tariq, S., Pramathan, T., Bayoumi, R., Kremer, Hubertus P. H., van de Warrenburg, Bart P., van den Akker, Willem M. R., Gilissen, C., Veltman, Joris A., Janssen, Irene M., Vulto-van Silfhout, Anneke T., van der Velde-Visser, S., Lefeber, Dirk J., Diekstra, A., Erasmus, Corrie E., Willemsen, Michèl A., Vissers, Lisenka E. L. M., Lammens, M., van Bokhoven, H., Brunner, Han G., Wevers, Ron A., Schenck, A., Al-Gazali, L., de Vries, Bert B. A., and de Brouwer, Arjan P. M. (2012) Mutations in DDHD2, Encoding an Intracellular Phospholipase A1, Cause a Recessive Form of Complex Hereditary Spastic Paraplegia. *The American Journal of Human Genetics* **91**, 1073-1081

114. Peter Hedera, M., PhD, FACMG. (2018) Hereditary Spastic Paraplegia Overview. University of Washington, Seattle

115. Synofzik, M., and Schule, R. (2017) Overcoming the divide between ataxias and spastic paraplegias: Shared phenotypes, genes, and pathways. *Mov Disord* **32**, 332-345

116. Citterio, A., Arnoldi, A., Panzeri, E., D'Angelo, M. G., Filosto, M., Dilena, R., Arrigoni, F., Castelli, M., Maghini, C., Germiniasi, C., Menni, F., Martinuzzi, A., Bresolin, N., and Bassi, M. T. (2014) Mutations in CYP2U1, DDHD2 and GBA2 genes are rare causes of complicated forms of hereditary spastic paraparesis. *J Neurol* **261**, 373-381

117. Kancheva, D., Atkinson, D., De Rijk, P., imon, M., Chamova, T., Mitev, V., Yaramis, A., Maria Fabrizi, G., Topaloglu, H., Tournev, I., Parman, Y., Parma, Y., Battaloglu, E., Estrada-Cuzcano, A., and Jordanova, A. (2016) Novel mutations in genes causing hereditary spastic paraplegia and Charcot-Marie-Tooth neuropathy identified by an optimized protocol for homozygosity mapping based on whole-exome sequencing. *Genet Med* **18**, 600-607

118. Coarelli, G., Romano, S., Travaglini, L., Ferraldeschi, M., Nicita, F., Spadaro, M., Fornasiero, A., Frontali, M., Salvetti, M., Bertini, E., and Ristori, G. (2018) Novel homozygous GBA2 mutation in a patient with complicated spastic paraplegia. *Clin Neurol Neurosurg* **168**, 60-63

119. Haugarvoll, K., Johansson, S., Rodriguez, C. E., Boman, H., Haukanes, B. I., Bruland, O., Roque, F., Jonassen, I., Blomqvist, M., Telstad, W., Mansson, J. E., Knappskog, P. M., and Bindoff, L. A. (2017) GBA2 Mutations Cause a Marinesco-Sjogren-Like Syndrome: Genetic and Biochemical Studies. *PLoS One* **12**, e0169309

120. Wei, Q., Dong, H. L., Pan, L. Y., Chen, C. X., Yan, Y. T., Wang, R. M., Li, H. F., Liu, . J., Tao, Q. Q., and Wu, . Y. (2019) Clinical features and genetic spectrum in Chinese patients with recessive hereditary spastic paraplegia. *Transl Neurodegener* **8**, 19

121. Yang, Y. J., hou, . F., Liao, X. X., Luo, Y. Y., han, . X., Huang, M. F., hou, L., Tang, B. S., Shen, L., and Du, J. (2016) SPG46 and SPG56 are rare causes of hereditary spastic paraplegia in China. *J Neurol* **263**, 2136-2138

122. Morais, S., Raymond, L., Mairey, M., Coutinho, P., Brandao, E., Ribeiro, P., Loureiro, J. L., Sequeiros, J., Brice, A., Alonso, I., and Stevanin, G. (2017) Massive sequencing of 70 genes reveals a myriad of missing genes or mechanisms to be uncovered in hereditary spastic paraplegias. *Eur J Hum Genet* **25**, 1217-1228

123. Merlini, L. (2008) Marinesco-Sjogren syndrome, fanfare, and more. *Neuromuscul Disord* **18**, 185-188

124. Ezgu, F., Krejci, P., Li, S., de Sousa, C., Graham, J. M., Jr., Hansmann, I., He, W., Porpora, K., Wand, D., Wertelecki, W., Schneider, A., and Wilcox, W. R. (2014) Phenotype-genotype correlations in patients with Marinesco-Sjogren syndrome. *Clin Genet* **86**, 74-84

125. Goto, M., Okada, M., Komaki, H., Sugai, K., Sasaki, M., Noguchi, S., Nonaka, I., Nishino, I., and Hayashi, Y. K. (2014) A nationwide survey on Marinesco-Sjogren syndrome in Japan. *Orphanet J Rare Dis* **9**, 58

126. Anttonen, A. K., Siintola, E., Tranebjaerg, L., Iwata, N. K., Bijlsma, E. K., Meguro, H., Ichikawa, Y., Goto, J., Kopra, O., and Lehesjoki, A. E. (2008) Novel SIL1 mutations and exclusion of functional candidate genes in Marinesco-Sjogren syndrome. *Eur J Hum Genet* **16**, 961-969

127. Anttonen, A. K., Mahjneh, I., Hamalainen, R. H., Lagier-Tourenne, C., Kopra, O., Waris, L., Anttonen, M., Joensuu, T., Kalimo, H., Paetau, A., Tranebjaerg, L., Chaigne, D., Koenig, M., Eeg-Olofsson, O., Udd, B., Somer, M., Somer, H., and Lehesjoki, A. E. (2005) The gene disrupted in Marinesco-Sjogren syndrome encodes SIL1, an HSPA5 cochaperone. *Nat Genet* **37**, 1309-1311

128. (2018) Focusing on mitochondrial form and function. *Nature Cell Biology* **20**, 735-735

129. Herst, P. M., Rowe, M. R., Carson, G. M., and Berridge, M. V. (2017) Functional Mitochondria in Health and Disease. *Front Endocrinol (Lausanne)* **8**, 296-296

130. Kühlbrandt, W. (2015) Structure and function of mitochondrial membrane protein complexes. *BMC Biology* **13**, 89

131. Picard, M., McEwen, B. S., Epel, E. S., and Sandi, C. (2018) An energetic view of stress: Focus on mitochondria. *Frontiers in Neuroendocrinology* **49**, 72-85

132. GRÉGOIRE, M., MORAIS, R., QUILLIAM, M. A., and GRAVEL, D. (1984) On auxotrophy for pyrimidines of respiration-deficient chick embryo cells. *European Journal of Biochemistry* **142**, 49-55

133. Calvo, S. E., Clauser, K. R., and Mootha, V. K. (2015) MitoCarta2.0: an updated inventory of mammalian mitochondrial proteins. *Nucleic Acids Research* **44**, D1251-D1257

134. El-Hattab, A. W., and Scaglia, F. (2016) Mitochondrial cytopathies. *Cell Calcium* **60**, 199-206

135. Li, M., hong, ., hu, J., Xiang, D., Dai, N., Cao, X., Qing, Y., Yang, ., Xie, J., Li, ., Baugh, L., Wang, G., and Wang, D. (2010) Identification and characterization of mitochondrial targeting sequence of human apurinic/apyrimidinic endonuclease 1. *J Biol Chem* **285**, 14871-14881

136. Omura, T. (1998) Mitochondria-Targeting Sequence, a Multi-Role Sorting Sequence Recognized at All Steps of Protein Import into Mitochondria. *The Journal of Biochemistry* **123**, 1010-1016

137. Paschen, S. A., and Neupert, W. (2001) Protein import into mitochondria. *IUBMB Life* **52**, 101-112

138. Liesa, M., Palacín, M., and orzano, A. (2009) Mitochondrial Dynamics in Mammalian Health and Disease. *Physiological Reviews* **89**, 799-845

139. Hoppins, S., Lackner, L., and Nunnari, J. (2007) The machines that divide and fuse mitochondria. *Annu Rev Biochem* **76**, 751-780

140. Youle, R. J., and van der Bliek, A. M. (2012) Mitochondrial Fission, Fusion, and Stress. *Science* **337**, 1062

141. Steffen, J., and Koehler, C. M. (2017) ER–mitochondria contacts: Actin dynamics at the ER control mitochondrial fission via calcium release. *The Journal of Cell Biology* **217**, 15-17

142. Friedman, J. R., Lackner, L. L., West, M., DiBenedetto, J. R., Nunnari, J., and Voeltz, G. K. (2011) ER Tubules Mark Sites of Mitochondrial Division. *Science* **334**, 358

143. El-Hattab, A. W., Suleiman, J., Almannai, M., and Scaglia, F. (2018) Mitochondrial dynamics: Biological roles, molecular machinery, and related diseases. *Molecular Genetics and Metabolism* **125**, 315-321

144. van der Bliek, A. M., Shen, Q., and Kawajiri, S. (2013) Mechanisms of mitochondrial fission and fusion. *Cold Spring Harb Perspect Biol* **5**

145. Lee, H., and Yoon, Y. (2018) Mitochondrial Membrane Dynamics-Functional Positioning of OPA1. *Antioxidants (Basel)* **7**

146. Delettre, C., Griffoin, J. M., Kaplan, J., Dollfus, H., Lorenz, B., Faivre, L., Lenaers, G., Belenguer, P., and Hamel, C. P. (2001) Mutation spectrum and splicing variants in the OPA1 gene. *Hum Genet* **109**, 584-591

147. Song, ., Chen, H., Fiket, M., Alexander, C., and Chan, D. C. (2007) OPA1 processing controls mitochondrial fusion and is regulated by mRNA splicing, membrane potential, and Yme1L. *The Journal of cell biology* **178**, 749-755

148. Olichon, A., Elachouri, G., Baricault, L., Delettre, C., Belenguer, P., and Lenaers, G. (2007) OPA1 alternate splicing uncouples an evolutionary conserved function in mitochondrial fusion from a vertebrate restricted function in apoptosis. *Cell Death Differ* **14**, 682-692

149. Baricault, L., Segui, B., Guegand, L., Olichon, A., Valette, A., Larminat, F., and Lenaers, G. (2007) OPA1 cleavage depends on decreased mitochondrial ATP level and bivalent metals. *Exp Cell Res* **313**, 3800-3808

150. Tulli, S., Del Bondio, A., Baderna, V., Mazza, D., Codazzi, F., Pierson, T. M., Ambrosi, A., Nolte, D., Goizet, C., Toro, C., Baets, J., Deconinck, T., DeJonghe, P., Mandich, P., Casari, G., and Maltecca, F. (2019) Pathogenic variants in the AFG3L2 proteolytic domain cause SCA28 through haploinsufficiency and proteostatic stress-driven OMA1 activation. *Journal of Medical Genetics* **56**, 499

151. Coarelli, G., Schule, R., van de Warrenburg, B. P. C., De Jonghe, P., Ewenczyk, C., Martinuzzi, A., Synofzik, M., Hamer, E. G., Baets, J., Anheim, M., Schöls, L., Deconinck, T., Masrori, P., Fontaine, B., Klockgether, T., Angelo, M. G., Monin, M.-L., De Bleecker, J., Migeotte, I., Charles, P., Bassi, M. T., Klopstock, T., Mochel, F., Ollagnon-Roman, E., Hooghe, M., Kamm, C., Kurzwelly, D., Papin, M., Davoine, C.-S., Banneau, G., Tezenas du Montcel, S., Seilhean, D., Brice, A., Duyckaerts, C., Stevanin, G., and Durr, A. (2019) Loss of paraplegin drives spasticity rather than ataxia in a cohort of 241 patients with <em>SPG7</em&gt. *Neurology* **92**, e2679

152. hang, K., Li, H., and Song, . (2014) Membrane depolarization activates the mitochondrial protease OMA1 by stimulating self-cleavage. *EMBO reports* **15**, 576-585

153. Baker, B. M., and Haynes, C. M. (2011) Mitochondrial protein quality control during biogenesis and aging. *Trends Biochem Sci* **36**, 254-261

154. Del Dotto, V., Mishra, P., Vidoni, S., Fogazza, M., Maresca, A., Caporali, L., McCaffery, J. M., Cappelletti, M., Baruffini, E., Lenaers, G., Chan, D., Rugolo, M., Carelli, V., and anna, C. (2017) OPA1 Isoforms in the Hierarchical Organization of Mitochondrial Functions. *Cell Rep* **19**, 2557-2571

155. Platt, F. M., Boland, B., and van der Spoel, A. C. (2012) The cell biology of disease: Lysosomal storage disorders: The cellular impact of lysosomal dysfunction. *J Cell Biol* **199**, 723-734

156. Sillence, D. J., and Allan, D. (1998) Repair of BHK cell surface ganglioside GM3 after its degradation by extracellular sialidase. *Mol Membr Biol* **15**, 229-235

157. Lutz, M. S., Jaskiewicz, E., Darling, D. S., Furukawa, K., and Young, W. W., Jr. (1994) Cloned beta 1,4 N-acetylgalactosaminyltransferase synthesizes GA2 as well as gangliosides GM2 and GD2. GM3 synthesis has priority over GA2 synthesis for utilization of lactosylceramide substrate in vivo. *J Biol Chem* **269**, 29227-29231

158. Fishman, P. H., Bradley, R. M., Hom, B. E., and Moss, J. (1983) Uptake and metabolism of exogenous gangliosides by cultured cells: effect of choleragen on the turnover of GM1. *J Lipid Res* **24**, 1002-1011

159. (2006) Elementary. in *Chemical Kinetics and Reaction Dynamics*, Springer Netherlands, Dordrecht. pp 1-45

160. Platt, F. M., Neises, G. R., Karlsson, G. B., Dwek, R. A., and Butters, T. D. (1994) N-butyldeoxygalactonojirimycin inhibits glycolipid biosynthesis but does not affect N-linked oligosaccharide processing. *Journal of Biological Chemistry* **269**, 27108-27114

161. Li, Y. T., and Li, S. C. (1989) Ceramide glycanase from leech, Hirudo medicinalis, and earthworm, Lumbricus terrestris. *Methods Enzymol* **179**, 479-487

162. hou, B., Li, S. C., Laine, R. A., Huang, R. T., and Li, Y. T. (1989) Isolation and characterization of ceramide glycanase from the leech, Macrobdella decora. *J Biol Chem* **264**, 12272-12277

163. Nilsson, O., and Svennerholm, L. (1982) Characterization and quantitative determination of gangliosides and neutral glycosphingolipids in human liver. *J Lipid Res* **23**, 327-334

164. Svennerholm, L., Fredman, P., Mansson, J. E., Nilsson, O., and Holmgren, J. (1982) Gangliosides of human intestinal mucosa: detection of a possible fetal antigen. *Adv Exp Med Biol* **152**, 333-342

165. Vieira, D. B., Thur, K., Sultana, S., Priestman, D., and van der Spoel, A. C. (2015) Verification and refinement of cellular glycosphingolipid profiles using HPLC. *Biochem Cell Biol* **93**, 581-586

166. Neville, D. C., Coquard, V., Priestman, D. A., te Vruchte, D. J., Sillence, D. J., Dwek, R. A., Platt, F. M., and Butters, T. D. (2004) Analysis of fluorescently labeled glycosphingolipid-derived oligosaccharides following ceramide glycanase digestion and anthranilic acid labeling. *Anal Biochem* **331**, 275-282

167. Neville, D. C. A., Dwek, R. A., and Butters, T. D. (2009) Development of a Single Column Method for the Separation of Lipid- and Protein-Derived Oligosaccharides. *Journal of Proteome Research* **8**, 681-687

168. Kobata, A. (1994) Size fractionation of oligosaccharides. *Methods Enzymol* **230**, 200-208

169. Neville, D. C. A., Coquard, V., Priestman, D. A., te Vruchte, D. J. M., Sillence, D. J., Dwek, R. A., Platt, F. M., and Butters, T. D. (2004) Analysis of fluorescently labeled glycosphingolipid-derived oligosaccharides following ceramide glycanase digestion and anthranilic acid labeling. *Analytical Biochemistry* **331**, 275-282

170. Paul, P., Kamisaka, Y., Marks, D. L., and Pagano, R. E. (1996) Purification and characterization of UDP-glucose:ceramide glucosyltransferase from rat liver Golgi membranes. *J Biol Chem* **271**, 2287-2293

171. Watanabe, R., Wu, K., Paul, P., Marks, D. L., Kobayashi, T., Pittelkow, M. R., and Pagano, R. E. (1998) Up-regulation of glucosylceramide synthase expression and activity during human keratinocyte differentiation. *J Biol Chem* **273**, 9651-9655

172. Bourne, C. R. (2014) Utility of the Biosynthetic Folate Pathway for Targets in Antimicrobial Discovery. *Antibiotics (Basel)* **3**, 1-28

173. Adams, J. C., Keiser, M. J., Basuino, L., Chambers, H. F., Lee, D. S., Wiest, O. G., and Babbitt, P. C. (2009) A mapping of drug space from the viewpoint of small molecule metabolism. *PLoS Comput Biol* **5**, e1000474

174. Ruan, S., and Lloyd, K. O. (1992) Glycosylation pathways in the biosynthesis of gangliosides in melanoma and neuroblastoma cells: relative glycosyltransferase levels determine ganglioside patterns. *Cancer Res* **52**, 5725-5731

175. Tettamanti, G. (2003) Ganglioside/glycosphingolipid turnover: New concepts. *Glycoconjugate Journal* **20**, 301-317

176. Matz, J., Gilyan, A., Kolar, A., McCarvill, T., and Krueger, S. R. (2010) Rapid structural alterations of the active zone lead to sustained changes in neurotransmitter release. *Proc Natl Acad Sci U S A* **107**, 8836-8841

177. Alvarez de la Rosa, D., Krueger, S. R., Kolar, A., Shao, D., Fitzsimonds, R. M., and Canessa, C. M. (2003) Distribution, subcellular localization and ontogeny of ASIC1 in the mammalian central nervous system. *J Physiol* **546**, 77-87

178. Dalvai, M., Loehr, J., Jacquet, K., Huard, C. C., Roques, C., Herst, P., Cote, J., and Doyon, Y. (2015) A Scalable Genome-Editing-Based Approach for Mapping Multiprotein Complexes in Human Cells. *Cell Rep* **13**, 621-633

179. Domann, R., and Martinez, J. (1995) Alternative to cloning cylinders for isolation of adherent cell clones. *Biotechniques* **18**, 594-595

180. Mathupala, S., and Sloan, A. A. (2009) An agarose-based cloning-ring anchoring method for isolation of viable cell clones. *Biotechniques* **46**, 305-307

181. Woeste, M. A., and Wachten, D. (2017) The Enigmatic Role of GBA2 in Controlling Locomotor Function. *Front Mol Neurosci* **10**, 386

182. Estrada-Cuzcano, A., Martin, S., Chamova, T., Synofzik, M., Timmann, D., Holemans, T., Andreeva, A., Reichbauer, J., De Rycke, R., Chang, D. I., van Veen, S., Samuel, J., Schols, L., Poppel, T., Mollerup Sorensen, D., Asselbergh, B., Klein, C., uchner, S., Jordanova, A., Vangheluwe, P., Tournev, I., and Schule, R. (2017) Loss-of-function mutations in the ATP13A2/PARK9 gene cause complicated hereditary spastic paraplegia (SPG78). *Brain* **140**, 287-305

183. Han, Y. H., Moon, H. J., You, B. R., and Park, W. H. (2009) The effect of MG132, a proteasome inhibitor on HeLa cells in relation to cell growth, reactive oxygen species and GSH. *Oncol Rep* **22**, 215-221

184. Craiu, A., Gaczynska, M., Akopian, T., Gramm, C. F., Fenteany, G., Goldberg, A. L., and Rock, K. L. (1997) Lactacystin and clasto-lactacystin beta-lactone modify multiple proteasome beta-subunits and inhibit intracellular protein degradation and major histocompatibility complex class I antigen presentation. *J Biol Chem* **272**, 13437-13445

185. Oda, K., Ikehara, Y., and Omura, S. (1996) Lactacystin, an inhibitor of the proteasome, blocks the degradation of a mutant precursor of glycosylphosphatidylinositol-linked protein in a pre-Golgi compartment. *Biochem Biophys Res Commun* **219**, 800-805

186. Li, W., and Ye, Y. (2008) Polyubiquitin chains: functions, structures, and mechanisms. *Cell Mol Life Sci* **65**, 2397-2406

187. Pickart, C. M., and Eddins, M. J. (2004) Ubiquitin: structures, functions, mechanisms. *Biochimica et Biophysica Acta (BBA) - Molecular Cell Research* **1695**, 55-72

188. Tanaka, K. (2009) The proteasome: overview of structure and functions. *Proc Jpn Acad Ser B Phys Biol Sci* **85**, 12-36

189. Meyer-Schwesinger, C. (2019) The ubiquitin–proteasome system in kidney physiology and disease. *Nature Reviews Nephrology* **15**, 393-411

190. Lecker, S. H., Goldberg, A. L., and Mitch, W. E. (2006) Protein Degradation by the Ubiquitin–Proteasome Pathway in Normal and Disease States. *Journal of the American Society of Nephrology* **17**, 1807

191. Sultana, S., Truong, N. Y., Vieira, D. B., Wigger, J. G., Forrester, A. M., Veinotte, C. J., Berman, J. N., and van der Spoel, A. C. (2016) Characterization of the ebrafish Homolog of beta-Glucosidase 2: A Target of the Drug Miglustat. *Zebrafish* **13**, 177-187

192. Lam, S. S., Martell, J. D., Kamer, K. J., Deerinck, T. J., Ellisman, M. H., Mootha, V. K., and Ting, A. Y. (2015) Directed evolution of APEX2 for electron microscopy and proximity labeling. *Nat Methods* **12**, 51-54

193. Martell, J. D., Deerinck, T. J., Lam, S. S., Ellisman, M. H., and Ting, A. Y. (2017) Electron microscopy using the genetically encoded APEX2 tag in cultured mammalian cells. *Nat Protoc* **12**, 1792-1816

194. Martell, J. D., Deerinck, T. J., Sancak, Y., Poulos, T. L., Mootha, V. K., Sosinsky, G. E., Ellisman, M. H., and Ting, A. Y. (2012) Engineered ascorbate peroxidase as a genetically encoded reporter for electron microscopy. *Nat Biotechnol* **30**, 1143-1148

195. Hein, M. Y., Hubner, N. C., Poser, I., Cox, J., Nagaraj, N., Toyoda, Y., Gak, I. A., Weisswange, I., Mansfeld, J., Buchholz, F., Hyman, A. A., and Mann, M. (2015) A human interactome in three quantitative dimensions organized by stoichiometries and abundances. *Cell* **163**, 712-723

196. Green, D. R., and Reed, J. C. (1998) Mitochondria and apoptosis. *Science* **281**, 1309-1312

197. Slee, E. A., Adrain, C., and Martin, S. J. (1999) Serial killers: ordering caspase activation events in apoptosis. *Cell Death Differ* **6**, 1067-1074

198. Slee, E. A., Harte, M. T., Kluck, R. M., Wolf, B. B., Casiano, C. A., Newmeyer, D. D., Wang, H. G., Reed, J. C., Nicholson, D. W., Alnemri, E. S., Green, D. R., and Martin, S. J. (1999) Ordering the cytochrome c-initiated caspase cascade: hierarchical activation of caspases-2, -3, -6, -7, -8, and -10 in a caspase-9-dependent manner. *J Cell Biol* **144**, 281-292

199. hang, J. H., and Xu, M. (2000) DNA fragmentation in apoptosis. *Cell Res* **10**, 205-211

200. Ellis, R. E., Yuan, J. Y., and Horvitz, H. R. (1991) Mechanisms and functions of cell death. *Annu Rev Cell Biol* **7**, 663-698

201. Bayot, A., Basse, N., Lee, I., Gareil, M., Pirotte, B., Bulteau, A. L., Friguet, B., and Reboud-Ravaux, M. (2008) Towards the control of intracellular protein turnover: mitochondrial Lon protease inhibitors versus proteasome inhibitors. *Biochimie* **90**, 260-269

202. Bross, P., Naundrup, S., Hansen, J., Nielsen, M. N., Christensen, J. H., Kruhoffer, M., Palmfeldt, J., Corydon, T. J., Gregersen, N., Ang, D., Georgopoulos, C., and Nielsen, K. L. (2008) The Hsp60-(p.V98I) mutation associated with hereditary spastic paraplegia SPG13 compromises chaperonin function both in vitro and in vivo. *J Biol Chem* **283**, 15694-15700

203. Hansen, J., Corydon, T. J., Palmfeldt, J., Durr, A., Fontaine, B., Nielsen, M. N., Christensen, J. H., Gregersen, N., and Bross, P. (2008) Decreased expression of the mitochondrial matrix proteases Lon and ClpP in cells from a patient with hereditary spastic paraplegia (SPG13). *Neuroscience* **153**, 474-482

204. Liu, C. I., Chen, C. C., Chen, J. C., Su, J. H., Huang, H. H., Chen, J. Y., and Wu, Y. J. (2011) Proteomic analysis of anti-tumor effects of 11-dehydrosinulariolide on CAL-27 cells. *Mar Drugs* **9**, 1254-1272

205. Luce, K., Weil, A. C., and Osiewacz, H. D. (2010) Mitochondrial protein quality control systems in aging and disease. *Adv Exp Med Biol* **694**, 108-125

206. Koppen, M., Metodiev, M. D., Casari, G., Rugarli, E. I., and Langer, T. (2007) Variable and tissue-specific subunit composition of mitochondrial m-AAA protease complexes linked to hereditary spastic paraplegia. *Mol Cell Biol* **27**, 758-767

207. Duvezin-Caubet, S., Koppen, M., Wagener, J., ick, M., Israel, L., Bernacchia, A., Jagasia, R., Rugarli, E. I., Imhof, A., Neupert, W., Langer, T., and Reichert, A. S. (2007) OPA1 processing reconstituted in yeast depends on the subunit composition of the m-AAA protease in mitochondria. *Mol Biol Cell* **18**, 3582-3590

208. Citterio, A., Arnoldi, A., Panzeri, E., D'Angelo, M. G., Filosto, M., Dilena, R., Arrigoni, F., Castelli, M., Maghini, C., Germiniasi, C., Menni, F., Martinuzzi, A., Bresolin, N., and Bassi, M. T. (2014) Mutations in CYP2U1, DDHD2 and GBA2 genes are rare causes of complicated forms of hereditary spastic paraparesis. *Journal of Neurology* **261**, 373-381

209. Arnoult, D. (2007) Mitochondrial fragmentation in apoptosis. *Trends Cell Biol* **17**, 6-12

210. Elmore, S. (2007) Apoptosis: a review of programmed cell death. *Toxicol Pathol* **35**, 495-516

211. Arnoult, D. (2007) Mitochondrial fragmentation in apoptosis. *Trends in Cell Biology* **17**, 6-12

212. Wong, R. S. Y. (2011) Apoptosis in cancer: from pathogenesis to treatment. *J Exp Clin Cancer Res* **30**, 87-87

213. Belenguer, P., and Pellegrini, L. (2013) The dynamin GTPase OPA1: More than mitochondria? *Biochimica et Biophysica Acta (BBA) - Molecular Cell Research* **1833**, 176-183

214. Twig, G., and Shirihai, O. S. (2011) The interplay between mitochondrial dynamics and mitophagy. *Antioxid Redox Signal* **14**, 1939-1951

215. Del Dotto, V., Mishra, P., Vidoni, S., Fogazza, M., Maresca, A., Caporali, L., McCaffery, J. M., Cappelletti, M., Baruffini, E., Lenaers, G., Chan, D., Rugolo, M., Carelli, V., and anna, C. (2017) OPA1 Isoforms in the Hierarchical Organization of Mitochondrial Functions. *Cell Reports* **19**, 2557-2571

216. Olichon, A., Guillou, E., Delettre, C., Landes, T., Arnauné-Pelloquin, L., Emorine, L. J., Mils, V., Daloyau, M., Hamel, C., Amati-Bonneau, P., Bonneau, D., Reynier, P., Lenaers, G., and Belenguer, P. (2006) Mitochondrial dynamics and disease, OPA1. *Biochimica et Biophysica Acta (BBA) - Molecular Cell Research* **1763**, 500-509

217. Consolato, F., Maltecca, F., Tulli, S., Sambri, I., and Casari, G. (2018) m-AAA and i-AAA complexes coordinate to regulate OMA1, the stress-activated supervisor of mitochondrial dynamics. *Journal of Cell Science* **131**, jcs213546

218. Rainbolt, T. K., Lebeau, J., Puchades, C., and Wiseman, R. L. (2016) Reciprocal Degradation of YME1L and OMA1 Adapts Mitochondrial Proteolytic Activity during Stress. *Cell Rep* **14**, 2041-2049

219. hang, K., Li, H., and Song, . (2014) Membrane depolarization activates the mitochondrial protease OMA1 by stimulating self-cleavage. *EMBO Rep* **15**, 576-585

220. Olichon, A., ElAchouri, G., Baricault, L., Delettre, C., Belenguer, P., and Lenaers, G. (2007) OPA1 alternate splicing uncouples an evolutionary conserved function in mitochondrial fusion from a vertebrate restricted function in apoptosis. *Cell Death & Differentiation* **14**, 682-692

221. Olichon, A., Emorine, L. J., Descoins, E., Pelloquin, L., Brichese, L., Gas, N., Guillou, E., Delettre, C., Valette, A., Hamel, C. P., Ducommun, B., Lenaers, G., and Belenguer, P. (2002) The human dynamin-related protein OPA1 is anchored to the mitochondrial inner membrane facing the inter-membrane space. *FEBS Lett* **523**, 171-176

222. Lelieveld, L. T., Mirzaian, M., Kuo, C. L., Artola, M., Ferraz, M. J., Peter, R. E. A., Akiyama, H., Greimel, P., van den Berg, R. J., Overkleeft, H. S., Boot, R. G., Meijer, A., and Aerts, J. (2019) Role of beta-glucosidase 2 in aberrant glycosphingolipid metabolism: model of glucocerebrosidase deficiency in zebrafish. *J Lipid Res*

223. Smith, D., Wallom, K.-L., Williams, I. M., Jeyakumar, M., and Platt, F. M. (2009) Beneficial effects of anti-inflammatory therapy in a mouse model of Niemann-Pick disease type C1. *Neurobiology of Disease* **36**, 242-251

224. Nietupski, J. B., Pacheco, J. J., Chuang, W.-L., Maratea, K., Li, L., Foley, J., Ashe, K. M., Cooper, C. G. F., Aerts, J. M. F. G., Copeland, D. P., Scheule, R. K., Cheng, S. H., and Marshall, J. (2012) Iminosugar-based inhibitors of glucosylceramide synthase prolong survival but paradoxically increase brain glucosylceramide levels in Niemann–Pick C mice. *Molecular Genetics and Metabolism* **105**, 621-628

225. Marques, A. R. A., Aten, J., Ottenhoff, R., van Roomen, C. P. A. A., Herrera Moro, D., Claessen, N., Vinueza Veloz, M. F., hou, K., Lin, ., Mirzaian, M., Boot, R. G., De eeuw, C. I., Overkleeft, H. S., Yildiz, Y., and Aerts, J. M. F. G. (2015) Reducing GBA2 Activity Ameliorates Neuropathology in Niemann-Pick Type C Mice. *PLOS ONE* **10**, e0135889

226. Chipuk, J. E., McStay, G. P., Bharti, A., Kuwana, T., Clarke, C. J., Siskind, L. J., Obeid, L. M., and Green, D. R. (2012) Sphingolipid metabolism cooperates with BAK and BAX to promote the mitochondrial pathway of apoptosis. *Cell* **148**, 988-1000

227. Oleinik, N., Kim, J., Roth, B. M., Selvam, S. P., Gooz, M., Johnson, R. H., Lemasters, J. J., and Ogretmen, B. (2019) Mitochondrial protein import is regulated by p17/PERMIT to mediate lipid metabolism and cellular stress. *Science Advances* **5**, eaax1978

228. Kurosaki, T., and Maquat, L. E. (2016) Nonsense-mediated mRNA decay in humans at a glance. *Journal of Cell Science* **129**, 461

229. Hug, N., Longman, D., and Cáceres, J. F. (2016) Mechanism and regulation of the nonsense-mediated decay pathway. *Nucleic Acids Res* **44**, 1483-1495

230. Golpich, M., Amini, E., Mohamed, ., Azman Ali, R., Mohamed Ibrahim, N., and Ahmadiani, A. (2017) Mitochondrial Dysfunction and Biogenesis in Neurodegenerative diseases: Pathogenesis and Treatment. *CNS Neuroscience & Therapeutics* **23**, 5-22

231. Johri, A., and Beal, M. F. (2012) Mitochondrial dysfunction in neurodegenerative diseases. *J Pharmacol Exp Ther* **342**, 619-630

232. Lezi, E., and Swerdlow, R. H. (2012) Mitochondria in neurodegeneration. *Adv Exp Med Biol* **942**, 269-286

233. Woeste, M. A., and Wachten, D. (2017) The Enigmatic Role of GBA2 in Controlling Locomotor Function. *Frontiers in Molecular Neuroscience* **10**

234. Yildiz, Y., Matern, H., Thompson, B., Allegood, J. C., Warren, R. L., Ramirez, D. M., Hammer, R. E., Hamra, F. K., Matern, S., and Russell, D. W. (2006) Mutation of beta-glucosidase 2 causes glycolipid storage disease and impaired male fertility. *J Clin Invest* **116**, 2985-2994